JOURNAL OF PALEONTOLOGY

THE STRUCTURE OF CRANIDIAL SHAPE VARIATION IN THREE EARLY PTYCHOPARIOID TRILOBITE SPECIES FROM THE DYERAN–DELAMARAN (TRADITIONAL "LOWER–MIDDLE" CAMBRIAN) BOUNDARY INTERVAL OF NEVADA, U.S.A.

MARK WEBSTER
Department of the Geophysical Sciences, University of Chicago, 5734 South Ellis Avenue, Chicago, Illinois 60637, <mwebster@geosci.uchicago.edu>

Journal of Paleontology, 85(2), 2011, p. 179–225

0022-3360/11/0085-0179$03.00

THE STRUCTURE OF CRANIDIAL SHAPE VARIATION IN THREE EARLY PTYCHOPARIOID TRILOBITE SPECIES FROM THE DYERAN–DELAMARAN (TRADITIONAL ''LOWER–MIDDLE'' CAMBRIAN) BOUNDARY INTERVAL OF NEVADA, U.S.A.

MARK WEBSTER
Department of the Geophysical Sciences, University of Chicago, 5734 South Ellis Avenue, Chicago, Illinois 60637, <mwebster@geosci.uchicago.edu>

ABSTRACT—The structure of cranidial shape variation in the early ptychoparioid trilobites *Crassifimbra walcotti*, *Crassifimbra*? *metalaspis* (new combination), and *Eokochaspis nodosa* is explored using landmark-based geometric morphometric techniques, and is found to be generally similar among the species. Allometry is the strongest single source of cranidial shape variation within each species. The species share several trends in their respective patterns of ontogenetic shape change, but differ in the relative magnitude of these shared trends. Species-specific trends are also present. Each species follows a unique trajectory of ontogenetic shape change. The species exhibit subtle but significant differences in mean cranidial shape even at small size (sagittal length 1.75 mm); the magnitude of interspecific differences becomes larger at larger size (sagittal length 4.2 mm).

For conspecific cranidia of a given size, the major pattern of covariance among anatomical parts is essentially identical to the pattern of covariance among those parts during ontogeny. Developmentally determined covariance patterns among cranidial regions might be responsible for ontogenetic shape change and a portion of non-allometric shape intraspecific variation. Interspecific differences in cranidial shape resulted from complex local modifications to growth pattern and cannot be attributed to simple ontogenetic scaling.

The new collections permit the first description of non-cranidial sclerites of *C. walcotti*. A cephalic median organ is documented on *C. walcotti*, representing the oldest known occurrence of this structure in trilobites.

INTRODUCTION

AN UNDERSTANDING of morphological variation is central to many issues in the evolutionary sciences (e.g., Hallgrímsson and Hall, 2005). Morphological variation within and between species can be both a raw material upon which natural selection operates and a product of that selection. The structure of intraspecific variation can constrain the rate and direction of evolution (Simpson, 1944; Wagner and Altenberg, 1996; Schluter, 1996; Renaud et al., 2006; Sniegowski and Murphy, 2006; Hunt, 2007). Our understanding of particular evolutionary trends or events may therefore be improved by knowledge of the degree and pattern of variation within the taxa involved. Study of morphological variation within and among fossil samples can also improve our ability to distinguish interspecific disparity from intraspecific variation, leading to more robust species delimitation, diversity estimates, and biostratigraphic correlation (e.g., Hughes, 1994; Adrain and Westrop, 2006; Webster, 2007b, 2009; Hopkins and Webster, 2009).

Evolutionary and taxonomic studies of early ptychoparioid trilobites would greatly benefit from better comprehension of their morphological variation. These Cambrian trilobites, typically assigned to the Ptychopariidae Matthew, 1887 (in the broad sense of Fortey in Whittington et al. [1997, p. 302], including the ''antagmines,'' ''kochaspids,'' alokistocarids, and others), are thought to be the plesiomorphic ancestral stock from which more derived trilobite clades arose (Fortey in Whittington et al., 1997, p. 296; Fortey, 2001, p. 1148) and thus occupy a pivotal place in trilobite evolution. However, systematic work is problematic because early ptychoparioid taxa must be discriminated and phylogenetic relationships resolved by reference to relatively minor morphological variation (often in continuously-varying traits) within a conservative, ''generalized'' bauplan (Lochman, 1947; Rasetti, 1951, 1955; Shaw, 1962; Palmer and Halley, 1979; Blaker and Peel, 1997; Fortey in Whittington et al., 1997, p. 295–297; Fortey, 2001; Cotton, 2001). Morphological intermediates blur supposed distinctions between many purported taxa (Lochman, 1947; Rasetti, 1955). Systematic work is further confounded by differences among specimens in size and preservation, which can introduce morphological variation of a nature and magnitude similar to that inferred to be of phylogenetic significance (discussed below). Most early ptychoparioids are known from very few specimens and typically only from cranidia, thus limiting assessment of the bounds of intra- versus interspecific variation in terms of statistical rigor and morphological representation. Although recent descriptive work and cladistic analyses have improved our knowledge of some early ptychoparioid clades (Cotton, 2001; Sundberg, 1999, 2004), the vast majority of species and higher taxa remain poorly diagnosed (see comments in Rasetti, 1951, 1955; Palmer, 1968; Geyer and Malinky, 1997; Blaker and Peel, 1997; Fortey in Whittington et al., 1997, p. 302; Cotton, 2001; Sundberg, 2004).

Workers have long recognized the need for a detailed study of variation within and among samples to clarify early ptychoparioid systematics (Lochman, 1947; Rasetti, 1951; Palmer, 1958) and important steps have been made towards filling this void (Palmer, 1958; Bright, 1959; Blaker and Peel, 1997; Smith, 1998; Sundberg, 1999, 2004; Sundberg and McCollum, 2000; discussed below). The present paper utilizes landmark-based geometric morphometric techniques to explore, explicitly quantify, and compare the degree and the structure of cranidial shape variation within single silicified samples of each of three species from the Dyeran–Delamaran (traditional Laurentian ''Lower–Middle'' Cambrian) boundary interval of Nevada: *Crassifimbra walcotti* (Resser, 1937), ''*Eokochaspis*'' *metalaspis* Sundberg and McCollum, 2000, and *Eokochaspis nodosa* Sundberg and McCollum, 2000 (Figs. 1–8). Taphonomic and allometric sources of variation are

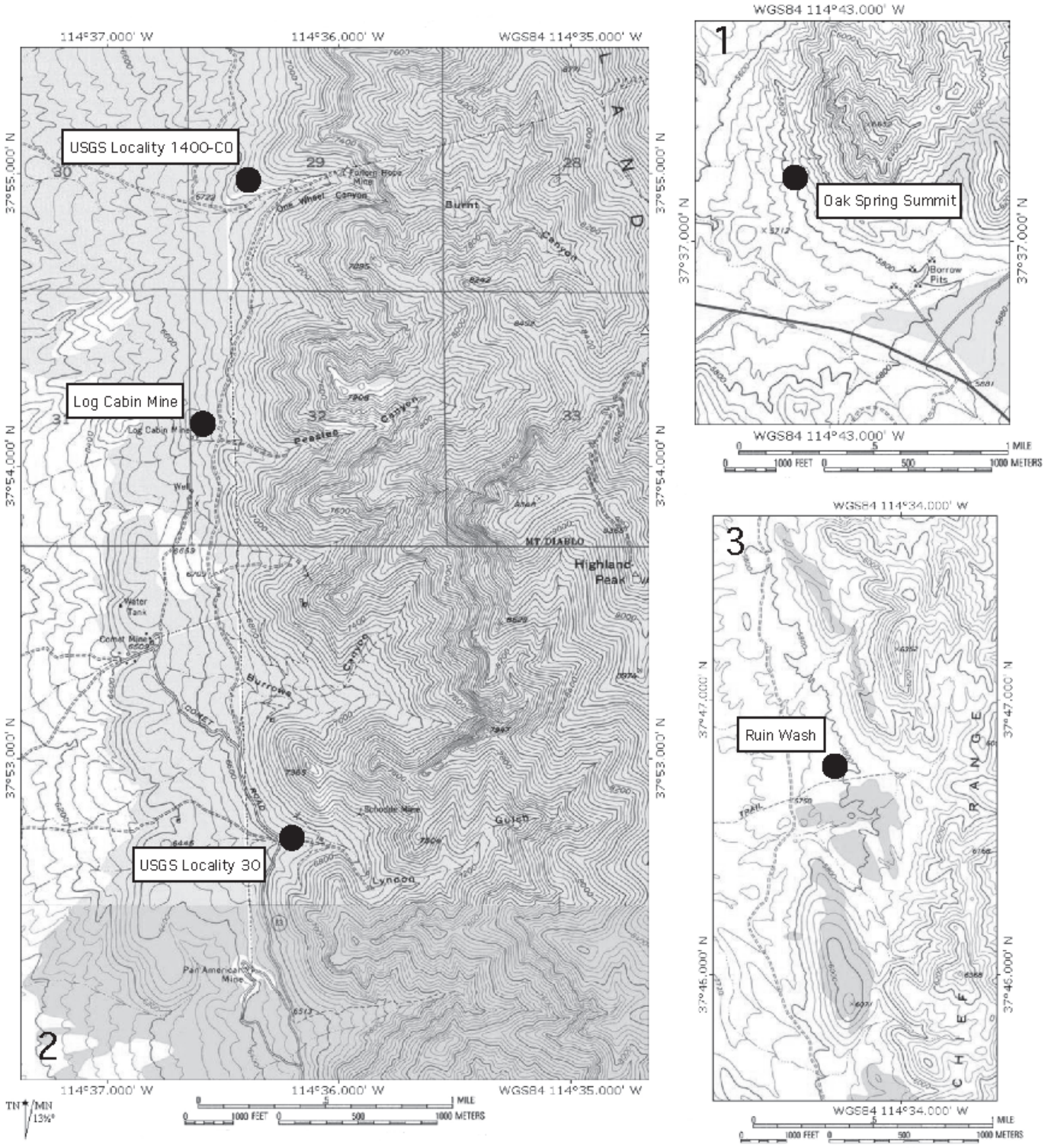

FIGURE *1*—Maps showing locations of sections in Lincoln County, east-central Nevada, U.S.A., studied and mentioned in the present work: *1,* Oak Spring Summit section (source of collection ICS-1029), Delamar Mountains. Major road south of section is Highway 93; *2,* Log Cabin Mine section (source of collection ICS-10124), west side of Highland Range. Location of USGS collection 1400-CO (One Wheel Canyon; type locality of *Crassifimba*? *metalaspis*) and approximate location of USGS locality 30 (?Lyndon Gulch; type locality of *C. walcotti*) also shown; *3,* Ruin Wash section (source of collection ICS-1192), Chief Range. See text for stratigraphic details. Maps created using TOPO! software (© National Geographic, 2002; <www.nationalgeographic.com/topo>).

controlled (below). In light of a critical review of previous work (below), this study is the first to provide directly comparable quantitative estimates of variation among early ptychoparioid species. The new silicified collections also permit the first description of non-cranidial sclerites of *C. walcotti*. Revised systematic descriptions of the species are provided. ''*Eokochaspis*'' *metalaspis* is excluded from the genus and provisionally reassigned to *Crassifimbra* Lochman,

1947. This detailed study of variation within and among early ptychoparioids represents a considerable advancement in our understanding of the paleobiology of these organisms. It establishes baseline data that will be useful for future systematic and evolutionary studies of this important but problematic group.

TERMINOLOGY AND SPECIES CONCEPT

Morphological terminology follows that of Whittington and Kelly in Whittington et al. (1997). Following Palmer (1998a), the length of a thoracic pleural spine is described as sentate when the spine length is less than half of the transverse width of the inner pleural region. Stratigraphic nomenclature for the Cambrian of Laurentia follows Palmer (1998b) and Sundberg (2005). Lithostratigraphic subdivision of the Pioche Formation follows Sundberg and McCollum (2000).

A pattern-based species concept is followed herein, whereby a species is defined as the least inclusive aggregation of comparable individuals diagnosable by a unique combination of character states. This essentially follows the phylogenetic species concept (Nixon and Wheeler, 1990; Wheeler and Platnick in Wheeler and Meier, 2000) and offers the most testable and defensible approach to species recognition in the fossil record (see Webster [2009] for further discussion and a case study).

PREVIOUS WORK

Several studies have explored the degree and structure of morphological variation within a limited number early ptychoparioid species (discussed below). However, these studies differ in the extent to which various sources of variation were controlled and in how variation was interpreted, complicating identification of generalities. These sources of variation and their impact on studies of variation (including the present study) are highlighted here.

Variation resulting from taphonomy.—Morphological variation attributable to difference in preservation between specimens is commonplace in paleontological samples but is typically biologically irrelevant. Compaction distorts shape and increases shape variation (Webster and Hughes, 1999) and fractures can sometimes be misinterpreted as biological structures (see discussion in Bright, 1959, p. 85). Features of potential phylogenetic significance such as furrow depth, relief of ocular ridges, and ornament can differ between internal and external surfaces of sclerites (Lochman, 1947; Rasetti, 1955; Palmer, 1958; Schwimmer, 1975; Blaker and Peel, 1997). The extent to which a sample is time-averaged can also affect variation within that sample (Hunt, 2004a, b).

Variation resulting from allometry.—Many morphological features are ontogenetically dynamic. Variation in these features may therefore reflect size differences rather than phylogenetic differences among specimens. Given the focus on cranidial shape herein, allometry (a non-zero relationship between size and shape) is particularly relevant. In the presence of allometry, estimates of intraspecific variation will be sensitive to the portion of ontogeny that is sampled.

All trilobites underwent considerable shape change during early ontogenetic stages. Conflicting views regarding the extent to which growth typically remained allometric during later ontogenetic stages (e.g., ''considerable allometric growth may take place during the holaspid period'' [Chatterton and Speyer in Whittington et al., 1997, p. 195]; ''shape changes [in the holaspid period] often approximated isometry'' [Hughes et al., 2006, p. 603]) might reflect taxon-specific differences. The few early ptychoparioid species for which ontogenetic data are available all seem to exhibit allometric growth even at large cranidial size (Rasetti, 1955, p. 7; Palmer, 1958; Bright, 1959; Sundberg, 1999; herein).

Geographic variation.—Single samples are not necessarily representative of the full range of morphology exhibited by a species. Geographic variation is well documented among extant arthropods (e.g., Riska, 1981; France, 1993; Avise, 2000; Hopkins and Thurman, 2010). Unambiguously distinguishing such geographically structured intraspecific variation from interspecific disparity can be difficult in the fossil record. Under the species concept adopted herein (above), two geographically and morphologically distinct samples would be assigned to different species unless the morphological differences between them are bridged by other samples. Hypotheses of species distinction are testable by addition of new data (geographic samples). Extensive geographic sampling coupled with careful analysis of inter- and intrasample variation has revealed geographic variation in one early Cambrian corynexochid trilobite (Hopkins and Webster, 2009), and has led to some supposedly widespread, variable late Cambrian trilobite species being reinterpreted as complexes of less variable species (Adrain and Westrop, 2005, 2006; Westrop and Adrain, 2007).

Previous estimates of variation in early ptychoparioids.—The above factors must be taken into account when evaluating variation in early ptychoparioids. Estimates of variation may not be readily comparable across studies that differ in the extent to which these factors are controlled.

The most exhaustive study to date of a basal ptychoparioid trilobite was presented by Palmer (1958), who described and quantitatively investigated the cranidial ontogeny of material that he assigned to *Crassifimbra walcotti*. Cranidial samples were recovered from three localities in east-central Nevada. Material from USGS locality 30 (type locality of *C. walcotti*; Fig. 1.2) was preserved as testate sclerites in limestone; material from USGS localities 1399-CO (near Pioche) and 1400-CO (Fig. 1.2) was silicified. All samples were represented by non-compacted material and were broadly comparable in terms of taphonomy, although morphological differences between internal and external cranidial surfaces were noted within the sample from USGS locality 30 (Palmer, 1958, p. 162). For each locality, traditional morphometric data for three cranidial variables (sagittal length of the frontal area, cranidial width [tr.] at the palpebral lobes, and the exsagittal distance between the posterior tip of the palpebral lobe to the occipital furrow) were regressed against sagittal cranidial length. Intrasample variation was assessed as the magnitude of deviations away from the regression line. For any cranidial length (and thus controlling for allometry), cranidia from USGS locality 1400-CO exhibited up to 20% variation (10% either side of the mean) in each of these variables, although most specimens exhibited values close to the mean (Palmer, 1958, p. 164). Differences between samples were found in some cranidial dimensions: at any cranidial length, cranidia from USGS locality 1399-CO exhibited a slightly longer frontal area compared to those from USGS locality 1400-CO, and cranidia from USGS locality 30 showed a relatively longer frontal area (sag.) and narrower cranidial width (tr.) at the palpebral lobes compared to those from USGS locality 1400-CO. These differences were small and all samples showed overlap in values for each trait, but were nevertheless found to be statistically significant. Palmer (1958, p. 164) preferred to interpret these differences as intraspecific because of ''the absence of any consistent observable difference other than proportion, and because the proportional differences even

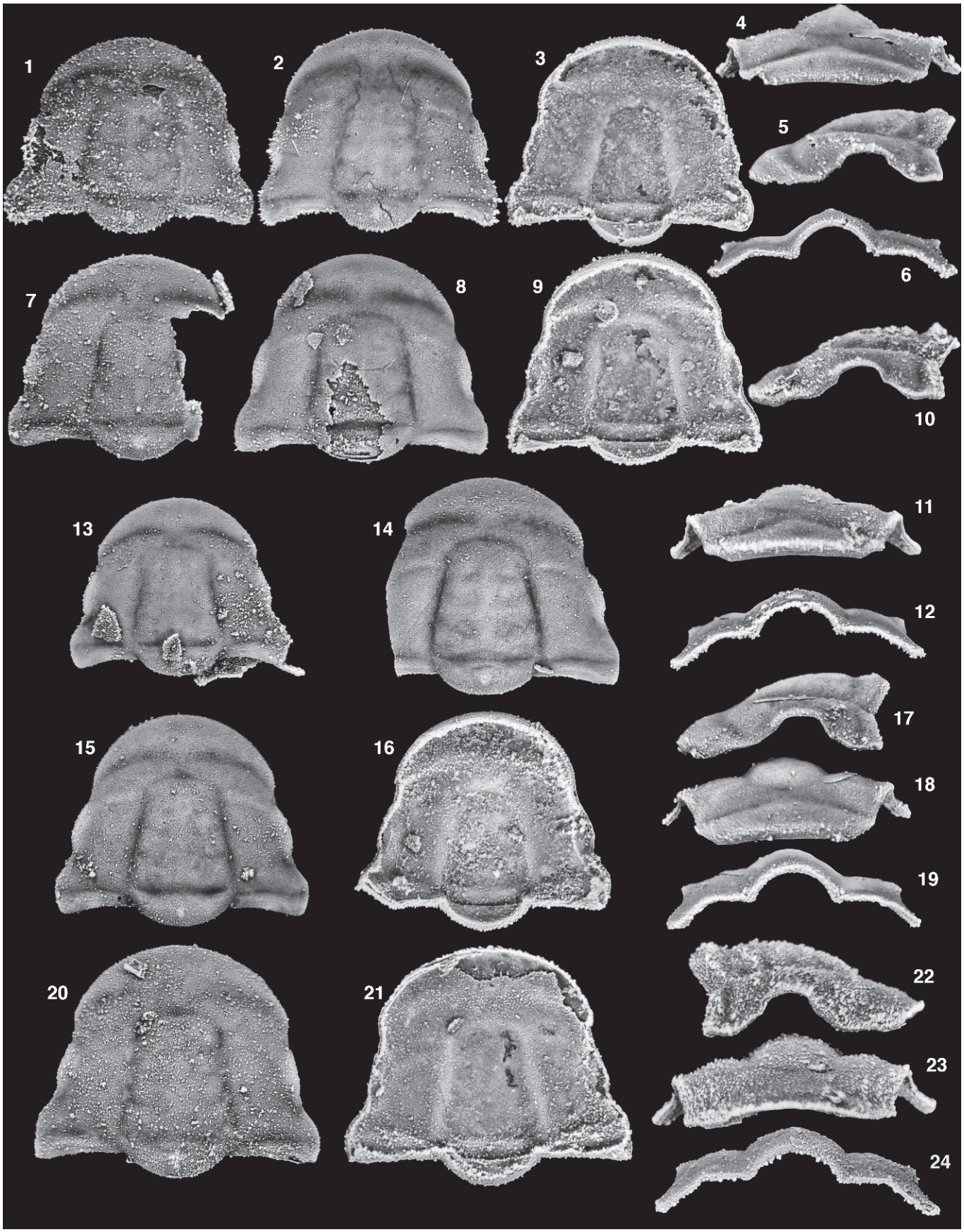

FIGURE 2—Large silicified cranidia of *Crassifimbra walcotti* (Resser, 1937): *1,* FMNH PE58241, dorsal view, ×12; *2–6,* FMNH PE58242, dorsal, ventral, anterior, left lateral, and posterior views, ×12; *7,* FMNH PE58243, dorsal view, ×12; *8–12,* FMNH PE58244, dorsal, ventral, left lateral,

though significant are small and not invariably sufficient alone for clear separation of any two specimens from two different localities.'' However, subsequent work emphasized the differences between cranidia from USGS localities 30 and 1400-CO (Fritz, 1968), and Sundberg and McCollum (2000) recognized the material from USGS locality 1400-CO as a new species, ''*Eokochaspis*'' *metalaspis* (herein provisionally reassigned to *Crassifimbra*; below). The collection from USGS locality 1399-CO has not been restudied since Palmer (1958), but seems to represent *C.*? *metalaspis*.

Growth and intraspecific variation in the Lincolnian (traditional Laurentian ''Middle'' Cambrian) early ptychoparioid *Elrathia kingii* (Meek, 1870) was assessed by Bright (1959). Six length variables summarizing basic body dimensions were measured on >300 (?late meraspids and) holaspids. The sample was recovered primarily from float in the Wheeler Amphitheater of the House Range, Utah (perhaps representing 250 ft of Wheeler Formation strata; Bright, 1959, p. 84), and is likely to be strongly time-averaged relative to single-bed samples. The ratio of cranidial width (tr., measured between the anterior tips of the palpebral lobes) to length (sag.) decreased from approximately 86% to approximately 80% as total body length increased from 5 mm to 40 mm. Of relevance to the present study, at any body size there was much variation in this ratio, with some specimens deviating from the mean by 15% (Bright, 1959, text-fig. 7). This degree of variation is similar to that reported in *C.*? *metalaspis* by Palmer (1958; above). Variation within *E. kingii* in the presence/absence and distribution of granular ornamentation and in thoracic segment number (10 to 13) was also noted (Bright, 1959).

Smith (1998) used landmark-based geometric morphometric techniques to quantify the degree of cranidial variation within nine trilobite species, including silicified samples of *C.*? *metalaspis* (identified as *C. walcotti*, following Palmer, 1958) and probably *Eokochaspis nodosa* (identified as *Eoptychoparia piochensis*; see below). For each species, intraspecific variation was quantified within a single collection of large sample size, covering ''the meraspid through holaspid ontogenetic stages'' (Smith, 1998, p. 18; how this was determined from isolated cranidia is unclear). There was no attempt to control for allometry, and the extent to which interspecific difference in variation may reflect difference in the portion of ontogeny sampled and/or in the magnitude of allometry over that portion of ontogeny is unknown. The Silurian aulacopleurid *Aulacopleura konincki* (Barrande, 1846) exhibited by far the highest variation. However, all specimens of this species had experienced compaction-related deformation, and the extent to which quantitative shape variation in this species represents biological signal and can be meaningfully compared to variation in the other species (specimens of which had experienced little to no compaction) is questionable. As in the present study, the samples of *C.*? *metalaspis* and (?)*E. nodosa* were silicified. However, Smith's (1998) summary of cranidial shape was less comprehensive and the metric for quantifying variation somewhat different than that used herein. Assuming that Smith's (1998) sample of ''*Eoptychoparia piochensis*'' did indeed represent *Eokochaspis nodosa*, his conclusion that *C.*? *metalaspis* and *E. nodosa* shared a similar level of variation is consistent with the findings of the present paper (below). The pattern of shape variation within each species was only cursorily discussed and presented in a rather abstract manner (Smith, 1998, p. 29, 30).

Blaker and Peel (1997) documented a remarkably high degree of cranidial variation in a single sample of early ptychoparioids from the Henson Gletscher Formation of North Greenland (upper Dyeran) that encompassed supposed distinctions between several genera. Although not investigated quantitatively, the variation was believed to be continuous and all specimens were assigned to a single species, *Ptychoparella* sp. A. Even allowing for the differential morphologies of internal versus external sclerite surfaces, the variation among illustrated specimens from this horizon is high (see Blaker and Peel, 1997, figs. 78, 79) and, if indeed continuous, would likely match or exceed the disparity among all three species documented herein. (It may be that the Greenland collection comprises two species.)

Sundberg (1999) studied variation in the Topazan (traditional Laurentian ''Middle Cambrian'') alokistocarid ptychoparioid *Alokistocare subcoronatum* (Hall and Whitfield, 1877). Bivariate analyses revealed that some features (basal cranidial width [tr.], anterior border width [sag.], exsagittal distance between the anterior border furrow and the anterior tip of the palpebral lobe, palpebral lobe length, and transverse width of the posterior wing of the fixigena) exhibited significant allometric growth with respect to cranidial length even among large cranidia (>2.5 mm sagittal length). Small but significant differences among samples were found for several measured variables (Sundberg, 1999, p. 1135, 1136). These differences did not seem to result from the collections having sampled different portions of the ontogeny. Sundberg (1999, p. 1136) interpreted these as intraspecific variation (stratigraphic and/or geographic) rather than interspecific disparity.

As part of a detailed systematic revision of kochaspid ptychoparioids, Sundberg and McCollum (2000) and Sundberg (2004) documented qualitative and quantitative intraspecific variation in several early ptychoparioid species including *C.*? *metalaspis* (as *Eokochaspis metalaspis*) and *E. nodosa*. In the cladistic analysis of the group (Sundberg, 2004), these two species were each coded from examination of 13 specimens (all stated to be holaspids), and each was found to be polymorphic in seven of the 69 and 68 (respectively) characters for which they were coded. The nature and absolute magnitude of the variation represented by each polymorphism obviously differs from character to character. Nevertheless, each coded polymorphism indicates a morphological feature in which intraspecific variation exceeds the distinction between (at least some of) the other species, and is therefore relevant to the issue of the magnitude of intraspecific variation relative to interspecific disparity. *Crassifimbra*? *metalaspis* was coded as polymorphic for glabellar length relative to cranidial length (character 1), glabellar tapering (character 2), length of the occipital ring relative to cranidial length (character 14), whether or not the posterior cranidial border furrow extended to the posterior facial suture (character 32), exsagittal length of the posterior wing of the fixigena relative to basal glabellar

←

anterior, and posterior views, ×11; *13,* FMNH PE58245, dorsal view, ×10; *14,* FMNH PE58246, dorsal view, ×10; *15–19,* FMNH PE58247, dorsal, ventral, left lateral, anterior, and posterior views, ×11; *20–24,* FMNH PE58248, dorsal, ventral, right lateral, anterior, and posterior views, ×10. All from ICS-1029, Combined Metals Member, Pioche Formation, Oak Spring Summit section, Delamar Mountains.

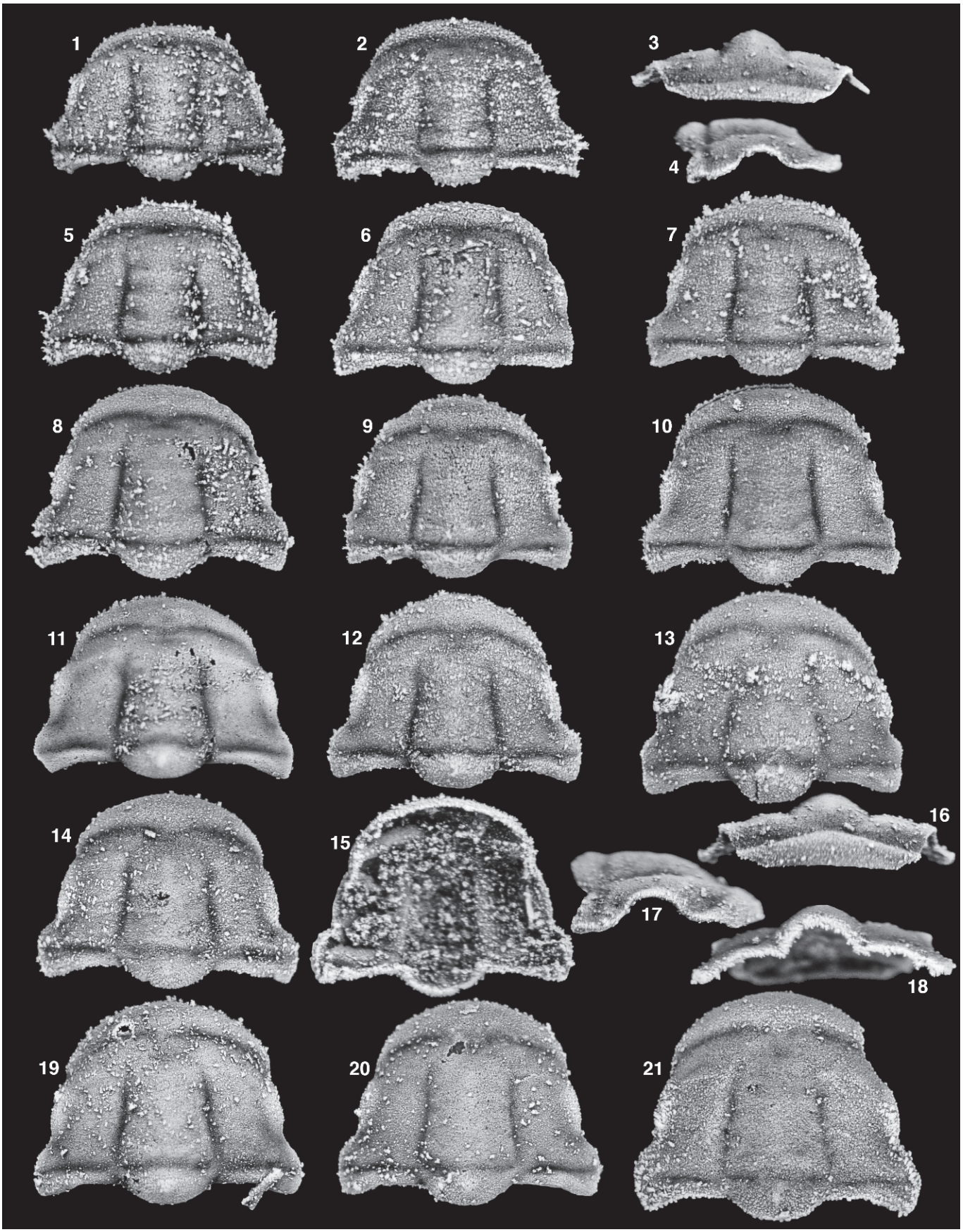

FIGURE 3—Small silicified cranidia of *Crassifimbra walcotti*: *1,* FMNH PE58249, dorsal view, ×30; *2–4,* FMNH PE58250, dorsal, anterior, and right lateral views, ×30; *5,* FMNH PE58251, dorsal view, ×28; *6,* FMNH PE58252, dorsal view, ×28; *7,* FMNH PE58253, dorsal view, ×27; *8,* FMNH

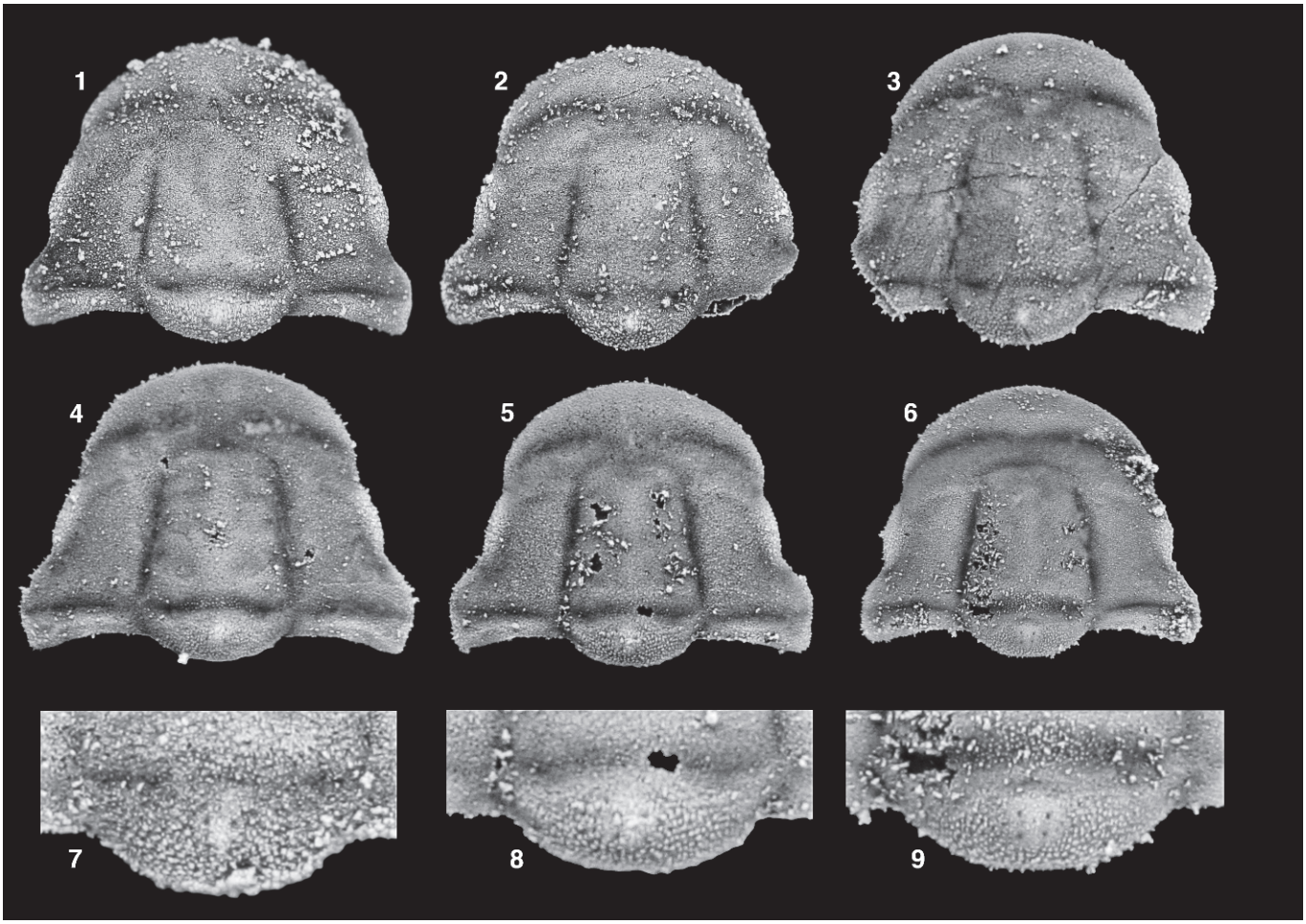

FIGURE 4—Small silicified cranidia of *Crassifimbra walcotti*: *1,* FMNH PE58264, dorsal view, ×19; *2,* FMNH PE58265, dorsal view, ×18; *3,* FMNH PE58266, dorsal view, ×18; *4,* FMNH PE58267, dorsal view, ×17; *5, 8,* FMNH PE58268, dorsal view (×15) and enlargement of occipital ring showing granulations and details of cephalic median organ (×30); *6, 9,* FMNH PE58269, dorsal view (×13) and enlargement of occipital ring showing granulations and details of cephalic median organ (×30); *7,* FMNH PE58263, enlargement of occipital ring showing details of cephalic median organ, ×40 (see also Fig. 3.21). All from ICS-1029, Combined Metals Member, Pioche Formation, Oak Spring Summit section, Delamar Mountains.

width (character 33), angle of divergence of the anterior branches of the facial suture (character 35), and palpebral lobe length relative to glabellar length (character 41). *Eokochaspis nodosa* was coded as polymorphic for length of the occipital ring relative to cranidial length (character 14), proportional length of the frontal area occupied by the preglabellar field (character 15), transverse width of the interocular portion of the fixigena relative to basal glabellar width (character 28), palpebral lobe length relative to glabellar length (character 41), palpebral lobe width relative to palpebral lobe length (character 42), orientation of the ocular ridges (character 44), and degree of rounding of the anterolateral corners of the pygidium (character 58). A meta-analysis of published trilobite cladistic analysis (Webster, 2007a) found that the degree of polymorphism coded in *C.*? *metalaspis* and *E. nodosa* documented by Sundberg (2004) is not unusual among early ptychoparioid trilobites, and that the frequency and level of intraspecific polymorphism coded in ptychoparioids (and other ''Early'' and ''Middle'' Cambrian trilobite groups) is significantly higher than in later groups.

Variation within single silicified samples of each of *C. walcotti*, *C.*? *metalaspis*, and *E. nodosa* from new collections is quantified and studied herein. The pattern of ontogenetic shape change is identified for each species. An analytical size-standardizing procedure is used to estimate intraspecific morphological variation with the effects of allometric shape change removed. Statistical comparison of the degree and structure of morphological variation (with and without size-standardization) and the pattern of ontogenetic shape change among samples provides novel insight into the nature of interspecific differences in cranidial shape. Geographic and stratigraphic variation within these species (including samples from the type localities and additional new collections), plus an investigation of the evolutionary significance of this variation, will be presented elsewhere.

←

PE58254, dorsal view, ×25; *9,* FMNH PE58255, dorsal view, ×24; *10,* FMNH PE58256, dorsal view, ×23; *11,* FMNH PE58257, dorsal view, ×22; *12,* FMNH PE58258, dorsal view, ×22; *13,* FMNH PE58259, dorsal view, ×21; *14–18,* FMNH PE58260, dorsal, ventral, anterior, right lateral, and posterior views, ×21; *19,* FMNH PE58261, dorsal view, ×21; *20,* FMNH PE58262, dorsal view, ×21; *21,* FMNH PE58263, dorsal view, ×20 (see also Fig. 4.7). All from ICS-1029, Combined Metals Member, Pioche Formation, Oak Spring Summit section, Delamar Mountains.

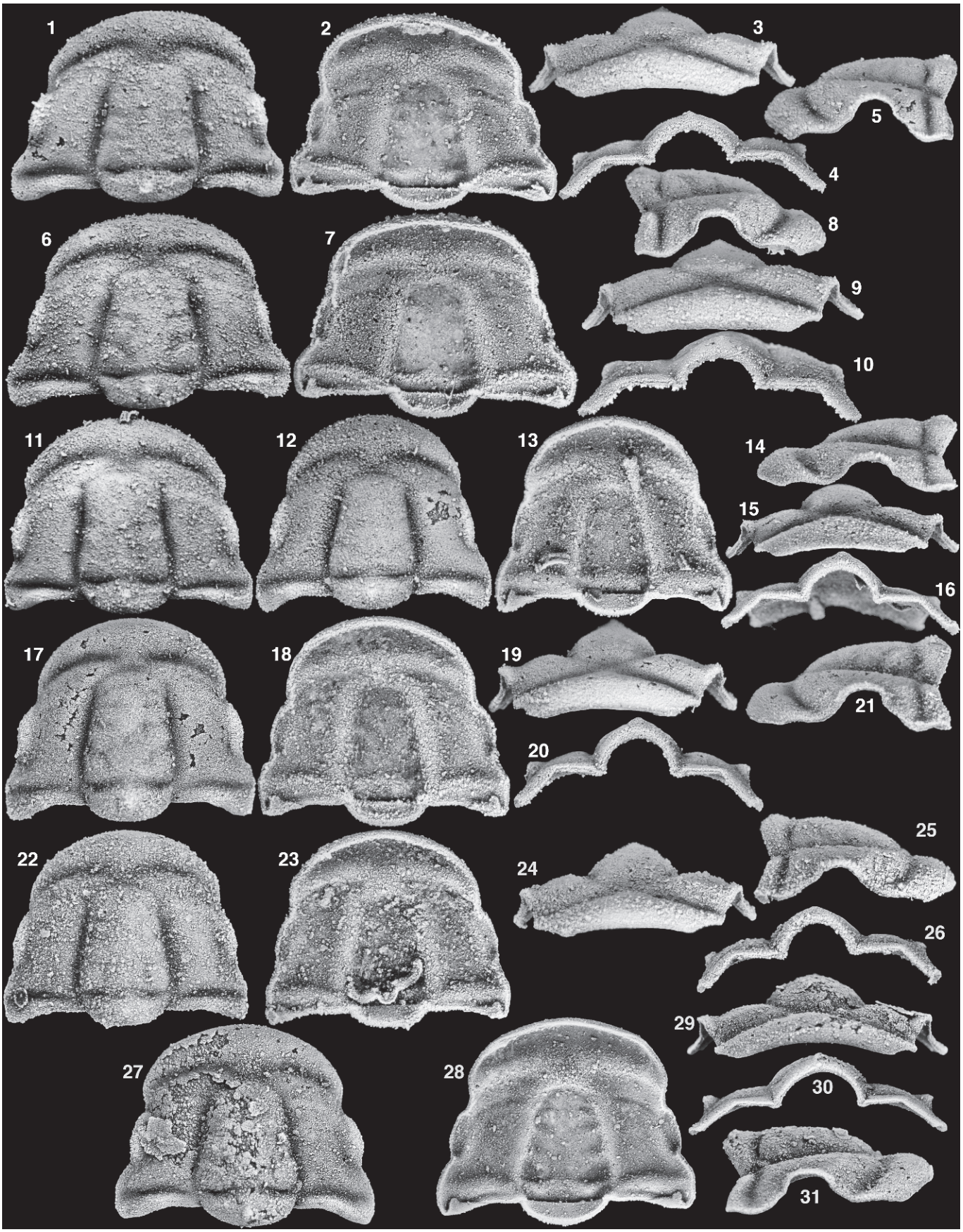

FIGURE 5—Large cranidia of *Crassifimbra*? *metalaspis* (Sundberg and McCollum, 2000): *1–5,* FMNH PE58270, dorsal, ventral, anterior, posterior, and left lateral views, ×9; *6–10,* FMNH PE58271, dorsal, ventral, right lateral, anterior, and posterior views, ×9; *11,* FMNH PE58272, dorsal view, ×9;

MATERIAL

Silicified sclerites of *C. walcotti*, *C.*? *metalaspis*, and *E. nodosa* were recovered from the Pioche Formation, east-central Nevada (Fig. 1). For each species, the material described and analyzed herein was extracted from a single, well-constrained horizon at a single locality: *C. walcotti* from collection ICS-1029 (carbonate nodules 11 m below the top of the Combined Metals Member, uppermost Dyeran, Oak Spring Summit section; Figs. 2–4); *C.*? *metalaspis* from collection ICS-10124 (thin carbonate ledge approximately 10.75 m above the base of the Combined Metals Member, uppermost Dyeran, Log Cabin Mine section; Figs. 5, 6); and *E. nodosa* from ICS-1192 (ribbon carbonate marking the base of the Comet Shale Member, lowermost Delamaran, Ruin Wash section; Figs. 7, 8). Taphonomic and stratigraphic data indicate that these three beds represent comparable, minimally time-averaged accumulations: all were deposited in a relatively deep subtidal environment as part of a transgressive to highstand system tract (Webster et al., 2008); the sampled portion of the beds are of similar thickness, each likely representing deposition over just decades to hundreds of years within the sequence; and the sclerites from each bed are typically in excellent condition, suggesting minimal transportion and reworking. The carbonates were dissolved in weak acetic acid, and silicified sclerites were picked from the insoluble residues. Cranidia were blackened with dilute Indian ink, whitened with ammonium chloride, and mounted for photography using the standard orientation of Shaw (1957), with the dorsal surface of the palpebral lobes being positioned horizontally below a vertically mounted digital camera.

More than 110, 240, and 120 cranidia of *C. walcotti*, *C.*? *metalaspis*, and *E. nodosa* (respectively) were photographed (Figs. 2–8). Morphometric data were collected for the subset of cranidia in each sample that were sufficiently large, complete, and well preserved to permit accurate and consistent digitization of all landmarks (below). Cranidia included in the morphometric analysis presented herein range in sagittal length from 0.99 mm to 4.37 mm (*C. walcotti*; N=57), from 1.71 mm to 5.43 mm (*C.*? *metalaspis*; N=116), and from 1.62 mm to 4.90 mm (*E. nodosa*; N=65) (Fig. 9). Many smaller cranidia in each sample were also examined, but were not photographed or included in the morphometric analyses because they are more difficult to mount and photograph in a consistent orientation and they exhibit relatively grainier preservation. Figured specimens are housed in the Field Museum of Natural History, Chicago (FMNH). Additional studied material is housed in the Institute for Cambrian Studies, University of Chicago (ICS) and the Smithsonian Institution, Washington, D.C. (USNM).

MORPHOMETRIC ANALYSIS OF CRANIDIAL SHAPE AND SHAPE VARIATION WITHIN AND BETWEEN SPECIES

Landmark-based geometric morphometric methods (Rohlf and Slice 1990; Bookstein, 1991; Dryden and Mardia, 1998; Zelditch et al., 2004; Webster and Sheets, 2010) are used herein to quantitatively study cranidial shape variation (including ontogenetic shape change) within each species, and to compare mean cranidial shape and patterns of shape change among the species. These methods extract information about shape variation by analyzing coordinates of landmarks (i.e., homologous, discrete, anatomical loci). A hallmark of these methods is their ability to retain information about the spatial relationships among landmarks throughout a study, making it possible to relate the abstract results of statistically powerful analyses to the physical structure of the original specimens (Bookstein, 1991; Zelditch et al., 2004; Slice, 2007; Webster and Sheets, 2010). Until fairly recently, landmark-based morphometrics was most useful for studies of landmark-rich structures but less effective for analyzing complex curves. Methodological developments now make it possible to incorporate information about outlines within the theoretical framework of landmark-based studies by sampling curves at a series of points called "semilandmarks." Semilandmarks are not discrete, anatomical loci and they contain less information than landmarks, but they capture information about curvature, making it possible to study complex curving morphologies where landmarks are sparse (Green, 1996; Bookstein, 1997; Sheets et al., 2004; Perez et al., 2006). Specialized methods are needed to superimpose semilandmarks (Green, 1996; Sampson et al., 1996; Bookstein, 1997; Andresen et al., 2000; Bookstein et al., 2002; Gunz et al., 2005). However, once superimposed, their coordinates can be analyzed just like those of landmarks except that semilandmarks have only one degree of freedom.

Landmark-based geometric morphometric techniques have been applied in many trilobite studies (Webster, 2007b and references therein; Hopkins and Webster, 2009). With sufficiently well-preserved material, the methods are capable of detecting even very subtle developmental signals in ancient organisms (Webster et al., 2001; Webster and Zelditch, 2005, 2008, 2009; Webster, 2007b).

A total of nine landmarks and 85 semilandmarks were digitized from the sagittal axis and right side of each cranidium (Fig. 10). Where the right side was incompletely preserved, landmarks and semilandmarks were digitized on the left side and computationally reflected across the midline. Landmarks and outlines were digitized using tpsDig (Rohlf, 2009). Coordinates of semilandmarks were calculated from the outline data in SemiLand6 (Sheets, 2009) using the minimized Procrustes distance method to optimize their location along the outline.

Variation among landmark configurations digitized from ten replicate images of the same specimen was almost two orders of magnitude smaller than variation among conspecific specimens from the same sample (data not presented). Measurement error associated with mounting of specimens and digitizing replicability is therefore deemed negligible. Distortion of inter-specimen distances associated with the projection from shape space into a tangent space approximation of that space is also negligible (correlation between all pairwise partial Procrustes distances and all pairwise Euclidean distances for all 238 specimens, $r^2=1.000$; slope=0.999766; analysis performed using tpsSmall [Rohlf, 2003]).

The structure of cranidial shape variation within samples.—Partial Procrustes superimposition of all landmark configurations (Fig. 11.1, 11.3, 11.5) confirms that each species exhibits

←

12–16, FMNH PE58273, dorsal, ventral, left lateral, anterior, and posterior views, ×9; *17–21,* FMNH PE58274, dorsal, ventral, anterior, posterior, and left lateral views, ×9; *22–26,* FMNH PE58275, dorsal, ventral, anterior, right lateral, and posterior views, ×8; *27–31,* FMNH PE58276, dorsal, ventral, anterior, posterior, and right lateral views, ×7. All from ICS-10124, Combined Metals Member, Pioche Formation, Log Cabin Mine section, Highland Range.

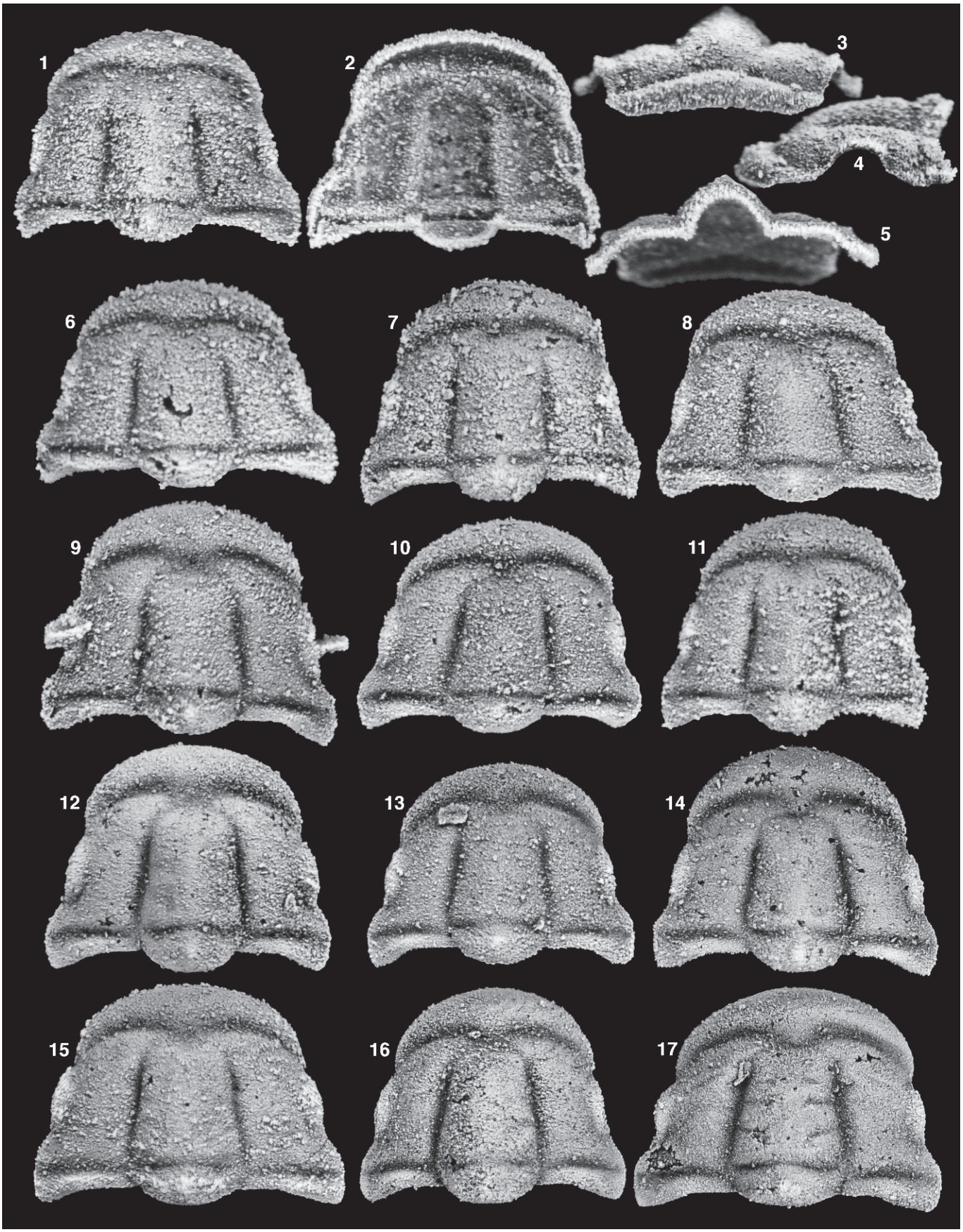

FIGURE 6—Small cranidia of *Crassifimbra*? *metalaspis*: *1–5,* FMNH PE58277, dorsal, ventral, anterior, left lateral, and posterior views, ×23; *6,* FMNH PE58278, dorsal view, ×22; *7,* FMNH PE58279, dorsal view, ×20; *8,* FMNH PE58280, dorsal view, ×17; *9,* FMNH PE58281, dorsal view, ×17;

considerable cranidial shape variation (see Figs. 2–8). The structure of this variation is explored through a principal components analysis (PCA) of shape data using PCAGen6p (Sheets, 2007a). In this case, the shape data are partial warp scores (including the two uniform terms) calculated for each configuration in a sample using the consensus of all configurations in that sample as the reference form (see Webster and Sheets [2010] and references within for details). For any configuration, each warp score quantifies the contribution of a mathematically independent style of deformation (a warp or one of the two uniform components) of the reference form to the shape difference between the reference and that configuration. A PCA of warp scores is termed a relative warp analysis (RWA), and each principal component can be referred to as a relative warp (RW). RWs are mathematically independent axes of shape variation and can be described in terms of the effect on particular anatomical regions. However, RWs do not necessarily relate to biologically independent modes of variation. Actual shape variation within a given anatomical region is described by the net effect of all RWs upon that region.

RWA of the configurations supports the hypothesis that each sample is monospecific: the data within each sample form a single cloud in morphospace with no outliers, and cranidial shape variation is continuous along all RW axes (Figs. 12–14).

Almost 80% of the shape variation among the 57 cranidia of *C. walcotti* is summarized by the first three relative warps (Fig. 12). RW1 explains 62% of the total shape variance in the sample and relates primarily to variation in the shape of the glabella, frontal area, and posterior wing of the fixigena: specimens with more positive scores have a glabella that is less anteriorly tapered, a proportionally shorter (sag., exsag.) and narrower (tr.) frontal area, and a more strongly posterolaterally oriented posterior cranidial margin distal to the fulcrum. RW2 explains 9% of the total shape variance in the sample and relates primarily to variation in relative area of the frontal area, interocular portion of the fixigena, and posterior wing of the fixigena: specimens with more positive scores have a proportionally more expansive (sag., exsag., and tr.) frontal area, interocular portion of the fixigena, and posterior wing of the fixigena relative to the glabella. RW3 explains 8% of the total shape variance in the sample and relates primarily to length (exsag.) of the palpebral lobe relative to the form of the posterior wing of the fixigena: specimens with more positive scores have a relatively longer palpebral lobe and a more compact posterior wing. Higher RWs each explain $<5\%$ of total variance and relate to trivial components of shape variation.

Almost three quarters of the shape variation among the 116 cranidia of *C.*? *metalaspis* is summarized by the first four relative warps (Fig. 13). RW1 explains 35% of the total shape variance in the sample and relates primarily to variation in the shape of the glabella, frontal area, and posterior wing of the fixigena: specimens with more positive scores have a glabella that is more anteriorly tapered, a proportionally longer (sag., exsag.) and wider (tr.) frontal area, and a less strongly posterolaterally oriented posterior cranidial margin distal to the fulcrum. RW2 explains 22% of the total shape variance in the sample and relates primarily to variation in relative anterior tapering of the cranidium: specimens with more positive scores have a proportionally wider (tr.) and longer (sag., exsag.) posterior portion of the cranidium (especially wider in the posterior portion of the glabella) and a relatively narrower (tr.) and shorter (sag., exsag.) frontal area. RW3 explains 9% of the total shape variance in the sample and relates primarily to area of the frontal area, interocular portion of the fixigena, and posterior wing of the fixigena: specimens with more positive scores have a proportionally more expansive (sag., exsag., and tr.) frontal area, interocular portion of the fixigena, and posterior wing of the fixigena relative to the glabella. RW4 explains 7% of the total shape variance in the sample and relates primarily to length (exsag.) of the palpebral lobe relative to the form of the posterior wing of the fixigena: specimens with more positive scores have a relatively longer palpebral lobe and a more compact posterior wing. Higher RWs each explain $<5\%$ of total variance and relate to trivial components of shape variation.

More than two-thirds of the shape variation among the 65 cranidia of *E. nodosa* is summarized by the first four relative warps (Fig. 14). RW1 explains 27% of the total shape variance in the sample and relates primarily to variation in the shape of the glabella, frontal area, and posterior wing of the fixigena: specimens with more positive scores have a glabella that is more anteriorly tapered, a proportionally longer (sag., exsag.) and wider (tr.) frontal area, and a less strongly posterolaterally oriented posterior cranidial margin distal to the fulcrum. RW2 explains 17% of the total shape variance in the sample and relates primarily to variation in relative anterior tapering of the cranidium: specimens with more positive scores have a proportionally wider (tr.) and longer (sag., exsag.) posterior portion of the cranidium (especially wider in the posterior portion of the glabella) and a relatively narrower (tr.) and shorter (sag., exsag.) frontal area. RW3 explains 16% of the total shape variance in the sample and relates primarily to area of the frontal area, interocular portion of the fixigena, and posterior wing of the fixigena: specimens with more positive scores have a proportionally more expansive (sag., exsag., and tr.) frontal area, interocular portion of the fixigena, and posterior wing of the fixigena relative to the glabella. RW4 explains 8% of the total shape variance in the sample and relates primarily to length (exsag.) of the abaxial portion of the frontal area: specimens with more positive scores have a relatively longer anterior branch of the facial suture and a proportionally more compact palpebral lobe and posterior wing. Higher RWs each explain $<6\%$ of total variance and relate to trivial components of shape variation.

Although the relative warps are not homologous across species (being based on PCA of warp scores from species-specific reference forms), some generalities regarding the structure of cranidial shape variation among these three species can be identified. The major axis of variation (RW1) in all three species describes a generally similar pattern of variation. (The polarity of the axis is arbitrary: the pattern of variation described by increasingly positive scores along RW1 of *C. walcotti* is similar to the pattern of variation described by increasingly negative scores along RW1 in *C.*? *metalaspis* and *E. nodosa*.) The pattern of variation described by RW2 in both *C.*? *metalaspis* and *E. nodosa* seems to be

←

10, FMNH PE58282, dorsal view, ×16; *11,* FMNH PE58283, dorsal view, ×16; *12,* FMNH PE58284, dorsal view, ×14; *13,* FMNH PE58285, dorsal view, ×14; *14,* FMNH PE58286, dorsal view, ×13; *15,* FMNH PE58287, dorsal view, ×13; *16,* FMNH PE58288, dorsal view, ×12; *17,* FMNH PE58289, dorsal view, ×12. All from ICS-10124, Combined Metals Member, Pioche Formation, Log Cabin Mine section, Highland Range.

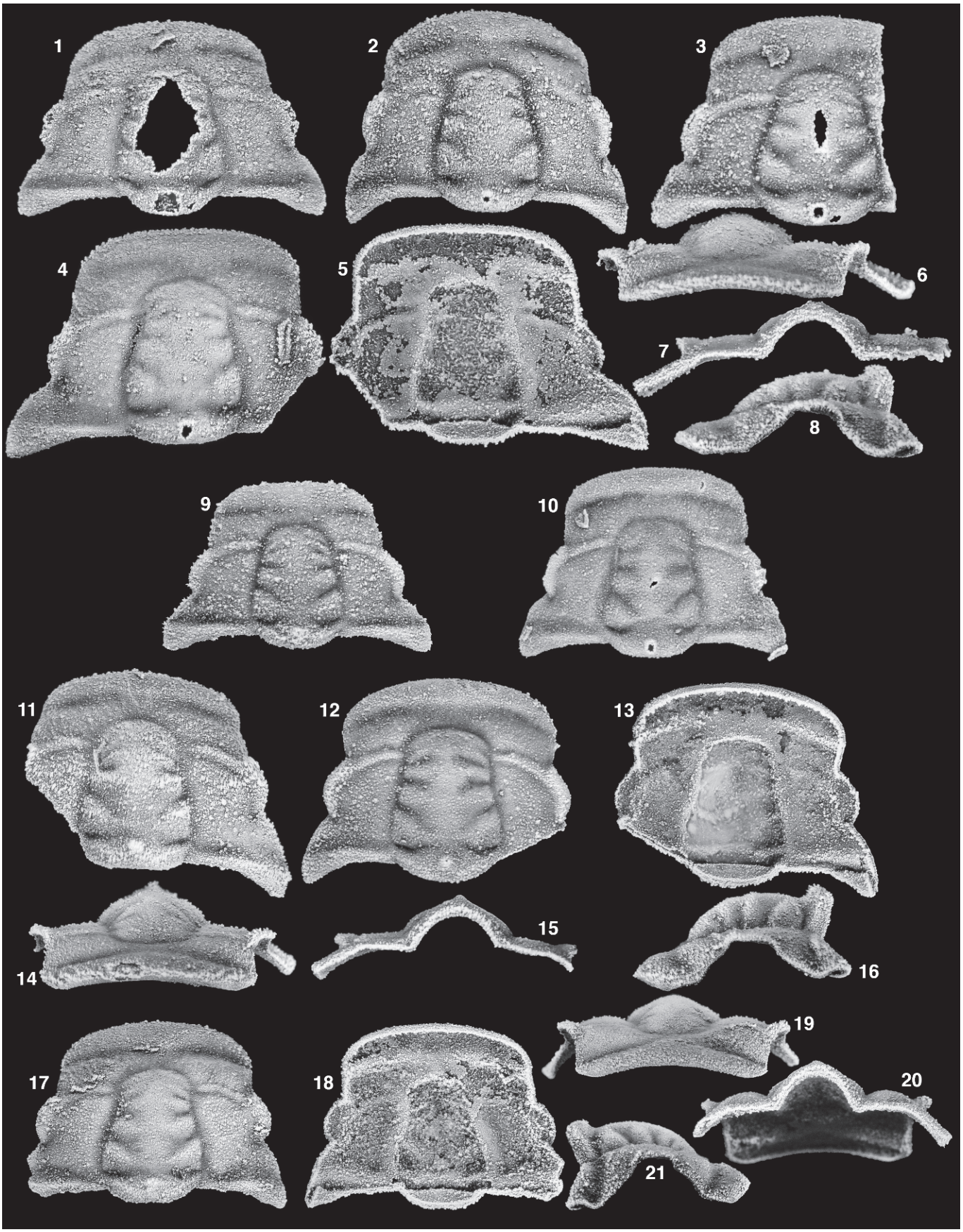

FIGURE 7—Large cranidia of *Eokochaspis nodosa* Sundberg and McCollum, 2000. *1,* FMNH PE58290, dorsal view, ×9; *2,* FMNH PE58291, dorsal view, ×9; *3,* FMNH PE58292, dorsal view, ×9; *4–8,* FMNH PE58293, dorsal, ventral, anterior, posterior, and left lateral views, ×9; *9,* FMNH PE58294,

incorporated into RW1 in *C. walcotti*. RW2 of *C. walcotti* describes a similar pattern of variation to that described by RW3 in the other species. RW3 of *C. walcotti* is analogous to RW4 of *C.*? *metalaspis* and shows some similarity to RW4 of *E. nodosa*, although the last relates more to relative length of the anterior facial suture than the palpebral lobe.

The presence and nature of cranidial ontogenetic shape change.—Given the size range of cranidia within each sample (Fig. 9), it is likely that some of the intraspecific variation in cranidial shape (above, Figs. 2–8, 11.1, 11.3, 11.5, 12–14) results from ontogenetic shape change. The presence and nature of allometric growth is here investigated in several ways.

First, the partial Procrustes distance of each specimen in a sample away from a reference configuration representing the typical form of the smallest cranidia in that sample was calculated (using the Regress6N software; Sheets, 2008). The reference configurations for *C. walcotti*, *C.*? *metalaspis*, and *E. nodosa* were designated as the consensuses of the smallest nine, six, and five specimens of each species, respectively. The partial Procrustes distance between two configurations is the square root of the summed squared distances between their corresponding landmarks after placing the configurations in partial Procrustes superimposition (see Webster and Sheets [2010] and references therein), and therefore quantifies the amount of difference in shape between those configurations. For each species the partial Procrustes distance away from the reference form shows a significant positive relationship to cranidial size (quantified as lnCS) (Fig. 15), demonstrating that shape changed as size increased during the sampled portion of ontogeny.

Second, the proportion of total shape variance explained by allometry was calculated for each species as follows (using the Regress6N software; Sheets, 2008). The mean cranidial shape of each species was calculated as the consensus of all configurations of that species. The total shape variance (SS_{total}) of that species was quantified as the summed squared partial Procrustes distances of all configurations of that species to its mean shape. Partial warp scores (including the two uniform terms) were then calculated for each configuration away from the reference configuration of that species, and those scores were regressed in a multivariate regression against lnCS to produce a vector of regression coefficients describing the nature of shape change over the sampled portion of ontogeny for each species. The summed squared residuals ($SS_{residual}$) from this regression, also expressed in Procrustes units, represent shape deviations not attributable to allometry. The difference between SS_{total} and $SS_{residual}$ gives the variance explained by the allometry regression (SS_{model}), and the ratio of SS_{model} to SS_{total} gives the proportion of total variance explained by allometry. Nonparametric resampling (1,600 bootstraps) determines the statistical significance of the multivariate regression. Using this method, allometry explains 48% of the total shape variation in the sample of *C. walcotti* ($P < 0.001$; Table 1). The proportion of total shape variance explained by allometry in *C.*? *metalaspis* and *E. nodosa* is much smaller (12% and 13%, respectively), but is nevertheless highly significant ($P < 0.001$ in each case; Table 1). Such a difference in strength of the allometric signal in the data between *C. walcotti* and the other species is not surprising given that the *C. walcotti* sample included small cranidia of a size not represented in the other samples (Fig. 9).

TABLE 1—Percentage of total variance (SS_{total}, measured as summed squared Procrustes units) explained by allometry in the samples of *Crassifimbra walcotti* (from ICS-1029; N=57), *Crassifimbra*? *metalaspis* (from ICS-10124; N=116), and *Eokochaspis nodosa* (from ICS-1192; N=65). P-value is based on 1,600 bootstraps. See text for details and interpretation.

Species	SS_{total}	$SS_{residual}$	Percent variance explained	*P*
Crassifimbra walcotti	0.0785	0.0406	48.33	<0.000625
Crassifimbra? *metalaspis*	0.0999	0.8884	11.55	<0.000625
Eokochaspis nodosa	0.0579	0.0502	13.42	<0.000625

As a third test of whether growth in these species was allometric, a multivariate vector of ontogenetic shape change was calculated for each species and compared to a vector of isometry using VecCompare6c (Sheets, 2003). The vector was calculated as follows. For each species, partial warp scores (including the two uniform terms) were calculated for each configuration away from a reference configuration (the consensus of all configurations of that particular species). These scores were then regressed in a multivariate regression against lnCS to produce a vector of regression coefficients describing the nature of shape change over the sampled portion of ontogeny for each species. (Bivariate plots of the x- and the y-component of each partial warp and the uniform terms against lnCS reveal that the ontogenetic vector of shape change for each species shows negligible deviation from linearity [data not shown].) The angle between the observed vector and the isometric vector is calculated as the inverse cosine of the dot product of the normalized regression coefficients between the two vectors. An angle of 0° between the vectors indicates that they do not differ in patterns of shape change. Confidence limits on the angle between the vectors are computed by 1,600 bootstraps of the sample data. The vector of shape change within a sample is considered to significantly differ from isometry if the observed angle between it and the isometric vector exceeded the 95% limits of the bootstrapped range of angles within the observed sample. Results of this test show that the angle between each ontogenetic vector and the vector of isometry is very large and far exceeds the range of within-species angles generated by bootstrap resampling (Table 2). Growth is significantly different from isometry (at >95% confidence) over the sampled portion of ontogeny in all species. The smaller range of within-species angles in *C. walcotti* relative to the other species (Table 2) reflects the stronger allometric signal within that sample (above).

A thin-plate spline deformation grid shows how the shape of each reference form is deformed when subjected to the corresponding vector of ontogenetic shape change for that species (Fig. 16). The pattern of ontogenetic shape change within each species closely matches the major axis of shape variation within that species (above, compare Fig. 16.1 to Fig. 12.3, Fig. 16.2 to Fig. 13.4, and Fig. 16.3 to Fig. 14.4). (The arbitrary polarity of RW1 for *C. walcotti* is reversed

←

dorsal view, ×8; *10,* FMNH PE58295, dorsal view, ×8; *11,* FMNH PE58296, dorsal view, ×8; *12–16,* FMNH PE58297, dorsal, ventral, anterior, posterior, and left lateral views, ×8; *17–21,* FMNH PE58298, dorsal, ventral, anterior, posterior, and right lateral views, ×7. All from ICS-1192, Comet Shale Member, Pioche Formation, Ruin Wash section, Chief Range.

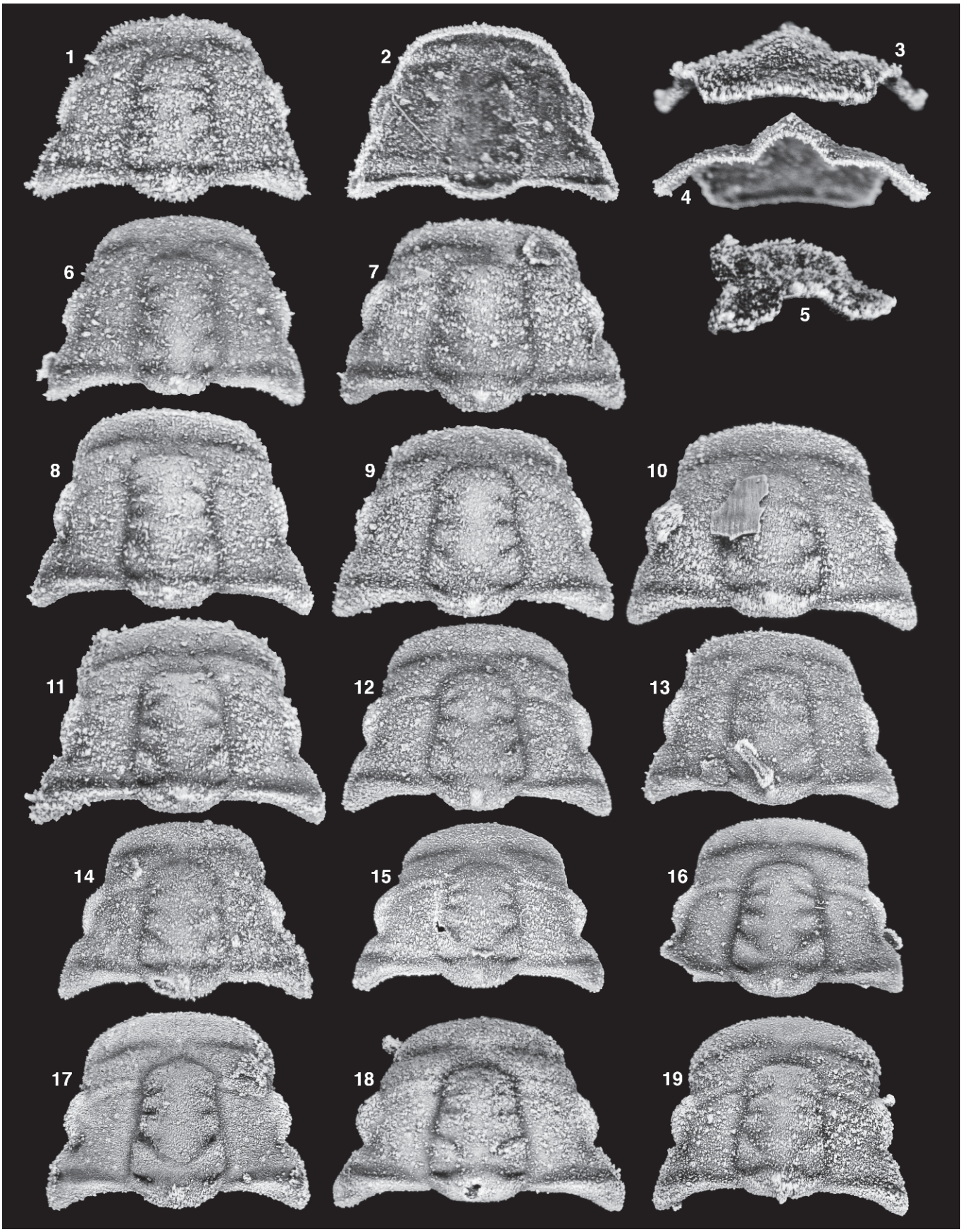

FIGURE 8—Small cranidia of *Eokochaspis nodosa*: *1–5,* FMNH PE58299, dorsal, ventral, anterior, posterior, and right lateral views, ×20; *6,* FMNH PE58300, dorsal view, ×20; *7,* FMNH PE58301, dorsal view, ×20; *8,* FMNH PE58302, dorsal view, ×19; *9,* FMNH PE58303, dorsal view, ×18; *10,*

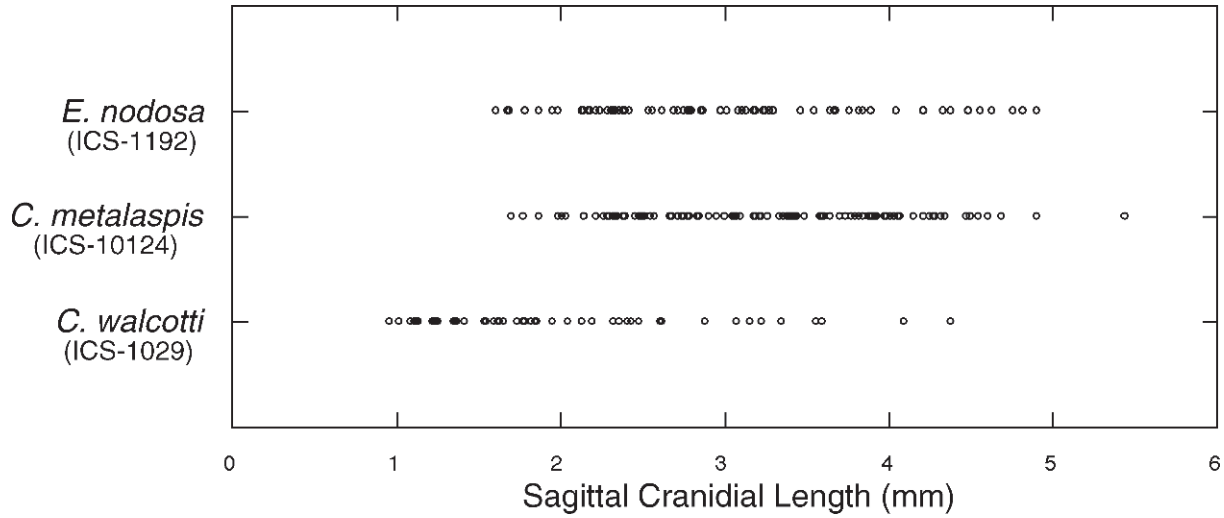

FIGURE 9—Sagittal length of cranidia of *Crassifimbra walcotti* (N=57), *C.*? *metalaspis* (N=116), and *Eokochaspis nodosa* (N=65) included in the morphometric analyses presented herein.

relative to the ontogenetic polarity for that species, as discussed above.) The primary pattern of variation in cranidial shape within a sample is therefore interpreted to result from ontogenetic shape change (further discussed below).

The three species show several general similarities in their respective patterns of ontogenetic shape change (Fig. 16): progressively larger cranidia of all species exhibit an increased anterior tapering of the glabella, elongation and lateral expansion of the frontal area, and rotation of the posterior cranidial margin distal to the fulcrum into a less strong posterolateral orientation. However, the species differ in the relative magnitude of each of these changes: the ontogenetic rotation of the distal portion of the posterior cranidial margin is strongest in *C. walcotti*, for example. Subtle species-specific ontogenetic trends are also superimposed upon these common trends (Fig. 16): *E. nodosa* exhibits a more extreme change in curvature of the distal margin of the palpebral lobe and the posterior wing of the fixigena becomes more extensiform (i.e., less blunt-tipped) relative to the other species; and the change in curvature of the distal margin of the palpebral lobe in *C.*? *metalaspis* is slightly stronger than in *C. walcotti*.

Comparison of trajectories of cranidial ontogenetic shape change.—Patterns of cranidial ontogenetic shape change were statistically compared among species by calculating the angle between their respective vectors of ontogenetic shape change (using the VecCompare6c software [Sheet, 2003]; see Webster et al. [2001] and Webster [2007b] for other trilobite examples using the same technique). The vectors for each species must be based on homologous variables (i.e., warps and uniform deformations). Partial warps and uniform terms for each species were therefore calculated using the consensus of the smallest three specimens in the combined data set (238 specimens) as the reference form. The regression coefficients of the x- and y-components of each warp score and the two uniform terms regressed against lnCS for each species represents the vector of ontogenetic shape change for that species. The angle between the vectors of two species was calculated as the inverse cosine of the dot product of the normalized regression coefficients between those vectors. An angle of 0° between the vectors indicates that they do not differ in patterns of shape change. Confidence limits on the range of angles that could be produced within a single species by chance were calculated by bootstrap resampling (1,600 replicates) of the sample of that species. Between-species vectors of shape change were considered to significantly differ if the between-species angle exceeded the 95% confidence limits of the within-species angles of both species.

Pairwise comparisons reveal that each species differs from all others in trajectory of shape change at >95% confidence (Table 3). Despite the ontogenetic trends common to all species (above), the differences in the magnitude of these changes and in subtle local allometry (above) result in each species following a unique trajectory of cranidial ontogenetic shape change. The smaller range of within-species angles in *C. walcotti* relative to the other species (Table 3) again reflects the stronger allometric signal within that sample (above).

Controlling for cranidial allometric variation by size-standardization.—The above analyses demonstrate that allometry is present over the sampled portion of ontogeny for each species (above; Figs. 15, 16). Shape variation within each sample is therefore a combination of "static" variation (i.e., non-

TABLE 2—Angle between vector of isometry and vector of ontogenetic shape change for *Crassifimbra walcotti* (from ICS-1029), *Crassifimbra*? *metalaspis* (from ICS-10124), and *Eokochaspis nodosa* (from ICS-1192). Difference between ontogenetic vector and isometric vector is significant at >95% for each species (based on 1,600 bootstraps). See text for details and interpretation.

Species	N	Angle to isometry	Within sample
Crassifimbra walcotti	57	96.6°	13.6°
Crassifimbra? *metalaspis*	116	93.6°	27.7°
Eokochaspis nodosa	65	91.3°	33.6°

←

FMNH PE58304, dorsal view, ×17; *11,* FMNH PE58305, dorsal view, ×16; *12,* FMNH PE58306, dorsal view, ×15; *13,* FMNH PE58307, dorsal view, ×12; *14,* FMNH PE58308, dorsal view, ×11; *15,* FMNH PE58309, dorsal view, ×11; *16,* FMNH PE58310, dorsal view, ×11; *17,* FMNH PE58311, dorsal view, ×10; *18,* FMNH PE58312, dorsal view, ×9; *19,* FMNH PE58313, dorsal view, ×9. All from ICS-1192, Comet Shale Member, Pioche Formation, Ruin Wash section, Chief Range.

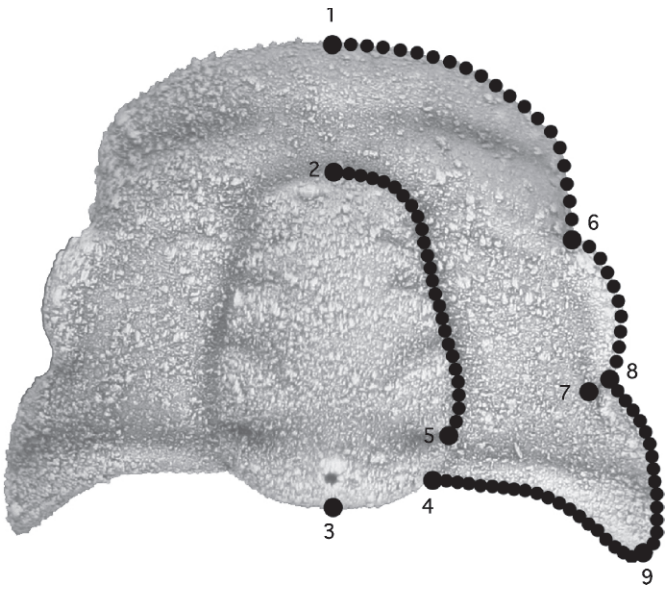

FIGURE *10*—Landmark and semilandmark selection. Landmarks (large circles, numbered): *1,* Anterior cranidial margin on sagittal axis; *2,* anterior of glabella on sagittal axis; *3,* posterior margin of occipital ring on sagittal axis; *4,* intersection of occipital ring and posterior cranidial margin in dorsal view; *5,* intersection of SO with axial furrow; *6,* anterior tip of palpebral lobe; *7,* posterior tip of palpebral lobe; *8,* intersection of posterior facial suture with distal margin of palpebral lobe in dorsal view; *9,* distal tip of posterior wing of fixigena. Semilandmarks (small circles, not numbered) summarize curvature of anterior cranidial margin and anterior branch of the facial suture (19 points between landmarks *1* and *6*), distal margin of palpebral lobe (9 points between landmarks *6* and *8*), posterior branch of the facial suture (14 points between landmarks *8* and *9*), posterior cranidial margin (19 points between landmarks *4* and *9*), and glabella anterior to SO (24 points between landmarks *2* and *5*). See text for details.

allometric variation among individuals of the same size) plus "dynamic" variation (i.e., allometric variation among individuals resulting from differences in size). Comparison of mean shape and shape variation among species is more meaningful when based on static variation alone; that is, with variance attributable to allometry having been controlled (above). In order to remove shape variation resulting from size variation, each sample was computationally size-standardized using the Standard6 software (Sheets, 2001). This procedure involves conducting a linear regression of shape variables against lnCS, then using this model to predict the shape of each specimen at a user-specified size. Residuals (shape deviations from the regression) remain associated with each specimen, so that the size-standardized shape of each specimen is the predicted shape of that specimen at the user-specified size plus its original residuals. When all specimens within a sample are size-standardized to the same log centroid size, shape variation is determined entirely by the residuals from the regression model and shape variation attributable to the regression (i.e., to allometry) has been removed. (This method is equivalent to that used to calculate the $SS_{residuals}$ term in the test for allometry, above.)

To permit comparison of cranidial shape at large size, the configurations of *C. walcotti*, *C.*? *metalaspis*, and *E. nodosa* were size-standardized to lnCS of 2.97, 3.03, and 3.10, respectively (Fig. 11.2, 11.4, 11.6): this is equivalent to a sagittal cranidial length of approximately 4.2 mm in all cases. To permit comparison of cranidial shape at small size, the configurations of *C. walcotti*, *C.*? *metalaspis*, and *E. nodosa* were also size-standardized to lnCS of 2.14, 2.20, and 2.20, respectively: this is equivalent to a sagittal cranidial length of approximately 1.75 mm in all cases. These values are close to the maximum and minimum size (but within the size range) of sampled specimens for each species. The size-standardizations therefore do not involve extrapolation of modeled ontogenetic vectors of shape change beyond the observed portion of ontogeny.

The effect of size-standardization on the amount of shape variation within each sample is investigated using the DisparityBox software (Sheets, 2007b). Intraspecific variation in cranidial shape for each sample is quantified as the variance in partial Procrustes distance of specimens from the mean form of the sample (Webster and Sheets, 2010). Bootstrap resampling (with replacement, 1,600 replicates) of each sample permits calculation of the 95% confidence limits on each sample variance. Variance values and 95% confidence limits are reported for both the non-size-standardized data and the size-standardized data (Table 4).

As expected, the estimate of intraspecific variation consistently decreases when data within each sample are size-standardized (Table 4; compare Fig. 11.1, 11.3, 11.5 to Fig. 11.2, 11.4, 11.6). However, this is significant at 95% confidence only for *C. walcotti* (Table 4), for which a far greater proportion of total shape variance is explained by allometry relative to the other species (above; Table 1).

This method also permits comparison of the level of variation among species. *Crassifimbra walcotti* is significantly more variable than other species when data are not size-standardized (Table 4). However, the estimate of variation in this species is more inflated by ontogenetic variation (above), and species do not significantly differ from each other (at 95% confidence) in estimate of variation based on size-standardized data (Table 4). This finding is consistent with that of Smith (1998; discussed above).

The structure of static variation within each species was investigated by a RWA of the size-standardized data (Figs. 17–19). More than 60% of the shape variation among the 57 cranidia of *C. walcotti* size-standardized to a sagittal length of approximately 4.2 mm is summarized by the first three relative warps (Fig. 17). RW1 explains 31% of the total shape variance in the sample. Specimens with more positive scores along this axis have a proportionally longer glabella that is less anteriorly tapered, a proportionally wider (tr.) posterior margin of the occipital ring, a proportionally longer (sag., exsag.) and wider (tr.) frontal area and fixigena, and a more strongly posteriorly oriented posterior cranidial margin distal to the fulcrum. RW2 explains 17% of the total shape variance in the sample. Specimens with more positive scores have a relatively longer (exsag.) interocular area and palpebral lobe and a more compact (exsag.) posterior wing. RW3 explains 14% of the total shape variance in the sample. Specimens with more positive scores have a proportionally more expansive (sag., exsag., and tr.) frontal area, interocular portion of the fixigena, and posterior wing of the fixigena relative to the glabella, and a wider (tr.) posterior margin of the occipital ring. Higher RWs each explain $<8\%$ of total variance and relate to trivial components of shape variation.

The structure of variation described by these RWs is strikingly similar to those produced by a RWA of the data prior to size-standardization (above; Fig. 12). RW1 in both cases essentially describes the pattern of ontogenetic shape change (with polarity again reversed; compare Figs. 12.3, 17.3, and 16.1). This is remarkable, given that the allometric signal was removed by size-standardization. This demonstrates that, for conspecific cranidia of a given size, the major pattern of covariance among anatomical regions reflects the pattern of

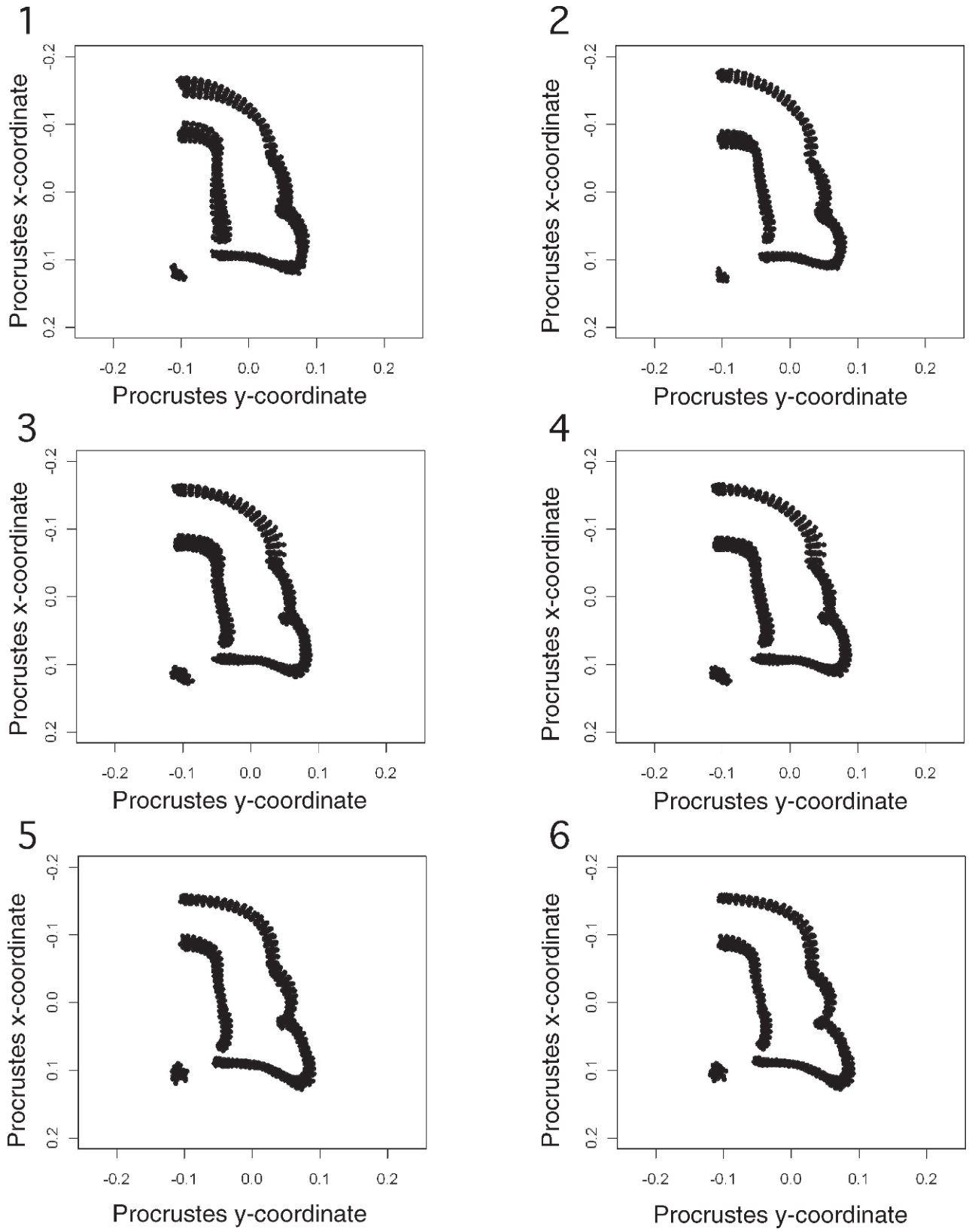

FIGURE *11*—Landmark configurations for *Crassifimbra walcotti: 1, 2,* from ICS-1029 (N=57); *C.*? *metalaspis: 3, 4,* from ICS-10124 (N=116); *E. nodosa: 5, 6,* from ICS-1192 (N=65) in partial Procrustes superimposition. The reference form for each plot is the consensus of all configurations in that sample. Axes have been switched and the y-axis reversed for ease of comparison to Fig. 10. Shape variation within a species (*1, 3, 5*) decreases when the variance attributable to size-related shape change is removed by size-standardization (*2, 4, 6*; representing predicted shape of all specimens at sagittal cranidial length of approximately 4.2 mm). See text and Table 4 for details.

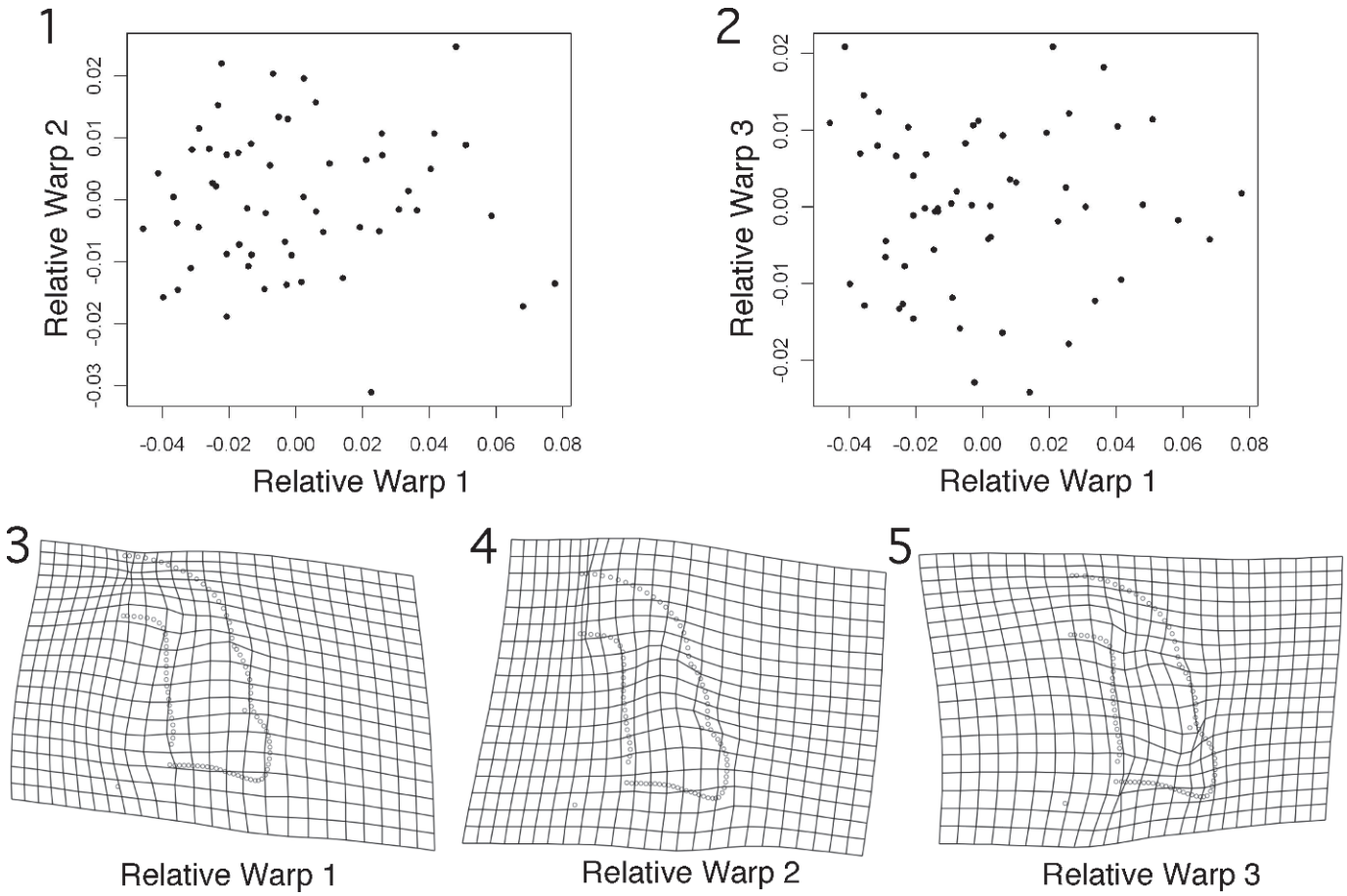

FIGURE *12*—Structure of cranidial shape variation in *Crassifimbra walcotti* from ICS-1029, as revealed by a principal components analysis of warp scores (relative warp analysis, RWA). Landmark configurations shown in Figs. 10, 11.1; reference form is mean of all 57 configurations in the sample. *1,* RW1 versus RW2; *2,* RW1 versus RW3; *3,* thin-plate spline deformation grid depicting shape variation along RW1 in a positive direction (62% variance explained); *4,* thin-plate spline deformation grid depicting shape variation along RW2 in a positive direction (9% variance explained); *5,* thin-plate spline deformation grid depicting shape variation along RW3 in a positive direction (8% variance explained). See text for details.

covariance among anatomical regions during ontogeny: the primary structure of static variation is also the structure of ontogenetic variation. The contribution of this pattern of variation to the total shape variation is approximately halved by the process of size-standardization. This is consistent with the test for allometry (above; Table 1), which found that allometry accounted for approximately one-half of the shape variance in the original data. Accordingly, the contribution of higher RWs (not relating to allometry) to total shape variance is approximately doubled following size-standardization. RW2 of the size-standardized data describes a similar pattern of variation to RW3 prior to size-standardization (compare Figs. 17.4 and 12.5), and RW3 of the size-standardized data describes a similar pattern of variation to RW2 prior to size-standardization (compare Figs. 17.5 and 12.4). RW2 and RW3 explain a similar proportion of total shape variance, and their order reversal as a result of size-standardization is understandable.

More than 55% of the shape variation among the 116 cranidia of *C.*? *metalaspis* size-standardized to a sagittal length of approximately 4.2 mm is summarized by the first two relative warps (Fig. 18). RW1 and RW2 explain 35% and 21% of the total shape variance in the sample, respectively. Higher RWs each explain <8% of total variance and relate to trivial components of shape variation. As for *C. walcotti* (above), the major patterns of shape variation in *C.*? *metalaspis* are essentially unchanged by size-standardization. The structure of variation described by RW1 of the size-standardized data is clearly similar to that described by RW1 prior to size-standardization and to the pattern of ontogenetic shape change (compare Figs. 18.2, 13.4, and 16.2); and RW2 of the size-standardized data is similar to that described by RW2 prior to size-standardization (compare Figs. 18.3 and 13.5). Again, the primary structure of static variation is also the structure of ontogenetic variation. The proportion of total variance explained by these axes of variation is not markedly changed by size-standardization. This is understandable given the relatively small contribution of allometry to total shape variation in this sample (above; Table 1).

More than 55% of the shape variation among the 65 cranidia of *E. nodosa* size-standardized to a sagittal length of approximately 4.2 mm is summarized by the first three relative warps (Fig. 19). RW1, RW2, and RW3 explain 25%, 19%, and 13% of the total shape variance in the sample, respectively. Higher RWs each explain <6% of total variance and relate to trivial components of shape variation. As for *C. walcotti* and *C.*? *metalaspis*, the major patterns of shape variation in *E. nodosa* are essentially unchanged by size-standardization. The structure of variation described by each of RW1, RW2, and RW3 of the size-standardized data is essentially identical to that of RWs 1 to 3 (respectively) prior to size-standardization, and RW1 again mirrors the pattern of

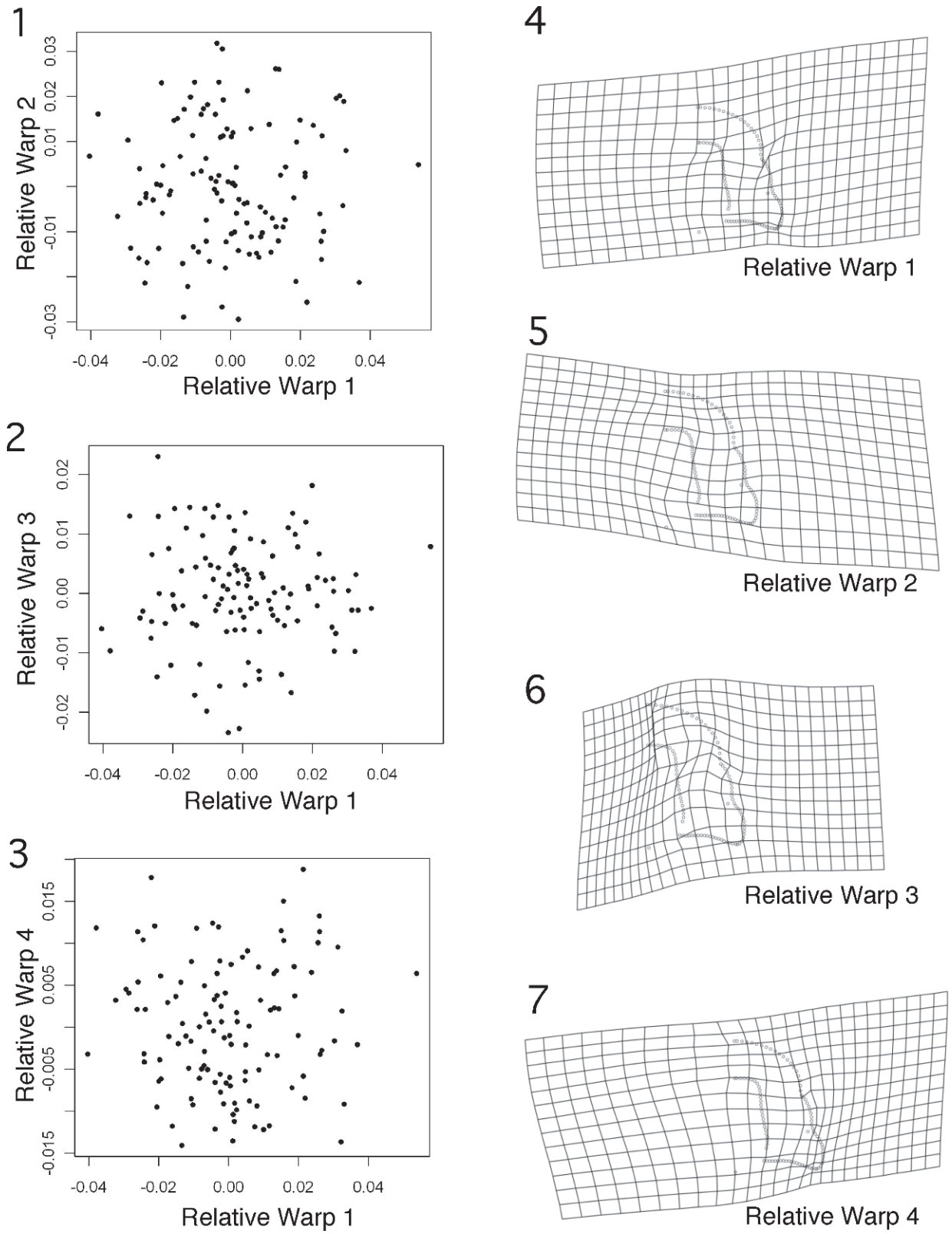

FIGURE *13*—Structure of cranidial shape variation in *Crassifimbra*? *metalaspis* from ICS-10124, as revealed by a principal components analysis of warp scores (relative warp analysis, RWA). Landmark configurations are shown in Figs. 10, 11.3. Reference form is mean of all 116 configurations in the sample. *1,* RW1 versus RW2; *2,* RW1 versus RW3; *3,* RW1 versus RW4; *4,* thin-plate spline deformation grid depicting shape variation along RW1 in a positive direction (35% variance explained); *5,* thin-plate spline deformation grid depicting shape variation along RW2 in a positive direction (22% variance explained); *6,* thin-plate spline deformation grid depicting shape variation along RW3 in a positive direction (9% variance explained); *7,* thin-plate spline deformation grid depicting shape variation along RW4 in a positive direction (7% variance explained). See text for details.

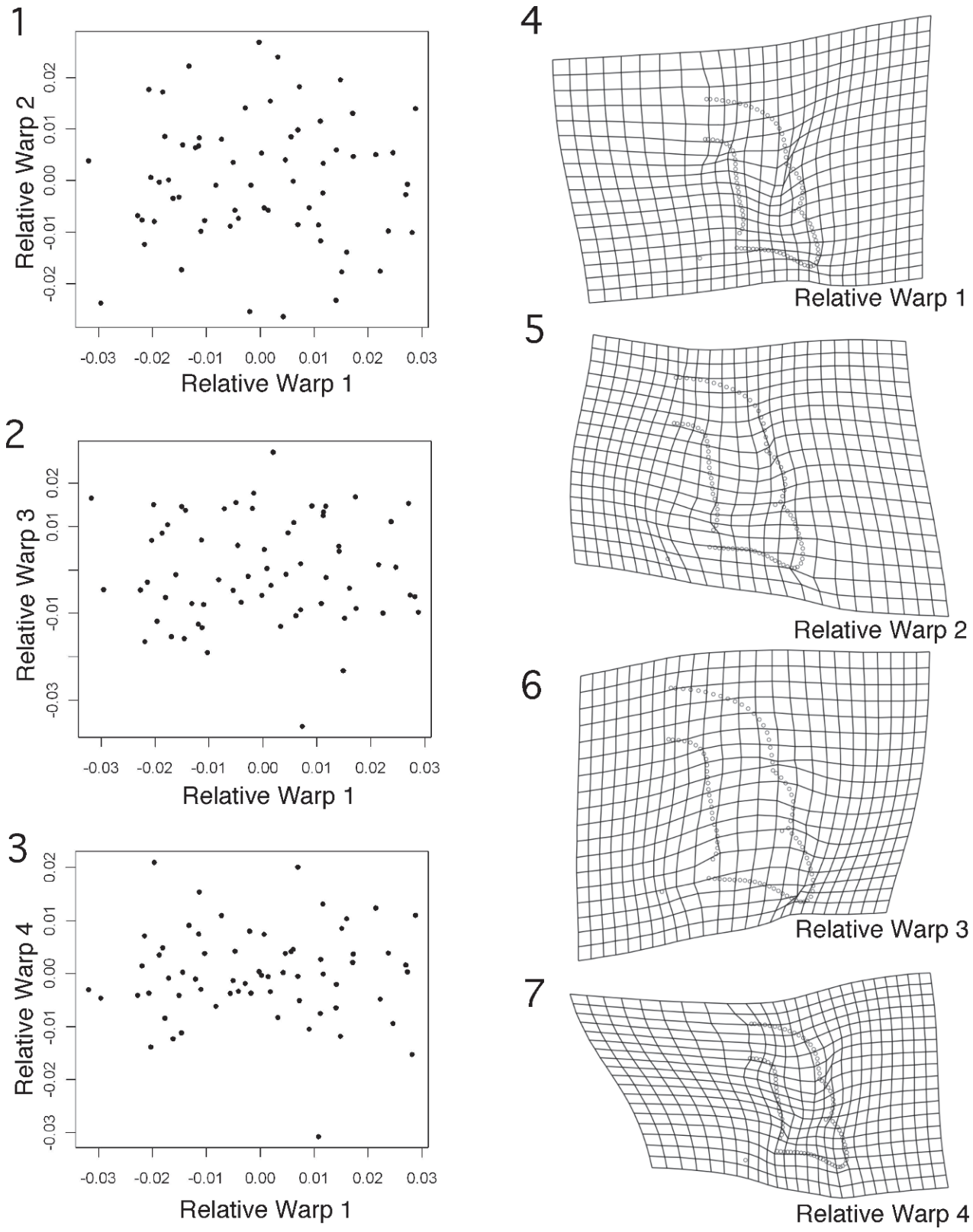

FIGURE *14*—Structure of cranidial shape variation in *Eokochaspis nodosa* from ICS-1192, as revealed by a principal components analysis of warp scores (relative warp analysis, RWA). Landmark configurations shown in Figs. 10, 11.5. Reference form is mean of all 65 configurations in the sample. *1,* RW1 versus RW2; *2,* RW1 versus RW3; *3,* RW1 versus RW4; *4,* thin-plate spline deformation grid depicting shape variation along RW1 in a positive direction (27% variance explained); *5,* thin-plate spline deformation grid depicting shape variation along RW2 in a positive direction (17% variance explained); *6,* thin-plate spline deformation grid depicting shape variation along RW3 in a positive direction (16% variance explained); *7,* thin-plate spline deformation grid depicting shape variation along RW4 in a positive direction (8% variance explained). See text for details.

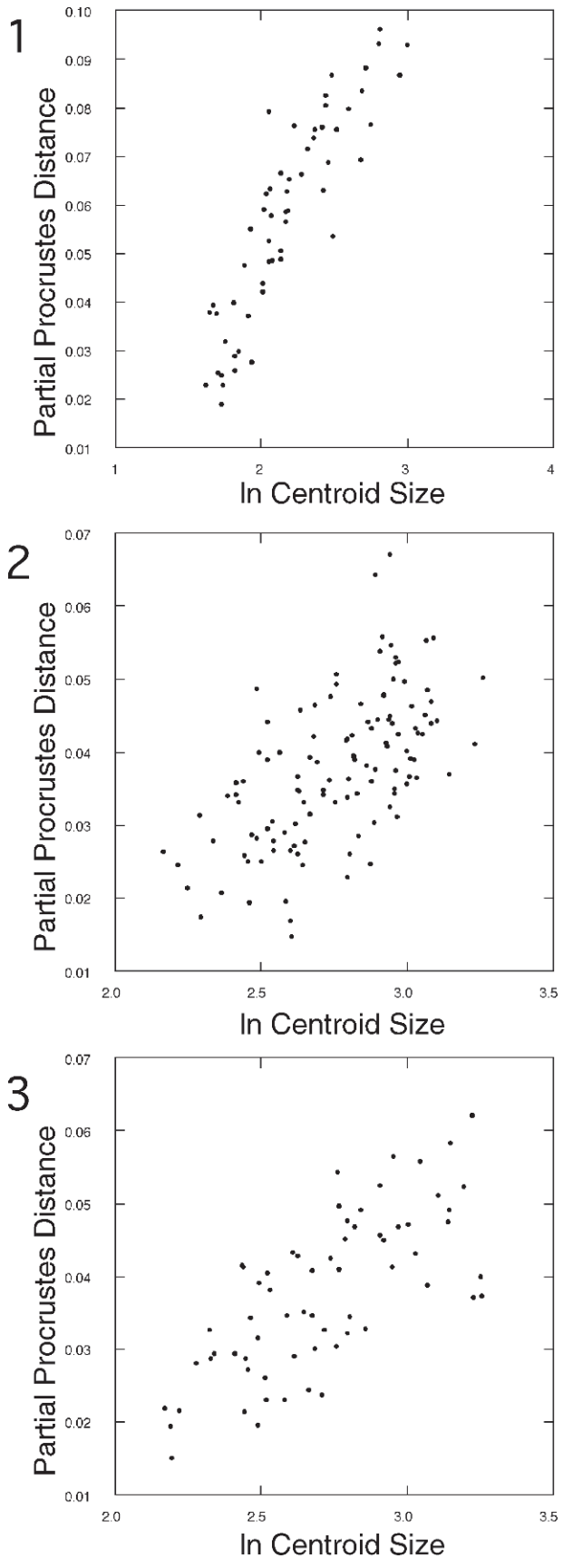

FIGURE 15—Amount of cranidial shape change over the sampled portion of ontogeny in *Crassifimbra walcotti: 1,* from ICS-1029 (N=57); *C.*? *metalaspis: 2,* from ICS-10124 (N=116); *Eokochaspis nodosa: 3,* from ICS-1192 (N=65). Shape change is quantified as partial Procrustes distance of each specimen in the sample away from a reference form representing the least mature morphology in that sample. Reference form for *C. walcotti*, *C.*? *metalaspis*, and *E. nodosa* is the consensus of the smallest nine, six, and five specimens in those samples, respectively. Landmark configurations are shown in Figs. 10, 11. Regression for each species is significant (*C. walcotti*, adjusted r^2=0.795, P=<0.001; *C.*? *metalaspis*, adjusted r^2=0.360, P=<0.001; *E. nodosa*, adjusted r^2=0.510, P=<0.001).

ontogenetic shape change (compare Figs. 14.4–14.6, 19.3–19.5, and 16.3). The relatively trivial changes in proportion of total variance explained by these axes of variation resulting from size-standardization is understandable given the relatively small contribution of allometry to total shape variation in this sample (above; Table 1).

Difference in mean cranidial shape.—For the purpose of species discrimination, it is important to determine whether the species differ in mean cranidial shape. Difference in mean shape between two species can be quantified as the partial Procrustes distance (above) between the consensus configurations of those species. The significance of the observed difference between species means must be determined in light of the shape variation within those species. Parametric tests of difference in mean shape between species are inappropriate because of the incorporation of semilandmarks in the configuration (this affects estimate of degrees of freedom, above). However, statistical tests based on bootstrap resampling, which do not require estimates of degrees of freedom, are appropriate. For each pairwise species comparison, two such nonparametric tests (below) were performed using the TwoGroup6h software (Sheets, 2005). Each test was performed on both size-standardized (to small and large cranidial sizes, above) and non-size-standardized data. Size-standardized data permit comparison of mean cranidial shape between species at a common ontogenetic size (above), and is arguably more biologically meaningful in terms of species discrimination. Tests based on data that have not been size-standardized are arguably more conservative when testing a null hypothesis of no difference in mean shape, because within-species variation is relatively higher (resulting from both static and dynamic variation, above) and the magnitude of any between-species difference in mean shape must be correspondingly greater to be deemed significant.

The first nonparametric test demonstrates that the partial Procrustes distance between the mean cranidial shape of each species significantly differs from zero in all pairwise comparisons both with and without size-standardization (Table 5; confidence limits determined by 1,600 bootstraps).

The second nonparametric test investigates between-sample differences in mean shape using a bootstrap-based approach utilizing Goodall's F-test (Goodall, 1991; Dryden and Mardia, 1998) of Procrustes distance between sample means as the test statistic (summarized in Webster and Sheets, 2010). The observed F-value is compared to the range of F-values obtained by randomly assigning specimens to samples (1,600 replicates). This test also finds significant differences in mean shape between all samples, both with and without size-standardization (Table 5).

For size-standardized data in both nonparametric tests, significant interspecific differences were found when samples shape was estimated at both small (sagittal cranidial length approximately 1.75 mm) and large (sagittal cranidial length approximately 4.2 mm) sizes (Table 5). In all pairwise species

comparisons, the difference between estimated species means at small size was smaller than that at large size (Table 5).

Interspecific differences in mean cranidial shape based on size-standardized data are visualized as thin-plate spline deformation grids (Fig. 20). At a sagittal length of approximately 4.2 mm, the mean cranidial shape of *C. walcotti* differs most obviously from that of *C.*? *metalaspis* and *E. nodosa* in the shape of the posterior portion of the cranidium, and in particular the posterior portion of the glabella (Fig. 20.2, 4). The posterior margin of the occipital ring between the sagittal axis and the intersection with the posterior cranidial margin is markedly wider (tr.), and the posterior cranidial margin distal to the fulcrum is oriented more strongly posteriorly, in *C.*? *metalaspis* and *E. nodosa* relative to *C. walcotti*. More subtle differences are also present: the frontal area, interocular portion of the fixigena, and posterior wing of the fixigena are wider (tr.) and the anterior cranidial margin less strongly arcuate in *C.*? *metalaspis* and *E. nodosa* than in *C. walcotti*; and the distal margin of the palpebral lobe is slightly more strongly arcuate in *C.*? *metalaspis* and *E. nodosa* than in *C. walcotti*. The frontal area is slightly shorter (sag.) and the posterior wing of the fixigena is more extensiform in *E. nodosa* than *C. walcotti* (Fig. 20.6).

Relative to comparisons involving *C. walcotti*, differences in mean cranidial shape of *C.*? *metalaspis* and *E. nodosa* at a sagittal length of approximately 4.2 mm are more subtle (Fig. 20.6), largely because of the closer similarity in width of the posterior margin of the occipital ring between the sagittal axis and the intersection to the posterior cranidial margin in these samples. However, the posterior cranidial margin is more strongly posteriorly oriented distal to the fulcrum, the posterior wing of the fixigena is more extensiform, the distal margin of the palpebral lobe is more strongly arcuate, and the glabella slightly more strongly anteriorly tapered in *E. nodosa* relative to *C.*? *metalaspis*.

The interspecific differences at cranidial length of 4.2 mm described above are also present at cranidial length of 1.75 mm (Fig. 20.1, 3, 5). However, the magnitude of the differences is much lower at this smaller size. This is consistent with the smaller Procrustes distance between species means at this size (above; Table 5).

Cranidial disparity.—Shape disparity of morphologically mature cranidia was explored through a RWA of configurations from all three species, based on shape data size-standardized to both large and small cranidial sizes (above) and using the consensus of all 476 configurations as the reference form (Fig. 21). Some 70% of the total shape variation among the 476 size-standardized configurations of the cranidia is summarized by the first three RWs (Fig. 21). RW1 explains 40% of the total shape variance. Specimens with more positive scores have a decreased anterior tapering of the glabella, shortening (sag.) of the frontal area, and rotation of the posterior cranidial margin distal to the fulcrum into a stronger posterolateral orientation (Fig. 21.3). This pattern of variance is similar to the general ontogenetic trends common to all species, although with reversed polarity (compare to Fig. 16). This interpretation is supported by the fact that, for each species, configurations size-standardized to small size (squares in Fig. 21.1, 21.2) have more positive scores than configurations size-standardized to large size (circles in Fig. 21.1, 21.2). The magnitude of ontogenetic offset along this axis is greatest in *C. walcotti*. RW2 explains 17% of the total shape variance. Specimens with more positive scores have a more elongate (sag., exsag.) cranidium, particularly in the interocular area of the fixigena and the posterior wing of the fixigena, and have slightly less strongly posteriorly oriented posterior cranidial margin distal to the fulcrum (Fig. 21.4). For each species, configurations size-standardized to small size (squares in Fig. 21.1) have more positive scores than configurations size-standardized to large size (circles in Fig. 21.1). The magnitude of ontogenetic offset along this axis is greatest in *C.*? *metalaspis* and smallest in *C. walcotti*. RW3 explains 13% of the total shape variance. Specimens with more positive scores have a more strongly posteriorly oriented posterior cranidial margin distal to the fulcrum, a more extensiform posterior wing of the fixigena, a more strongly arcuate distal margin of the palpebral lobe, and a slightly more strongly anteriorly tapered glabella (Fig. 21.5). Both *C. walcotti* and *E. nodosa* show considerable ontogenetic offset along this axis (towards more positive scores at larger cranidial size). At each cranidial size, scores on this axis for *E. nodosa* are markedly higher than for the other species. Higher RWs each explain $<7\%$ of total variance and relate to trivial components of shape variation. Similar results are obtained for a RWA of landmark configurations for all 238 specimens without size-standardization (not shown).

The morphospace depicted in Fig. 21.1 and Fig. 21.2 confirms that interspecific differences are of greater magnitude at larger cranidial size (see above). The three species cluster more tightly along RW1 and RW2 at small cranidial size (square symbols in Fig. 21.1) but are more distinctly separated at large cranidial size (circle symbols in Fig. 21.1). Similarly, *C. walcotti* and *C.*? *metalaspis* exhibit similar scores on RW1 and RW3 at small cranidial size but are clearly distinct at large cranidial size (Fig. 21.2).

Summary and implications of the analyses of cranidial shape.—With regard to the structure of cranidial shape variation (above), the following generalities hold true for the three species studied herein: 1) The structure of cranidial shape variation is generally similar among the species; 2) All species exhibit significant allometric growth over the sampled portion of their respective cranidial ontogenies. Cranidial growth did not become isometric at large size; 3) The species share several general similarities in their respective patterns of ontogenetic shape change. These include an increased anterior tapering of the glabella, an elongation and lateral expansion of the frontal area, and rotation of the posterior cranidial margin into a less strong posterolateral orientation; 4) For conspecific cranidia of a given size, the major pattern of covariance among anatomical parts is essentially identical to the pattern of covariance among those parts during ontogeny of that species. The primary structure of static morphological variation is also the structure of ontogenetic variation.

The second and third findings are likely general to many early ptychoparioids. Rasetti (1955, p. 7) identified a general ontogenetic trend towards a proportionally shorter glabella (i.e., longer frontal area) relative to cranidial length, and an increased anterior tapering of the glabella among large (presumed holaspid) cranidia of early ptychoparioids such as *Periomma gaspensis* Rasetti, 1955 and *Periommella yorkensis* Resser, 1938.

The fourth finding listed above potentially offers considerable insight into the nature of intraspecific variation and warrants further discussion. Great caution must be employed when relating a particular mathematically derived axis of variation to a particular biological phenomenon. As mentioned above, actual shape variation within a given anatomical region is described by the net effect of all RWs. The deformation of an anatomical region described by one RW may be modified or offset by that described by another RW.

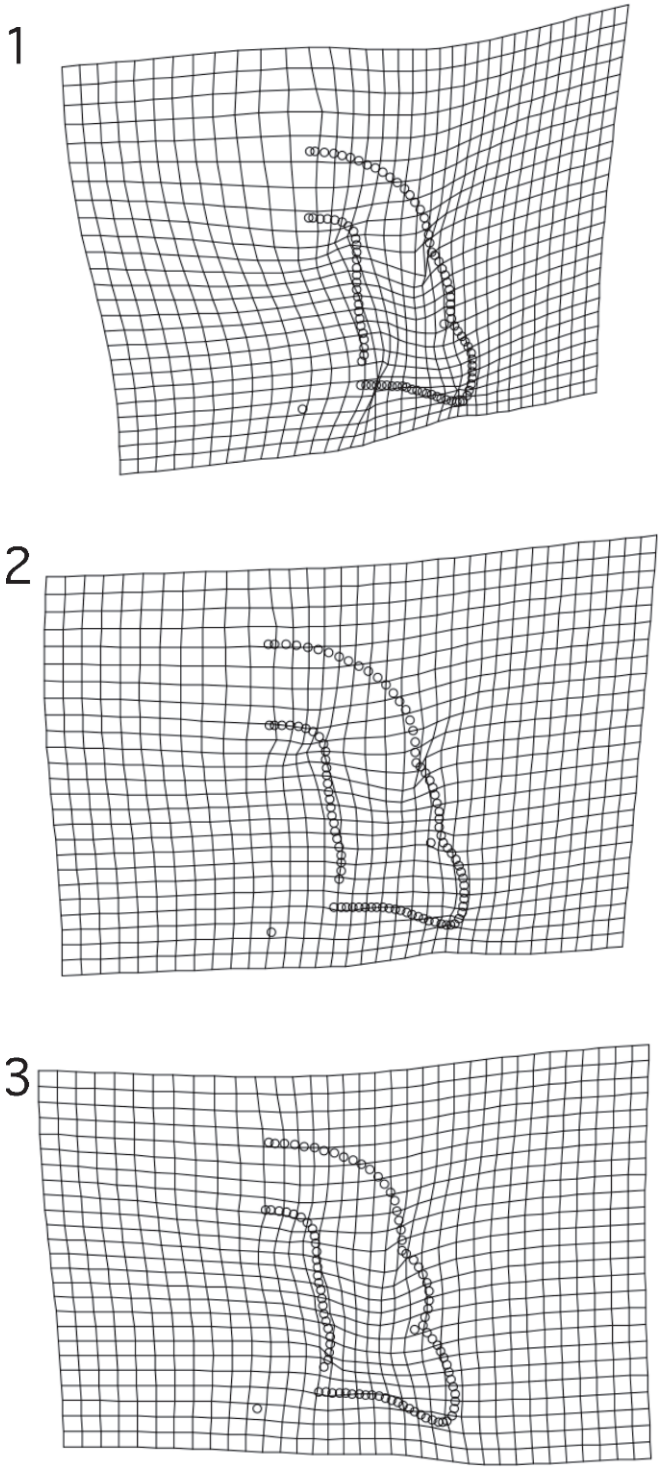

FIGURE *16*—Thin-plate spline deformation grids depicting shape changes during the sampled portion of ontogeny of *1, Crassifimbra walcotti; 2, C.? metalaspis; 3, Eokochaspis nodosa*. Landmark configurations shown in Figs. 10, 11. Shape changes calculated by a regression of shape variables against lnCS for each sample. Reference form in each plot is consensus of all configurations in that sample. See text for details. Deformation has been exaggerated 1.5 times for clarity.

TABLE *3*—Angle between vectors of ontogenetic shape change for *Crassifimbra walcotti* (from ICS-1029), *Crassifimbra*? *metalaspis* (from ICS-10124), and *Eokochaspis nodosa* (from ICS-1192). Interspecific difference between ontogenetic vectors is significant at >95% for all species comparisons (based on 1,600 bootstraps). See text for details and interpretation.

Species comparison	N	Between species	Within species 1	Within species 2
C. walcotti to *C.*? *metalaspis*	57, 116	44.0°	13.6°	36.1°
C. walcotti to *E. nodosa*	57, 65	50.5°	13.6°	35.3°
C.? *metalaspis* to *E. nodosa*	116, 65	52.1°	33.3°	33.0°

Nevertheless, the remarkable similarity between RW1 of the size-standardized data and the pattern of ontogenetic shape change for each species is consistent with a hypothesis that the two share a common underlying cause: namely, the developmentally determined pattern of covariance among cranidial regions. Under this hypothesis, approximately 25–35% of the shape difference between cranidia of the same size can be explained by among-individual decoupling between size and the trajectory of shape change for that species. Intraspecific heterochrony would therefore be an important source of static cranidial shape variation within these early ptychoparioids. (Heterochrony is usually used in the evolutionary sense as a parallelism between ontogenetic shape change and phylogenetic shape change [see Webster and Zelditch, 2005]. Here it refers to a parallelism between ontogenetic shape change and intraspecific shape difference.)

Even if RW1 is interpreted as resulting from intraspecific heterochrony, the total structure of intraspecific cranidial shape variation cannot. In each species, the combined effect of RW2 and higher, accounting for 65–75% of shape variation among conspecific cranidia of the same size, adds to and locally modifies the variation described by RW1. The underlying controls dictating the structure of intraspecific cranidial shape variation in these trilobites are therefore manifold.

With regard to interspecific differences and cranidial disparity (above), the following conclusions can be drawn: 1) The species exhibit subtle but significant differences in mean cranidial shape even at small size (sagittal cranidial length 1.75 mm); 2) The species differ in the relative magnitude of the shared trends in ontogenetic shape change, and subtle species-specific trends are superimposed upon the common trends. Each species therefore follows a unique trajectory of ontogenetic shape change; 3) As a result, cranidial disparity and the magnitude of interspecific differences in mean cranidial shape become larger at larger size (sagittal cranidial length 4.2 mm).

Phylogenetic analyses indicate that the species studied herein share relatively recent common ancestry (Sundberg, 2004; unpublished data; see also discussion in systematic section below). None are considered to share direct ancestor-descendant relationship with each other. Interspecific differences are therefore not interpreted as direct evolutionary modifications from one species into the other. Rather, observed differences are the product of divergence from an unsampled common ancestor. However, the nature of interspecific differences can be used to test hypotheses regarding particular modes of evolution.

Some of the interspecific differences in size-standardized cranidial shape (Fig. 20) parallel ontogenetic trends within the species (e.g., the differences in anterior tapering of the glabella and orientation of the posterior cranidial margin distal to the fulcrum). These differences might be interpreted as having arisen through heterochrony. However, the lack of parallelism between vectors of ontogenetic shape change

TABLE 4—Amount of cranidial shape variation in *Crassifimbra walcotti* (from ICS-1029), *Crassifimbra*? *metalaspis* (from ICS-10124), and *Eokochaspis nodosa* (from ICS-1192). Variation within each species quantified as variance in partial Procrustes distance away from mean form of that species. Variation in size-standardized data is based on configurations size-standardized to a size equivalent to approximately 4.2 mm sagittal cranidial length. Lower and upper 95% confidence limits based on 1,600 bootstraps. See text for details and interpretation.

		Without size-standardization			With size-standardization		
Species	N	Variation	Lower 95% limit	Upper 95% limit	Variation	Lower 95% limit	Upper 95% limit
C. walcotti	57	0.00140	0.00109	0.00168	0.00072	0.00060	0.00083
C.? *metalaspis*	116	0.00087	0.00077	0.00095	0.00077	0.00069	0.00085
E. nodosa	65	0.00091	0.00079	0.00098	0.00078	0.00069	0.00085

demonstrates that interspecific differences in cranidial shape resulted from complex local modifications to growth pattern (''allometric repatterning'') and cannot be attributed to simple ontogenetic scaling (''global heterochrony''; see Webster and Zelditch [2005] for discussion of these concepts). It is conceivable that local heterochrony may explain interspecific differences in particular anatomical features, and that such local heterochronies were dissociated across features. However, hypotheses of evolution being restricted to rate and/or timing modifications become less tenable as the number of inferred local heterochronies approaches the number of anatomical features being studied: hypotheses involving allometric repatterning then become increasingly viable (Webster and Zelditch, 2005). The more extensiform shape of the posterior wing of the fixigena in *E. nodosa* is not easily explicable in terms of extrapolation of a shared ontogenetic trajectory, but rather seems to be a novel autapomorphy of that species.

The fact that allometric growth is the strongest single source of cranidial shape variation within each species is inconvenient

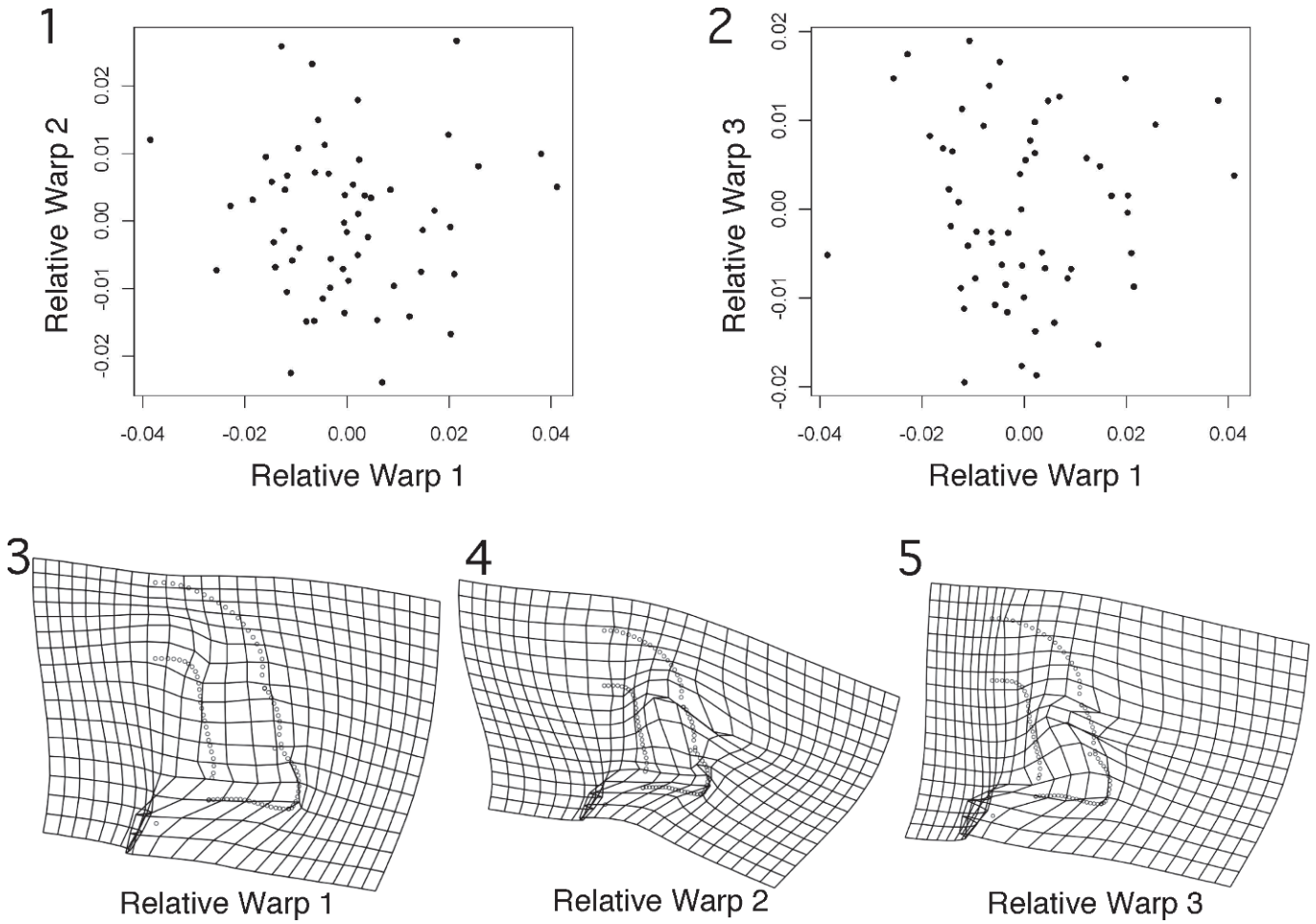

FIGURE 17—Structure of cranidial shape variation in *Crassifimbra walcotti* from ICS-1029, as revealed by a principal components analysis of warp scores (relative warp analysis, RWA) of size-standardized data (sagittal cranidial length approximately 4.2 mm). Landmark configurations are shown in Figs. 10, 11.2. Reference form is mean of all 57 configurations in the sample. *1,* RW1 versus RW2; *2,* RW1 versus RW3; *3,* thin-plate spline deformation grid depicting shape variation along RW1 in a positive direction (31% variance explained); *4,* thin-plate spline deformation grid depicting shape variation along RW2 in a positive direction (17% variance explained); *5,* thin-plate spline deformation grid depicting shape variation along RW3 in a positive direction (14% variance explained). See text for details.

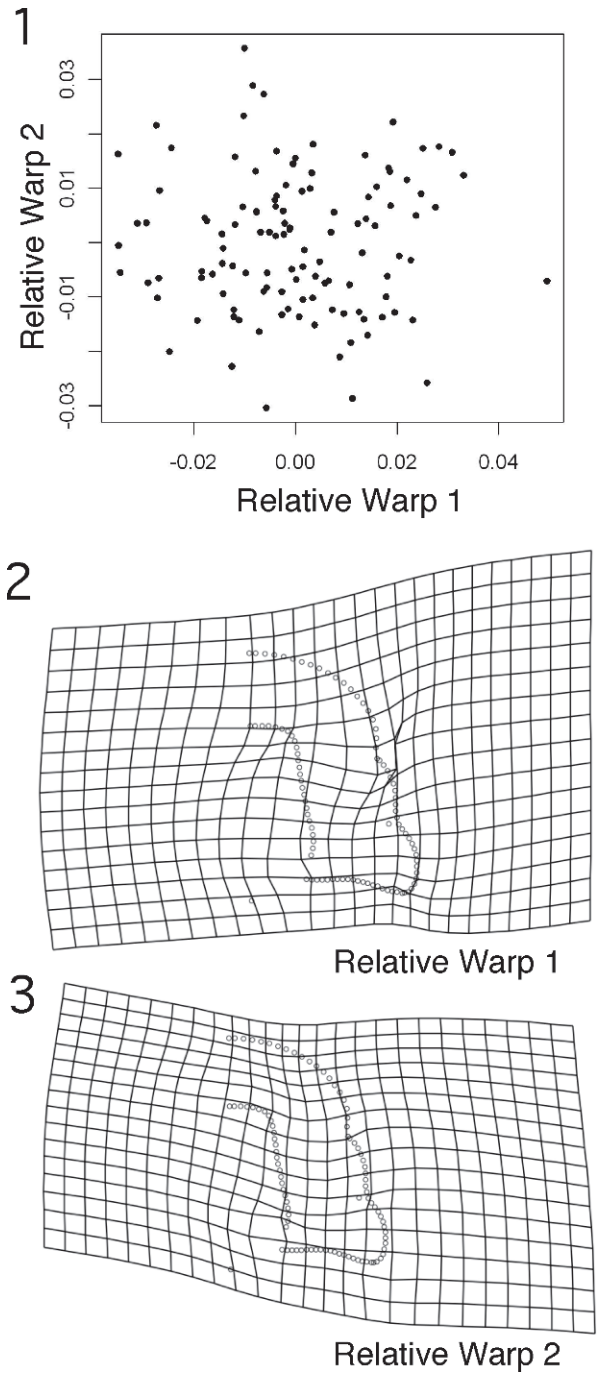

FIGURE *18*—Structure of cranidial shape variation in *Crassifimbra*? *metalaspis* from ICS-10124, as revealed by a principal components analysis of warp scores (relative warp analysis, RWA) of size-standardized data (sagittal cranidial length approximately 4.2 mm). Landmark configurations are shown in Figs. 10, 11.4. Reference form is mean of all 116 configurations in the sample. *1,* RW1 versus RW2; *2,* thin-plate spline deformation grid depicting shape variation along RW1 in a positive direction (35% variance explained); *3,* thin-plate spline deformation grid depicting shape variation along RW2 in a positive direction (21% variance explained). See text for details.

for systematists. It confirms that morphological differences between cranidia of different size can represent either ontogeny or phylogeny. Careful study of a wide size range of cranidia is recommended before such differences are interpreted as interspecific disparity or intraspecific variation. Establishment of new species of early ptychoparioid species based on a limited number of specimens is not encouraged.

However, the fact that interspecific differences between the three species studied herein are established at cranidial length smaller than 1.75 mm is good news for early ptychoparioid systematists. It suggests that, with careful study, ptychoparioid species can be distinguished even at very small cranidial size. The fact that the species studied herein exhibit divergent ontogenetic trajectories of shape change confirms that diagnosis of early ptychoparioid species is easier when comparing large cranidia.

SYSTEMATIC PALEONTOLOGY

Family "PTYCHOPARIIDAE" Matthew, 1887

Discussion.—Resolving systematic relationships among the vast number of taxa assigned to this problematic (and probably paraphyletic; Fortey in Whittington et al., 1997; Fortey, 2001) family is beyond the scope of the present paper. Several supposed clades have been identified within the "Ptychopariidae," including the kochaspids (Palmer and Halley, 1979; Sundberg, 2004) and the antagmines (sometimes recognized as the distinct family Antagmidae Hupé, 1953; e.g., Geyer and Malinky, 1997; Jell in Jell and Adrain, 2003). Cladistic analysis supports monophyly of a kochaspid clade (Sundberg, 2004), although several plesiomorphic genera are polyphyletic and the clade diagnosis was left ambiguous (Sundberg, 2004, p. 923). The monophyly of antagmines has yet to be demonstrated (see comments by Cotton, 2001, p. 167).

Crassifimbra is a very poorly diagnosed genus typically considered to be an antagmine (e.g., Jell in Jell and Adrain, 2003). *Eokochaspis* was initially considered to be a basal kochaspid genus (Sundberg and McCollum, 2000), but has since been demonstrated to be polyphyletic (discussed below). Pending full revision of early ptychoparioids and clear demonstration of antagmine and kochaspid monophyly, *Crassifimbra* and *Eokochaspis* are here assigned to a broadly inclusive "Ptychopariidae."

Genus CRASSIFIMBRA Lochman, 1947

Discussion.—Five named species plus three in open nomenclature have been assigned to this genus. Prior to the present work, all were known only from cranidia except for a single librigena of *C. walcotti* (the type species) figured and cursorily described by Sundberg and McCollum (2003). The genus is very poorly diagnosed, and hypotheses regarding its monophyly and distinction from other (equally poorly diagnosed) "antagmine" genera such as *Onchocephalus* Resser, 1937 and *Antagmus* Resser, 1936 have yet to be tested. The present paper does not attempt such a cladistic reappraisal. However, non-cranidial sclerites of *C. walcotti* are fully described herein for the first time: this new information will be valuable to future systematic studies.

Sundberg and McCollum (2000, p. 611) distinguished *Crassifimbra* from *Eokochaspis* based on the "higher relief of cranidial features, better defined cranidial furrows, and subtrapezoidal outline of the cranidium of *Eokochaspis*." The present study reveals that there is considerable intraspecific variation in these features (above). However, the type species of these genera also exhibit marked differences in librigenal, thoracic, and pygidial morphology (below). Based on non-cranidial sclerite morphology, "*Eokochaspis*" *metalaspis* Sundberg and McCollum, 2000 is herein provisionally reassigned to *Crassifimbra*.

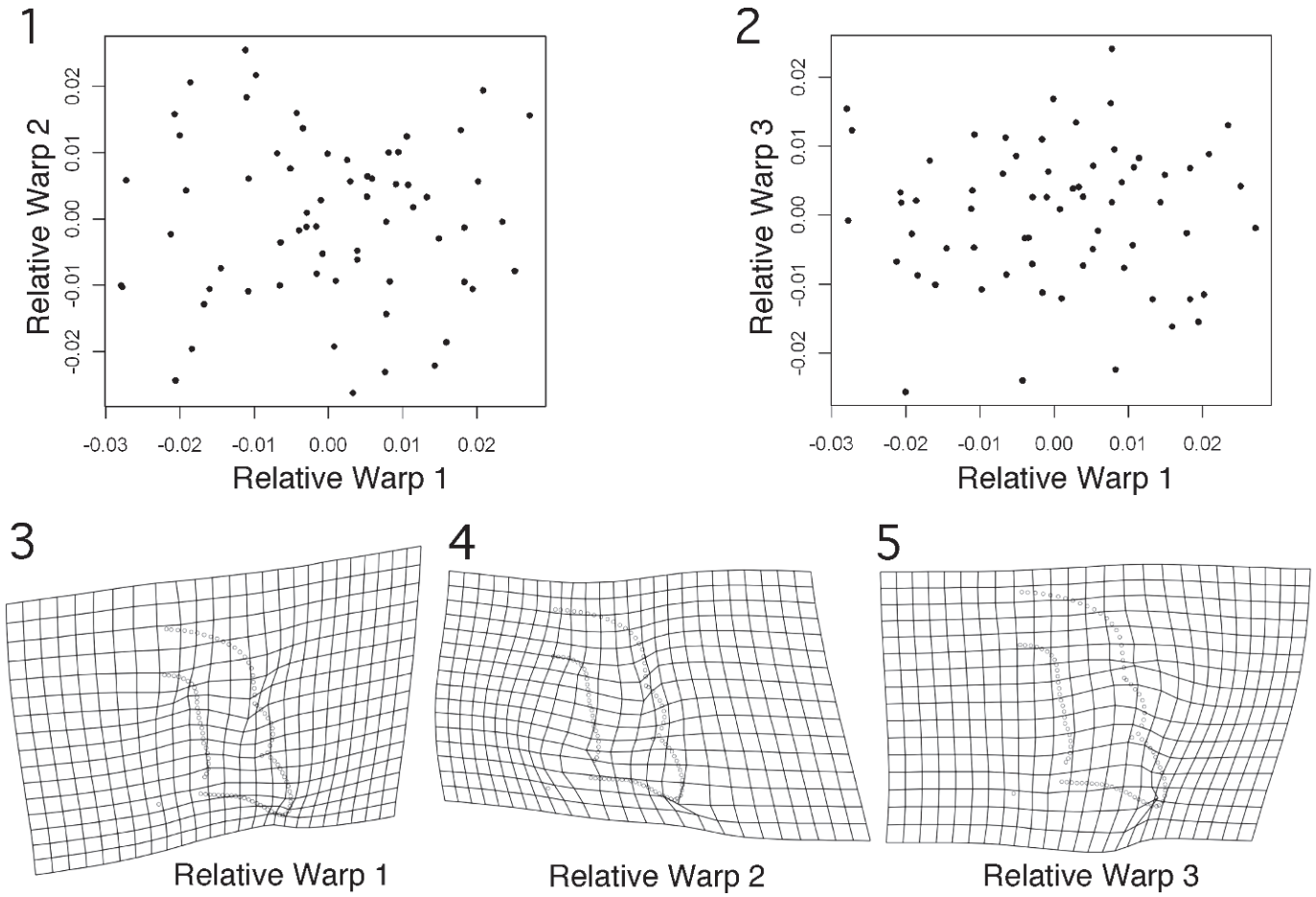

FIGURE *19*—Structure of cranidial shape variation in *Eokochaspis nodosa* from ICS-1192, as revealed by a principal components analysis of warp scores (relative warp analysis, RWA) of size-standardized data (sagittal cranidial length approximately 4.2 mm). Landmark configurations are shown in Figs. 10, 11.6. Reference form is mean of all 65 configurations in the sample. *1,* RW1 versus RW2; *2,* RW1 versus RW3; *3,* thin-plate spline deformation grid depicting shape variation along RW1 in a positive direction (25% variance explained); *4,* thin-plate spline deformation grid depicting shape variation along RW2 in a positive direction (19% variance explained); *5,* thin-plate spline deformation grid depicting shape variation along RW3 in a positive direction (13% variance explained). See text for details.

CRASSIFIMBRA WALCOTTI (Resser, 1937)
Figures 2, 3, 4, 22, 23

Onchocephalus walcotti RESSER, 1937, p. 21.

Crepicephalus augusta WALCOTT, 1886 (part), p. 208–209. pl. 28, fig. 2b only; WALCOTT, 1890 (part), p. 653, pl. 96, fig. 9 only; WALCOTT, 1916 (part), pl. 29, fig. 6 only.

Crassifimbra walcotti LOCHMAN, 1947, p. 64, 71, text-figs. 1–3; PALMER, 1958 (part), p. 157, pl. 25, figs. 1–3 only [not pl. 25, figs. 4, 7–25, pl. 26, figs. 1–24, text-figs. 3–7; = *C.*? *metalaspis*]; ?PALMER, 1998a, fig. 4 [occurrences in range chart]; not SMITH, 1998, p. 103–106 [morphometric data only; = *C.*? *metalaspis*]; SUNDBERG AND MCCOLLUM, 2000, p. 619, figs. 11.1–11.8; SUNDBERG AND MCCOLLUM, 2003,

TABLE *5*—Pairwise nonparametric statistical comparisons of mean cranidial shape between *Crassifimbra walcotti* (from ICS-1029; N = 57), *Crassifimbra*? *metalaspis* (from ICS-10124; N = 116), and *Eokochaspis nodosa* (from ICS-1192; N = 65). Size-standardization (Size-standn.) column specifies whether and how configurations were size-standardized: small = size-standardized to sagittal cranidial length of approximately 1.75 mm; large = size-standardized to sagittal cranidial length of approximately 4.2 mm. Lower and upper 95% confidence limits and significance value of Goodall's F-test based on 1,600 bootstraps. See text for details and interpretation.

		Partial procrustes distance			Goodall's F-test	
Species comparison	Size-standn.	Between species means	Lower 95% limit	Upper 95% limit	F	*P*
C. walcotti to *E. nodosa*	none	0.0457	0.0433	0.0491	55.81	0.0006
	small	0.0404	0.0381	0.0435	65.56	0.0006
	large	0.0784	0.0751	0.0819	247.42	0.0006
C. walcotti to *C.*? *metalaspis*	none	0.0362	0.0335	0.0404	47.9	0.0006
	small	0.0303	0.0294	0.0321	46.64	0.0006
	large	0.0530	0.0496	0.0565	142.48	0.0006
C.? *metalaspis* to *E. nodosa*	none	0.0459	0.0436	0.0486	99.31	0.0006
	small	0.0408	0.0392	0.0429	89.57	0.0006
	large	0.0510	0.0488	0.0535	139.91	0.0006

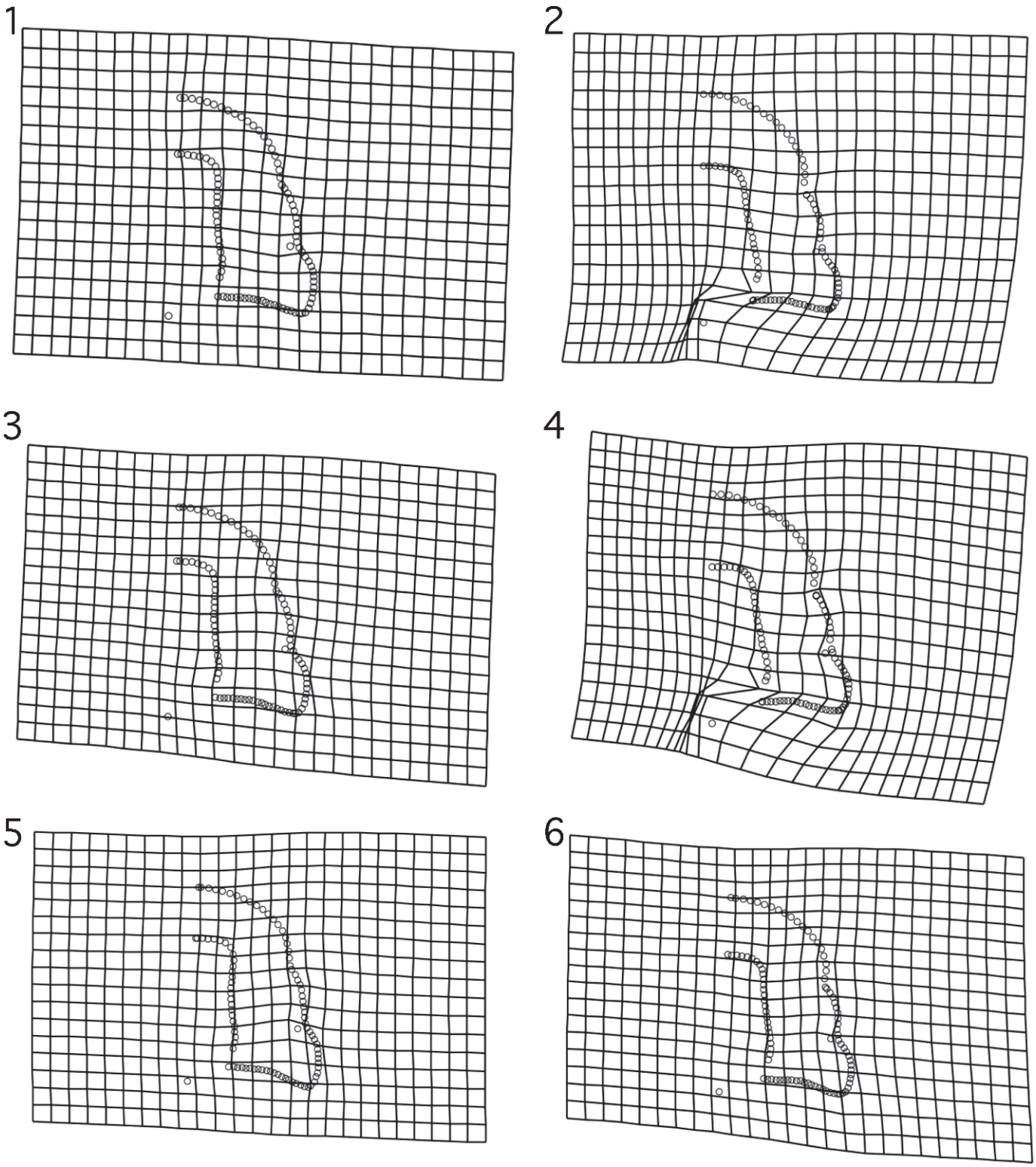

FIGURE *20*—Thin-plate spline deformation grids depicting interspecific difference in mean cranidial shape based on data that have been size-standardized to represent estimated cranidial shape at a sagittal length of approximately 1.75 mm (*1, 3, 5*) and approximately 4.2 mm (*2, 4, 6*). *1, 2,* deformation of mean size-standardized cranidial shape of *C. walcotti* into that of *C.*? *metalaspis*; *3, 4,* deformation of mean size-standardized cranidial shape of *C. walcotti* into that of *E. nodosa*; *5, 6,* deformation of mean size-standardized cranidial shape of *C.*? *metalaspis* into that of *E. nodosa*. See text for details.

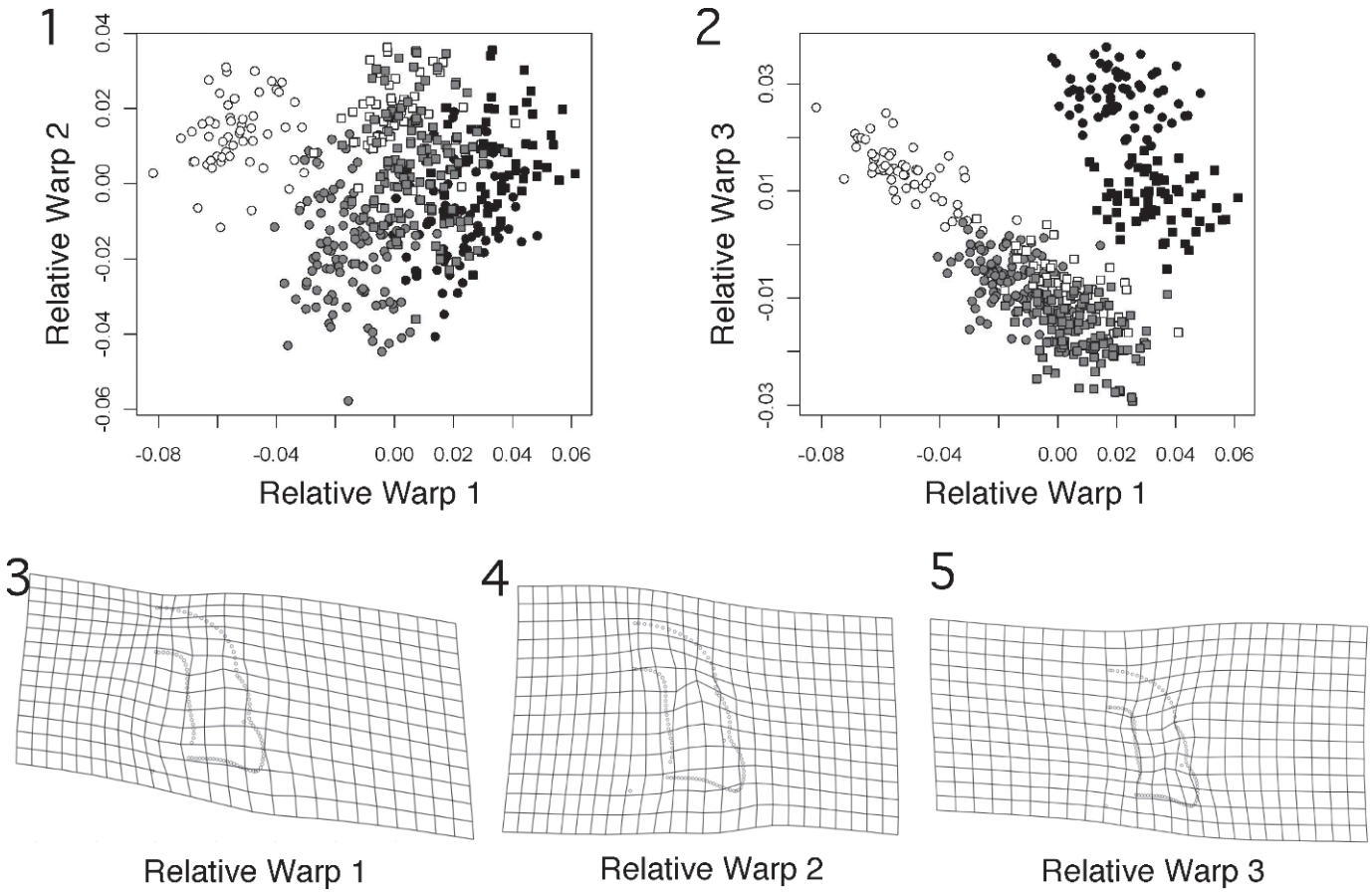

FIGURE *21*—Structure of cranidial shape disparity in Crassifimbra walcotti from ICS-1029 (white symbols), *C.*? *metalaspis* from ICS-10124 (gray symbols), and *Eokochaspis nodosa* from ICS-1192 (black symbols), as revealed by a PCA of warp scores (relative warp analysis). The configuration of each specimen is size-standardized to produce an estimate of the shape of that specimen at sagittal cranidial length of 1.75 mm (square symbols) and at 4.2 mm (circle symbols); each specimen therefore appears twice in the morphospace. Landmark configurations are shown in Figs. 10, 11. Reference form is mean of all 476 configurations. *1,* RW1 versus RW2; *2,* RW1 versus RW3; *3,* thin-plate spline deformation grid depicting shape variation along RW1 in a positive direction (40% variance explained); *4,* thin-plate spline deformation grid depicting shape variation along RW2 in a positive direction (17% variance explained); *5,* thin-plate spline deformation grid depicting shape variation along RW3 in a positive direction (13% variance explained). Higher RWs each explain <7% of total variance and relate to trivial components of shape variation.

p. 967, pl. 1, figs. 9, 10; Jell in JELL AND ADRAIN, 2003, p. 361 [mentioned in list].

Antagmus (Antagmus) walcotti SHAW, 1962, p. 334–335.

Crassifimbra walcotti? FRITZ, 1968, p. 223, 224, pl. 37, figs. 23–26.

Description.—Cranidia >3 mm in sagittal glabellar length (Fig. 2) subtriangular in outline; sagittal length 83–94% of transverse distance between posterolateral corners of posterior limbs; distance (tr.) between anterior branches of facial suture at γ 79–89% of distance between posterolateral corners of posterior limbs. Facial suture opisthoparian; anterior branches sigmoidal abaxially, anteriorly convergent (each side oriented 10–29° inwards relative to exsagittal axis when followed anteriorly) and dipping ventrally at 32–40° between contact with palpebral lobes and anterior border furrow, parallel and approximately horizontal across posterior portion of anterior border, strongly anteriorly convergent and dipping ventrally across anterior portion of anterior border, merging smoothly with anterior cranidial margin in plan view; posterior branches sigmoidal or convex abaxially, dipping at approximately 30–35° posteroventrally away from palpebral lobe, approximately horizontal across posterior border furrow and posterior cranidial margin. Glabella elongate trapezoidal, length 69–73% of cranidial length (sag.); glabellar width at SO (tr.) 59–70% of glabellar length (sag.), tapering anteriorly, width (tr.) at contact with ocular ridge 48–54% of glabellar length (sag.); highest and prominently dorsally arched (tr.) posteriorly, less vaulted anteriorly. Occipital ring semilunate in plan view; sagittal length 23–26% of glabellar length (sag.); exsagittal length from anterolateral corner (contact between axial furrow and SO) to contact with posterior cranidial margin approximately 11–14% of glabellar length (sag.); width (tr.) between contacts with posterior cranidial margins 90–99% of width (tr.) between anterolateral corners; posterior margin convex posteriorly. SO transglabellar; broad (sag., exsag.), shallow, and transverse to convex anteriorly over sagittal axis; narrows, deepens, and becomes convex posteriorly each side of axis; shallows at contact with axial furrow. L1 subtriangular, narrowing anteriorly, lateral margins bow very slightly outwards. S1 and S2 very shallow, convex anteriorly, oriented strongly posterolaterally when traced adaxially from axial furrow (S1 more strongly so than S2); absent over axis. Lateral margins of L2 bow very slightly outwards. Contact between S2 and axial furrow located opposite point approximately three-fifths of distance along sagittal axis from SO to anterior glabellar margin. S3 absent or defined only distally by extremely shallow furrow; roughly transverse or weakly convex anteriorly either side of axis when

present. S4 absent or defined only distally by extremely shallow furrow; oriented strongly anterolaterally when traced adaxially from axial furrow. Frontal lobe bluntly rounded anteriorly. Axial furrows converge between contact with SO and contact with S2 or S3, less convergent anterior to this; deepest and broadest between lateral margins of S1 and S3, shallow around anterior margin of glabella and lateral margins of occipital ring. Anterior cranidial border crescent-shaped with distal portions strongly flexed posteriorly relative to sagittal portion in plan view and dorsally weakly flexed into subtle anterior arch (tr.); broad (sag., exsag.), accounting for approximately one-half to two-thirds of frontal area close to sagittal axis (excluding plectrum), tapering distally to anterior facial suture; convex dorsally (sag., exsag.), slopes ventrally out of anterior border furrow, slope steeper in anterior two-thirds. Medial portion of anterior border furrow widens (sag., exsag.), shallows, and deflects posteriorly at broad (tr.), low plectrum extending from anterior border across anterior half of preglabellar field; more or less confluent with axial furrow around frontal lobe sagittally in some specimens (Fig. 2.15). Palpebral lobe reniform in plan view, width (tr.) just posterior to midlength 20–25% of length (exsag.), length (exsag.) 25–29% of cranidial length (sag.), weakly defined adaxially by break in slope that strengthens posterolaterally, suture-bound margin convex abaxially; axis between anterior and posterior tips oriented outwards by 6–15° relative to sagittal axis); anterior tip located opposite point 79–86% of distance from posterior to anterior end of glabella along sagittal axis, posterior tip located opposite point 42–48% of distance from posterior to anterior end of glabella along sagittal axis; gently convex dorsally (tr.); palpebral suture more or less horizontal along summit of palpebral lobe, dipping ventrally at 52–73° anteriorly and 59–68° posteriorly to merge with anterior and posterior branches of facial suture. Poorly defined ocular ridge contacts axial furrow just anterior to S4, gently arcs posterolaterally across interocular area; more prominently defined on ventral surface. Fixigenal field anterior to ocular ridge arcs steeply ventrally into anterior border furrow. Interocular area parallelogram-shaped; width (tr.) opposite posterior tip of palpebral lobe 35–42% of sagittal glabellar length; slightly arched dorsally (tr., sag., exsag.), distal portion lower than proximal portion, dorsal summit of palpebral lobe at lower dorsal elevation than axial furrow. Posterior limb of fixigena projects laterally beyond posterior tip of palpebral lobe; width (tr.) from axial furrow to posterolateral tip 73–90% of distance between intersections of posterior cranidial margins with occipital ring. Proximal portion of posterior margin of fixigena transversely oriented and horizontal; distal portion flexing posteriorly by 8–21° relative to transverse line and dipping ventrally at 30–38° relative to horizontal plane at fulcrum. Posterior border well defined by more or less transversely oriented broad border furrow that shallows adjacent to axial furrow and at distal end of posterior limb of fixigena; slightly narrower (exsag.) than distance (exsag.) from anterolateral corner of occipital ring to intersection of posterior cranidial margin with posterior margin of occipital ring; proportionally widens (exsag.) distally. Prominent occipital node on posterior portion of occipital ring. Anterior margin of doublure below occipital ring runs almost transversely between posterolateral corners of occipital ring. Triangular doublure below posterior cranidial border extends from fulcrum to terminate slightly adaxial to facial suture, broadening (exsag.) abaxially; anterior margin oriented weakly anteriorly when traced distally, with distinct sub-triangular extension projecting anteriorly at abaxial end. Low boss-like process projects ventrally at posterior margin of axial furrow on ventral surface. Rostral suture runs slightly inside margin on ventral cranidial surface. External surface of cranidium smooth except for fine granular ornament on posterior half of occipital ring and sagittal portion of SO. Well-preserved specimens bear four pits arranged in a square around the base of the occipital node (Fig. 4.7–4.9). Internal surface bears granulations, particularly evident below anterior border furrow and sagittal portion of preglabellar field (Fig. 2.21).

Rostral plate (Fig. 22.1, 22.2) subrectangular in plan view, width (tr.) between anterolateral corners 440% of distance between anterior and posterior tips of connective sutures; transversely bowed dorsally into broad arch. Anterior and posterior margins weakly convex anteriorly; anterior margin steeply upturned dorsally; posterior margin bears broad, subcentral posterior extension mirroring sagittal posterior deflection of anterior cranidial border. Connective sutures concave adaxially; narrowest (tr.) point of rostral plate approximately one-third of distance from anterior to posterior end of connective sutures. Terrace ridges run transversely along anterior margin.

Mature hypostome (Fig. 22.7, 22.8) subrectangular in outline, maximum length approximately 140% of width across anterior margin (excluding anterior wings). Anterior margin weakly convex anteriorly; posterior margin strongly rounded posteriorly (tr.). Anterior and lateral border narrow, separated from middle body by distinct furrow. Anterior wing slender, elongate, blunt-tipped, oriented strongly dorsolaterally, distance (tr.) between tips of anterior wings 110% of maximum hypostome length (sag.); base located approximately one-fifth distance down hypostomal length on large specimens, more anteriorly located on smaller specimens (Fig. 22.3–22.6). Posterior wing short, slender, oriented dorsally; base located approximately two-thirds distance down hypostomal length. Middle body weakly inflated (tr., sag., exsag.); central portion of anterior lobe not preserved and perhaps not strongly mineralized in life on large specimens; posterior lobe crescentic, maximum width approximately 75% of maximum hypostomal width, length (sag.) approximately one-quarter that of middle body. Narrow doublure developed interior to lateral and posterior border.

Librigena (Fig. 22.9–22.18) relatively narrow (tr.). Librigenal field slightly wider (tr.) than lateral border opposite midlength of eye socle, sloping steeply from eye socle into broad, very shallow lateral border furrow. Posterior border furrow and posterior portion of lateral border furrow represented only by subtle break in slope. Posterior librigenal margin very short, approximately one-fifth to one-half width (tr.) of base of genal spine. Lateral border convex dorsally in cross-section, broadening slightly posteriorly to base of genal spine. Base of genal spines developed opposite lateral margin of occipital ring. Genal spine broad-based, evenly tapering to pointed tip; length typically 18–30% (rarely 40%; Fig. 22.14, 22.15) of distance between anteriormost and posteriormost points of facial suture; curvature of distal margin more or less continuous with that of lateral librigenal margin; genal spine slopes ventrally at approximately 15° relative to plane defined by summit of eye socle (Fig. 22.13, 22.18); faint groove-like depression at base may represent extension of border furrow onto genal spine. Doublure broadly convex ventrally, terminates below lateral border furrow; broadest at base of genal spine; projects adaxially beyond facial suture below anterior and posterior cranidial borders. Connective suture concave adaxially. Doublure of lateral border and ventral surface of

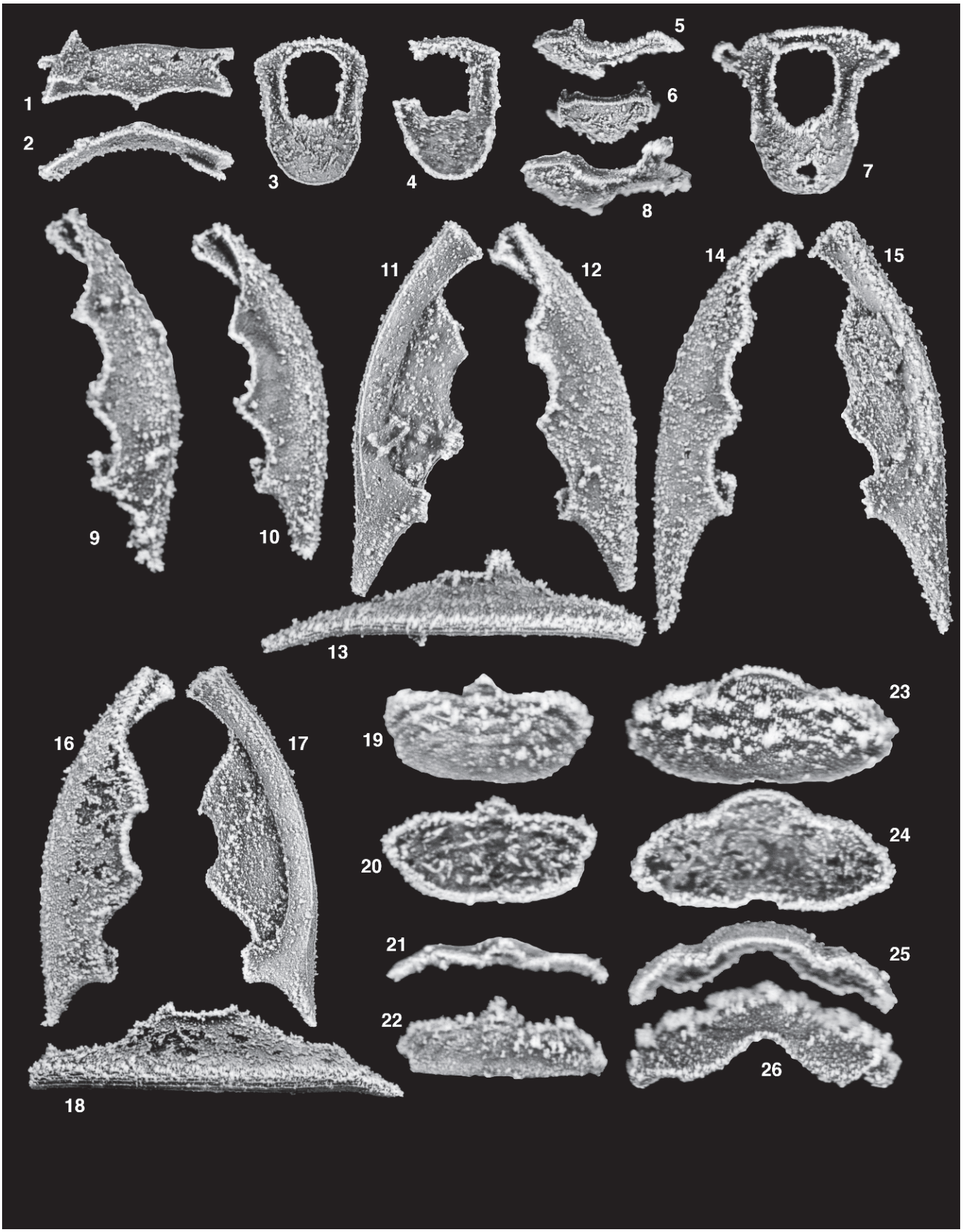

FIGURE *22*—Rostral plate, hypostomes, librigenae, and pygidia of *Crassifimbra walcotti*: *1, 2,* ventral and posterior view of rostral plate, FMNH PE58314, ×15; *3–6,* hypostome in ventral, dorsal, lateral, and posterior views, FMNH PE58315, ×20; *7, 8,* hypostome in ventral and right lateral views,

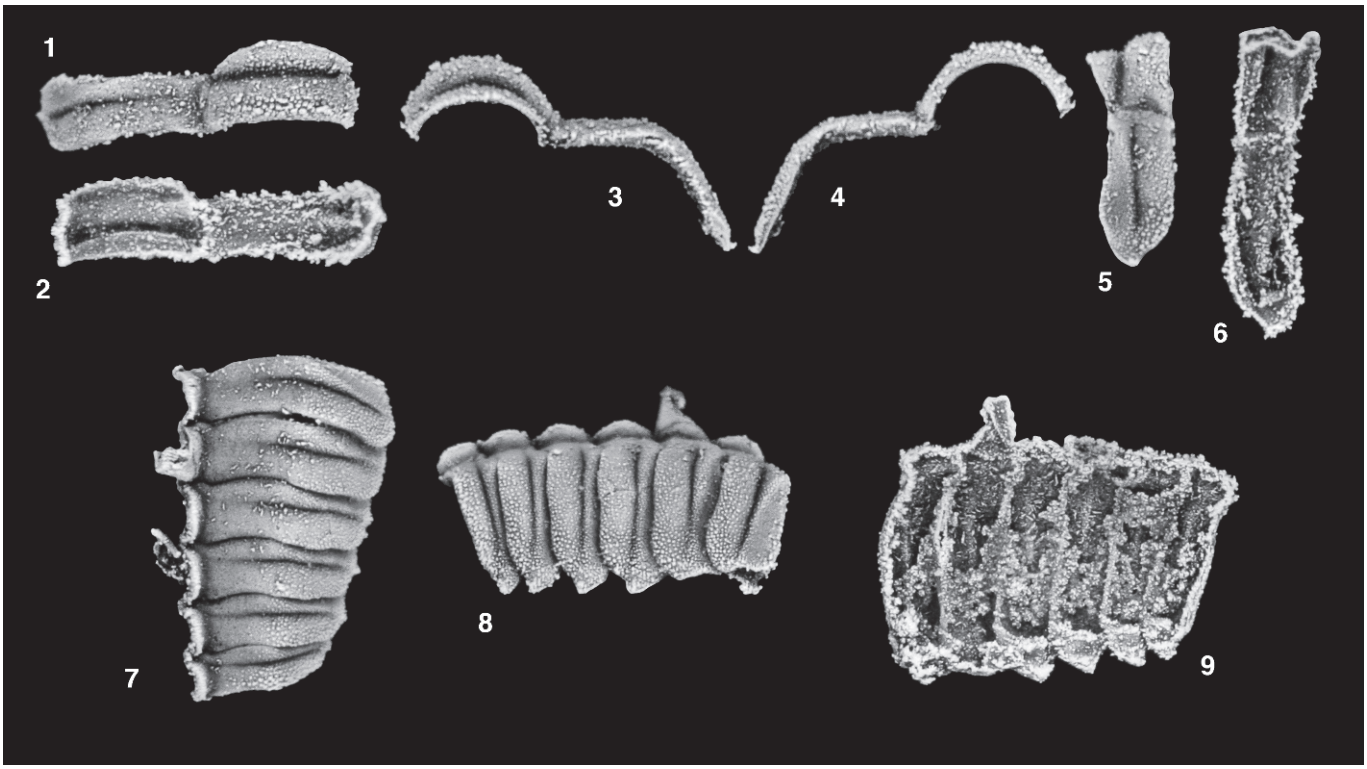

FIGURE *23*—Thorax of *Crassifimbra walcotti*: *1–6,* isolated thoracic segment (right pleura missing) in dorsal, ventral, anterior, posterior, left lateral, and oblique interior views, FMNH PE58324, ×20; *7–9,* run of six articulated right thoracic pleurae in dorsal, right lateral, and oblique interior views, FMNH PE58325, ×15. Both from ICS-1029, Combined Metals Member, Pioche Formation, Oak Spring Summit section, Delamar Mountains.

genal spine ornamented with terrace ridges; external surface otherwise smooth. Visual surface unknown.

Total number of thoracic segments at maturity unknown. Isolated segment (Fig. 23.1–23.6) with horizontal inner pleural region, dipping ventrally at approximately 60° relative to horizontal plane at fulcrum located approximately midway (tr.) across pleura. Axial ring subrectangular in plan view, width (tr.) approximately 150% width (tr.) of distance from axial furrow to fulcrum; strongly arched dorsally (tr.). Articulating half ring semilunate; maximum length (sag.) approximately two-thirds length (sag.) of axial ring; well defined by clear articulating furrow. Anterior and posterior margins of pleura sinuous (tr.); small process on anterior margin immediately adjacent to axial furrow nestles into subtle socket immediately distal to axial furrow along posterior margin of next anterior segment (Fig. 23.7, 23.8); anterior margin immediately distal to this process bears subtle indentation corresponding to subtle posterior protuberance along posterior margin of next anterior segment. Pleural furrow runs posterolaterally across pleura from close to axial furrow, terminating short of pleural tip; deepest distal to fulcrum. Articulating facet developed distal to fulcrum on anterior band (Fig. 23.5, 23.7, 23.8). Pleural tip bears small, sentate pleural spine. Semilunate doublure beneath posterior margin of axial ring. Narrow triangular doublure extends along posterior margin from fulcrum to pleural tip, broadening (exsag.) distally; panderian notch and protuberance well developed in broad doublure below pleural tip; panderian protuberance clear in posterior view (Fig. 23.4). Fine granular ornament on dorsal surface of pleural lobe distal to fulcrum; absent on facet (Fig. 23.5, 23.7, 23.8). Run of six articulated pleurae (Fig. 23.7–23.9) demonstrates that the pleural spine is barely developed on more anterior segments, and that the fulcrum becomes relatively more proximally located (tr.) along the pleura on more posterior segments.

Mature pygidium (Fig. 22.23–22.26) micropygous, suboval in dorsal outline; sagittal length (excluding articulating half ring) 35–40% of maximal width (tr.); anterior margin slopes slightly dorsally when traced away from axial furrow, more or less transversely oriented to fulcrum located approximately 35–40% of distance along margin from axial furrow to anterolateral corner of pygidium; anterior margin distal to fulcrum oriented slightly posteriorly, dips ventrally at approximately 45° relative to horizontal plane to anterolateral corner of pygidium; maximum pygidial width (tr.) slightly posterior to anterolateral corner. Articulating socket developed ventrally below anterior pygidial margin immediately abaxial to lateral margin of pygidial axis; visible only in ventral view (Fig. 22.24). Posterior pygidial margin with subtle sagittal notch in plan view; vaulted dorsally into strong posterior arch (Fig. 22.26). Pygidial axis defined only by break in slope; weakly dorsally vaulted above summit of pleural field (tr.);

←

FMNH PE58316, ×20; *9,* right librigena, dorsal view, FMNH PE58317, ×28; *10,* right librigena, dorsal view, FMNH PE58318, ×20; *11–13,* right librigena in ventral, dorsal, and right lateral view, FMNH PE58319, ×18; *14, 15,* left librigena in dorsal and ventral views, FMNH PE58320, ×18; *16–18,* left librigena in dorsal, ventral, and left lateral view FMNH PE58321, ×15; *19–22,* pygidium in dorsal, ventral, anterior, and posterior views, FMNH PE58322, ×40; *23–26,* pygidium in dorsal, ventral, anterior, and posterior views, FMNH PE58323, ×35; All from ICS-1029, Combined Metals Member, Pioche Formation, Oak Spring Summit section, Delamar Mountains.

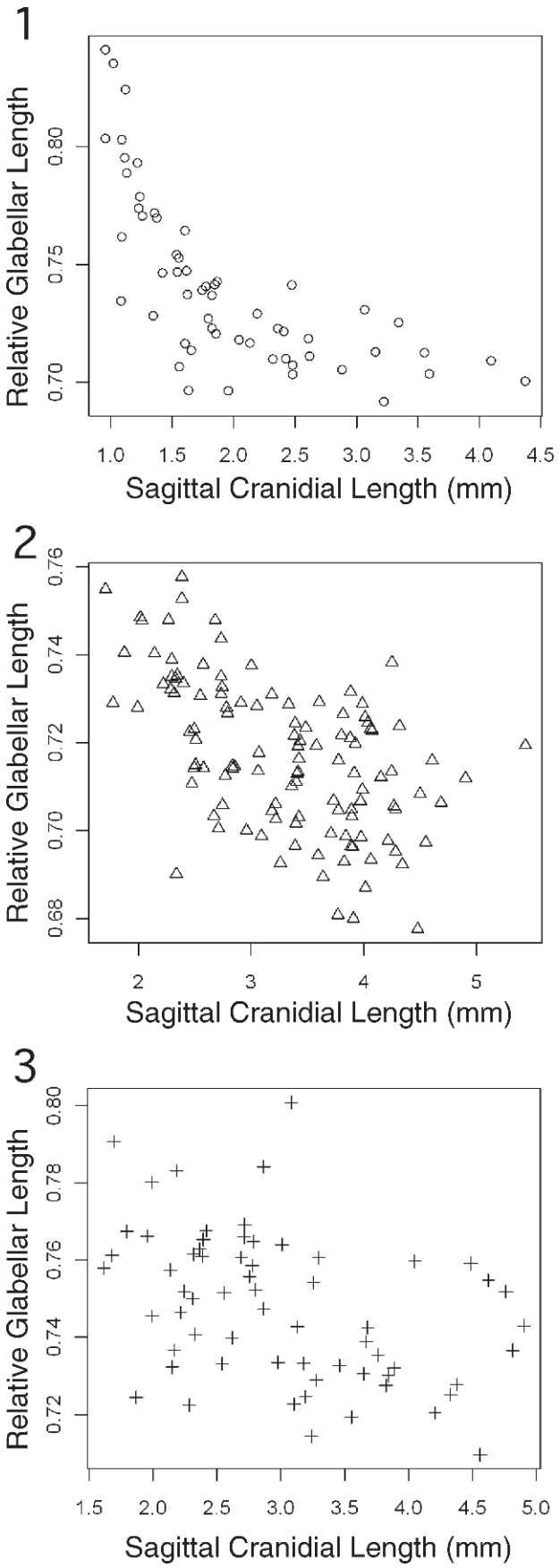

FIGURE *24*—Ontogenetic changes in relative glabellar length (quantified as sagittal glabellar length divided by sagittal cranidial length) for *Crassifimbra walcotti:1,* from ICS-1029 (N=57); *C.? metalaspis: 2,* from ICS-10124 (N=116); *Eokochaspis nodosa: 3,* from ICS-1192 (N=65). See text for details.

length 85–90% of pygidial length (sag.), anterior width approximately 130–150% that of pleural field (tr.) in dorsal view; tapers to bluntly rounded posterior tip; more or less effaced. Articulating half ring crescent-shaped, extends full width of axis; posteriorly defined by very shallow furrow. Pleural field moderately vaulted; inner portion more or less horizontal, distal portion sloping ventrally at approximately 35–40° before slightly flattening into narrow border that narrows posteriorly; border furrow not developed. First pleural furrow and weaker first interpleural furrow on dorsal surface of pleural field; each deepens and widens (exsag.) away from axial furrow, does not extend to margin. Pygidial doublure broadest at anterolateral corner of pygidium, narrowing posteriorly, absent sagittally; innermost margin below and paralleling break in slope defining pygidial border.

Ontogeny.—Morphometric analysis of cranidia ranging from 0.96 mm to 4.37 mm in sagittal length reveals several ontogenetic trends in cranidial morphology (above; Figs. 2–4, 16.1). The glabella proportionally narrows (tr.) anteriorly and widens (tr.) posteriorly, becoming more anteriorly tapered; L1 proportionally expands (tr.) more dramatically than more anterior glabellar lobes. Sagittal glabellar length is approximately 73% to 84% of sagittal cranidial length on the smallest sampled specimens (sagittal cephalic length <1.1 mm) and decreases to approximately 69% to 73% of sagittal cranidial length over the sampled portion of ontogeny (Fig. 24.1). SO is straighter (tr.) and shallows only slightly over the axis on cranidia <1.5 mm in sagittal length relative to larger specimens (Fig. 3.1, 3.2, 3.5). The portion of the posterior cranidial margin distal to the fulcrum becomes less strongly posterolaterally oriented. The anterior cranidial margin and the anterior branch of the facial suture migrate away from the anterior margin of the glabella as the anterior cranidial border widens (tr., sag., exsag.). The anterior end of the palpebral lobe initially more or less contacts the anterior border furrow (Fig. 3.3, 3.4), but becomes separated from it as a strip of exoskeleton anterior to the ocular ridge elongates (exsag.) (Fig. 3.16, 3.17). The palpebral lobe proportionally shortens (exsag.).

Shape change in the hypostome and librigena over the sampled portion of ontogeny are minimal. Small pygidia (Fig. 22.19–22.22) have a proportionally narrower (tr.) axis and lack a posterior arch.

Holotype.—USNM 61642, figured by Walcott (1886, pl. 28, fig. 2b; Walcott, 1890, pl. 96, fig. 9; Walcott, 1916, pl. 29, fig. 6; Lochman, 1947, figs. 1, 2; Palmer, 1958, pl. 25, fig. 1; Sundberg and McCollum, 2000, fig. 11.1–11.3.), from USGS locality 30 (Fig. 1.2). This specimen was erroneously identified as USNM 61641 by Palmer (1958, figure caption on p. 160).

Other material examined.—Descriptions and morphometric analyses presented herein based on examination of FMNH PE58241-PE58269, FMNH PE58314–PE58325, plus >70 other cranidia in the ICS collections, all from ICS-1029 (stratigraphic and locality details above). For comparative purposes, the following specimens were also examined: USNM 517486 (external mold of cranidium, uppermost Dyeran micritic limestone at base [“1 m”] of Emigrant Formation, Split Mountain, “Split Mountain East Section”; Sundberg and McCollum, 2003); USNM 517487 (cranidium

plus librigena, uppermost Dyeran micritic limestone at base [''1 m''] of Emigrant Formation, Split Mountain, ''Split Mountain East Section''; Sundberg and McCollum, 2003); USNM 508988 (five cranidia on dark micritic limestone; USGS locality 30, 8 mi north of Bennetts Spring, west slope of Highland Range); USNM 508989 (26 cranidia on dark micritic limestone; USGS locality 30, 8 mi north of Bennetts Spring, west slope of Highland Range); USNM 61642 (three cranidia [including the holotype] on dark micritic limestone; USGS locality 30 [?=352y], 8 mi north of Bennetts Spring, west slope of Highland Range); USNM 61642a (cranidium on dark micritic limestone; USGS locality 30, 8 mi north of Bennetts Spring, west slope of Highland Range); USNM 61642b (3 cranidia on dark micritic limestone; USGS locality 30, 8 mi north of Bennetts Spring, west slope of Highland Range); USNM 153562 and USNM 153563 (two cranidia preserved in a crystalline packstone/wackestone; locality 1085 of Fritz [1968], float about 223 ft above base of Pioche Formation, Campbell Ranch section, within T20N near boundary of R62 and R63E, Egan Range, White Pine County, Nevada).

Discussion.—Prior to the present paper, *C. walcotti* was known almost exclusively from isolated cranidia. A single librigena was figured and cursorily described by Sundberg and McCollum (2003). The rostral plate, pygidium, and thorax of *C. walcotti* are figured and described herein for first time, and a full description of the librigena is also provided. This information, combined with detailed knowledge of the cranidial ontogeny and morphological variation within the species (above), will greatly assist in future systematic studies of antagmine ptychoparioids. Comparison of the silicified material described herein to material from other localities (including the type locality at USGS locality 30; Fig. 1.2) will be presented elsewhere.

There has been some ambiguity regarding the presence and nature of sculpture on the cranidial surface of *C. walcotti*. Palmer (1958, p. 162; also Sundberg and McCollum, 2000, figs. 7, 8) described the internal surface of cranidia from USGS locality 30 as ''punctate.'' The internal surfaces of cranidia described herein bear granulations (Fig. 2.21), which would be represented as pits (?punctae) on internal molds. The external cranidial surface has been described as ''apparently smooth'' (Lochman, 1947, p. 71) and ''nearly smooth'' (Fritz, 1968, p. 223). Rasetti (1955, p. 19, 20) also considered the surface of *C. walcotti* to be non-granular. The silicified material described here clearly shows a fine granular ornament on the posterior half of occipital ring and the sagittal portion of SO of at least some cranidia (Fig. 4.8, 4.9). A similar ornament is locally present on the thorax (above). Examination of 38 cranidia from the type locality revealed that at least one specimen appears to bear fine granulations on the posterior margin of the occipital ring (the external cranidial surface in this region is preserved on extremely few large cranidia in the type lot). Intraspecific variation in the presence and distribution of granular ornamentation may be widespread among early ptychoparioids (see also Bright, 1959).

The structure consisting of four pits arranged in a square around the base of the occipital node has been termed the cephalic median organ by Lerosey-Aubril and McNamara (2008). Although rarely preserved and/or mentioned in the literature, the structure has been documented on members of most major trilobite groups, including on at least three other ptychoparioids, ranging in age from the ''Middle'' Cambrian to the Devonian (e.g., Whittington, 1965, p. 297; Whittington and Wilmot in Whittington et al., 1997, p. 79, fig. 72.2; Lerosey-Aubril and McNamara, 2008). The presence on *C. walcotti* (Fig. 4.7–4.9) represents the oldest known occurrence of the cephalic median organ in trilobites. That *C. walcotti* is a basal ptychoparioid lends credence to the claim by Lerosey-Aubril and McNamara (2008) that the structure was ancestrally present among (at least non-olenelline) trilobites.

Crassifimbra walcotti was not included in Sundberg's (2004) cladistic analysis of early ptychoparioids. Nevertheless, the coding would be similar to that for ''*Eokochaspis*'' *metalaspis* (Sundberg, 2004; below), differing only in *C. walcotti* having a shorter occipital ring relative to cranidial length (character 14); a longer preglabellar field relative to frontal area length (character 15); a more strongly bowed anterior border furrow (character 18); a downturned rather than level anterior border (character 19); a shallower anterior border furrow (character 20); a less steeply downsloping anterior portion of the fixigena (character 29); and a longer and wider posterior fixigena relative to basal glabellar width (characters 33, 34). The two species also differ in offset of the anterior and posterior branches of the facial suture (character 37); in the presence of fine granules (character 46); and in the development of pygidial pleural bands (character 67). The two species would also be coded as exhibiting different degrees of variation (i.e., intraspecific polymorphism in one or both species with partial overlap of states between species) in fixigenal width relative to basal glabellar width (character 28); in lateral extension of posterior border furrow (character 32); in angle of convergence of the anterior branch of the facial suture (character 35); in palpebral lobe length relative to glabellar length (character 41); in palpebral lobe width relative to palpebral lobe length (character 42); and in orientation of the ocular ridge (character 44). The number of thoracic segments (character 56) is unknown in *C. walcotti* (coded as state 1 [15 segments] for ''*E.*'' *metalaspis*). The two species are firmly supported as sister-taxa when *C. walcotti* is added to the analysis (analysis not presented).

CRASSIFIMBRA? METALASPIS (Sundberg and McCollum, 2000)
Figures 5, 6, 25, 26, 27

Crassifimbra walcotti PALMER, 1958 (part), p. 157–169, pl. 25, figs. 4, 7–25 only, pl. 26, figs. 1–24, text-fig. 5; SMITH, 1998, p. 103–106 [morphometric data only].

Eokochaspis metalaspis SUNDBERG AND MCCOLLUM, 2000, p. 618–619 [reassignment only]; SUNDBERG, 2004, p. 923, 924 [in cladogram], 925 [in cladogram], 934 [character codings], 939 [apomorphy list]; HOPKINS AND WEBSTER, 2009, p. 537.

Description.—Cranidia >4 mm in sagittal glabellar length (Fig. 5) wide (tr.), subtrapezoidal in outline; sagittal length 72–89% of transverse distance between posterolateral corners of posterior limbs; distance (tr.) between anterior branches of facial suture at γ 77–90% of distance between posterolateral corners of posterior limbs. Facial suture opisthoparian; anterior branches convex or sigmoidal abaxially, anteriorly convergent (each side oriented 10–25° inwards relative to exsagittal axis when followed anteriorly) and dipping ventrally at approximately 45° between contact with palpebral lobes and anterior border furrow, parallel or anteriorly divergent and approximately horizontal across posterior portion of anterior border, strongly anteriorly convergent and dipping slightly ventrally across anterior portion of anterior border, merging smoothly with anterior cranidial margin when viewed from above; posterior branches sigmoidal or convex abaxially, dipping at approximately 30–45° posteroventrally away from

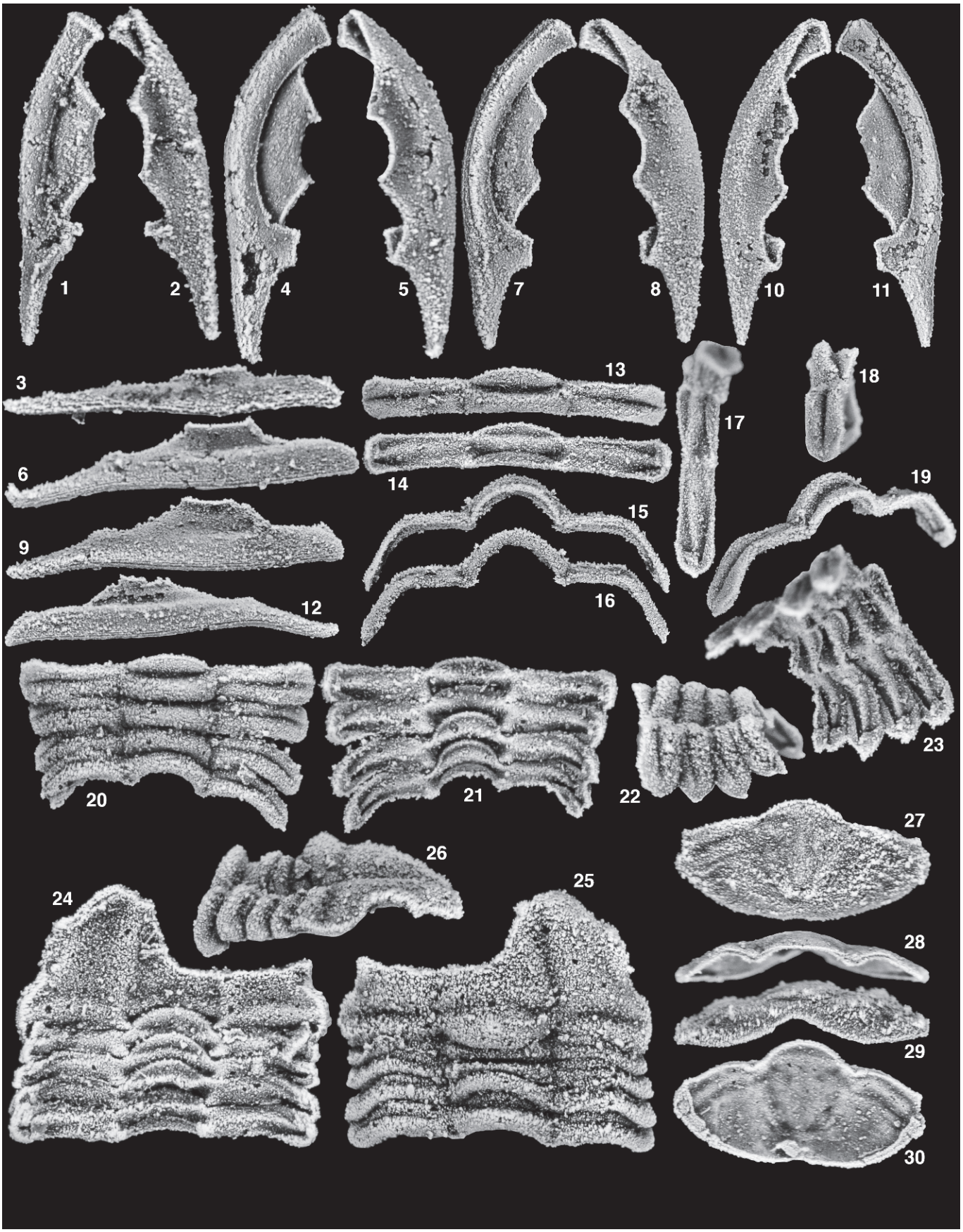

FIGURE *25*—Librigenae, thorax, and pygidium of *Crassifimbra*? *metalaspis*: *1–3,* right librigena in ventral, dorsal, and right lateral views, FMNH PE58326, ×18; *4–6,* right librigena in ventral, dorsal, and right lateral views, FMNH PE58327, ×18; *7–9,* right librigena in ventral, dorsal, and right

palpebral lobe, approximately horizontal across posterior border furrow and posterior cranidial margin. Glabella elongate to squat trapezoidal, length 68–74% of cranidial length (sag.); glabellar width at SO (tr.) 57–80% of glabellar length (sag.), tapering anteriorly, width (tr.) at contact with ocular ridge 47–58% of glabellar length (sag.); highest and prominently dorsally arched (tr.) posteriorly, less vaulted anteriorly. Occipital ring semilunate in plan view; sagittal length 22–29% of glabellar length (sag.); exsagittal length from anterolateral corner (contact between axial furrow and SO) to contact with posterior cranidial margin approximately 11–16% of glabellar length (sag.); width (tr.) between contacts with posterior cranidial margins 86–100% of width (tr.) between anterolateral corners; posterior margin convex posteriorly. SO transglabellar; broad (sag., exsag.), shallow, and transverse to convex anteriorly over sagittal axis; narrows, deepens, and becomes convex posteriorly each side of axis; shallows at contact with axial furrow. L1 subtriangular, narrowing anteriorly, lateral margins bow slightly outwards. S1 and S2 very shallow, convex anteriorly, oriented strongly posterolaterally when traced adaxially from axial furrow (S1 more strongly so than S2); absent over axis. Lateral margins of L2 bow very slightly outwards. Contact between S2 and axial furrow located opposite point approximately three-fifths of distance along sagittal axis from SO to anterior glabellar margin. S3 absent or defined only distally by extremely shallow furrow; roughly transverse or weakly convex anteriorly either side of axis when present. S4 absent or defined only distally by extremely shallow furrow; oriented strongly anterolaterally when traced adaxially from axial furrow. Frontal lobe bluntly rounded anteriorly. Axial furrows converge between contact with SO and contact with S2, less convergent or subparallel anterior to S2; deepest and broadest between lateral margins of S1 and S3, shallow around anterior margin of glabella and lateral margins of occipital ring. Anterior cranidial border crescent-shaped with distal portions moderately to strongly flexed posteriorly relative to sagittal portion in plan view and typically dorsally flexed into broad anterior arch (tr.); broad (sag., exsag.), accounting for approximately two-thirds of frontal area close to sagittal axis (excluding plectrum), tapering distally to anterior facial suture; convex dorsally (sag., exsag.), sloping steeply down to anterior margin and less steeply into broad anterior border furrow. Medial portion of anterior border furrow widens (sag., exsag.), shallows, and deflects posteriorly at broad (tr.), low plectrum extending from anterior border almost to frontal lobe of glabella; more or less confluent with axial furrow around frontal lobe sagittally. Palpebral lobe reniform in plan view, width (tr.) just posterior to midlength 22–37% of length (exsag.), length (exsag.) 23–28% of cranidial length (sag.), weakly defined adaxially by break in slope that strengthens posterolaterally, suture-bound margin convex abaxially; axis between anterior and posterior tips oriented outwards by 4–15° relative to sagittal axis); anterior tip located opposite point 75–86% of distance from posterior to anterior end of glabella along sagittal axis, posterior tip located opposite point 38–48% of distance from posterior to anterior end of glabella along sagittal axis; gently convex dorsally (tr.); palpebral suture horizontal along summit of palpebral lobe, dipping ventrally at approximately 60–85° anteriorly and posteriorly to merge with anterior and posterior branches of facial suture. Poorly defined ocular ridge contacts axial furrow just anterior to S4, gently arcs posterolaterally across interocular area; more prominently defined on ventral surface. Fixigenal field anterior to ocular ridge arcs steeply ventrally into anterior border furrow. Interocular area parallelogram-shaped; width (tr.) opposite posterior tip of palpebral lobe 41–47% of sagittal glabellar length; slightly arched dorsally (tr. and exsag.), distal portion lower than proximal portion, dorsal summit of palpebral lobe at lower dorsal elevation than axial furrow. Posterior limb of fixigena projects laterally beyond posterior tip of palpebral lobe; width (tr.) from axial furrow to posterolateral tip 76–99% of distance between intersections of posterior cranidial margins with occipital ring. Proximal portion of posterior margin of fixigena transversely oriented and horizontal; distal portion flexing posteriorly by 8–27° relative to transverse line and dipping ventrally by 35–45° relative to horizontal plane at fulcrum. Posterior border well defined by more or less transversely oriented broad border furrow that shallows adjacent to axial furrow and at distal end of posterior limb of fixigena; slightly narrower (exsag.) than distance (exsag.) from anterolateral corner of occipital ring to intersection of posterior cranidial margin with posterior margin of occipital ring; proportionally widens (exsag.) distally. Prominent occipital node on posterior portion of occipital ring. Anterior margin of doublure below occipital ring runs almost transversely between posterolateral corners of occipital ring. Triangular doublure below posterior cranidial border extends from fulcrum to terminate slightly adaxial to facial suture, broadening (exsag.) abaxially; anterior margin approximately transverse but for distinct subtriangular extension projecting anteriorly at abaxial end. Low boss-like process projects slightly posteriorly and ventrally at posterior margin of axial furrow on ventral surface. Rostral suture runs slightly inside margin on ventral cranidial surface. External surface of cranidium smooth.

Librigena (Fig. 25.1–25.12) relatively narrow (tr.). Librigenal field approximately equal in width (tr.) to lateral border opposite midlength of eye socle, sloping steeply from eye socle into broad, shallow lateral border furrow. Posterior border furrow and posterior portion of lateral border furrow represented only by subtle break in slope. Posterior librigenal margin very short, one-third to one-half width (tr.) of base of genal spine. Lateral border convex dorsally in cross-section, broadening slightly posteriorly to base of genal spine. Base of genal spines located approximately opposite (tr.) posterior margin of occipital ring (Figs. 26, 27). Genal spine broad-based, evenly tapering to pointed tip; length 30–38% of distance between anteriormost and posteriormost points of facial suture; curvature of distal margin more or less continuous with that of lateral librigenal margin; genal spine slopes ventrally at 10–15° relative to plane defined by summit of eye socle, slope at tip decreases to become approximately coplanar with summit of eye socle on some specimens

←

lateral views, FMNH PE58328, ×12; *10–12,* left librigena in dorsal, ventral, and left lateral views, FMNH PE58329, ×11; *13–19,* isolated thoracic segment in dorsal, ventral, anterior, posterior, oblique interior, right lateral, and oblique anterolateral views, FMNH PE58330, ×10; *20–23,* run of four articulated thoracic segments in dorsal, ventral, left lateral, and oblique interior views, FMNH PE58331, ×15; *24–26,* incomplete cranidium associated with anteriormost four thoracic segments in ventral, dorsal, and right lateral views, FMNH PE58332, ×15; *27–30,* pygidium in dorsal, anterior, posterior, and ventral views, FMNH PE58333, ×20. All from ICS-10124, Combined Metals Member, Pioche Formation, Log Cabin Mine section, Highland Range.

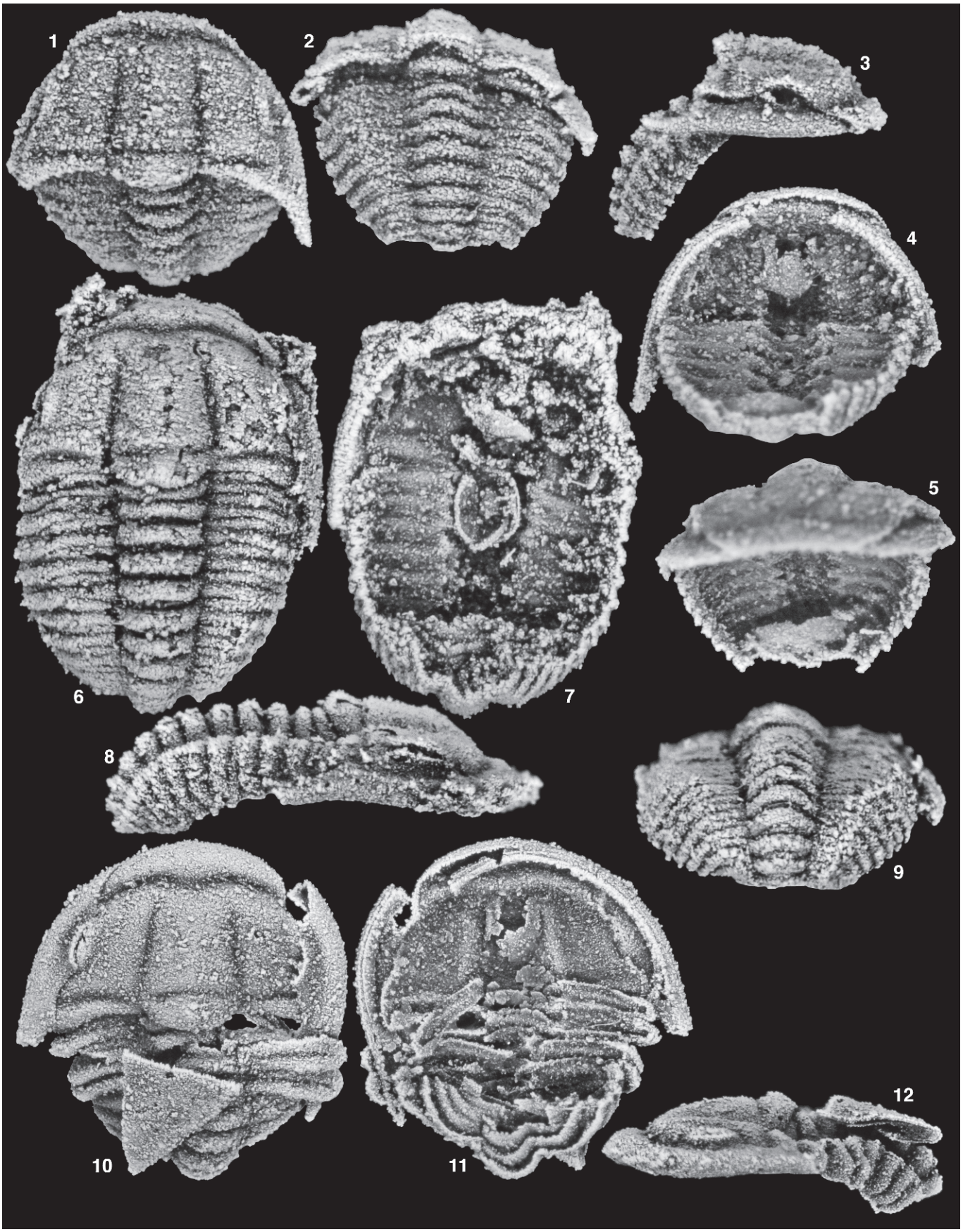

FIGURE *26*—Articulated specimens of *Crassifimbra*? *metalaspis*: *1–5,* articulated dorsal exoskeleton with 11 thoracic segments and pygidium, plus hypostome and rostral plate, viewed perpendicular to cranidium, perpendicular to thorax, right lateral view, ventral to cranidium, and interior of thorax

(Fig. 25.12); faint groove-like depression at base may represent extension of border furrow onto genal spine. Doublure broadly convex ventrally, terminates below lateral border furrow; broadest at base of genal spine; projects adaxially beyond facial suture below anterior and posterior cranidial borders. Connective suture concave adaxially. Doublure of lateral border and ventral surface of genal spine ornamented with terrace ridges; external surface otherwise smooth. Visual surface unknown.

Pygidium (Fig. 25.27–25.30) micropygous, suboval in dorsal outline; sagittal length (excluding articulating half ring) approximately 40% of maximal width (tr.); anterior margin slopes slightly dorsally when traced away from axial furrow, more or less transversely oriented to fulcrum located approximately 33–40% of distance along margin from axial furrow to anterolateral corner of pygidium; anterior margin distal to fulcrum oriented slightly posteriorly, dips ventrally at approximately 30–35° relative to horizontal plane to anterolateral corner of pygidium; maximum pygidial width (tr.) slightly posterior to anterolateral corner. Articulating socket developed ventrally below anterior pygidial margin immediately abaxial to lateral margin of pygidial axis; visible only in ventral view (Fig. 25.30). Posterior pygidial margin with subtle sagittal notch in plan view; vaulted dorsally into strong posterior arch (Fig. 25.29). Pygidial axis defined only by break in slope; weakly dorsally vaulted above summit of pleural field (tr.); length (excluding articulating half ring) approximately 80% of pygidial length (sag.), anterior width approximately equal to that of pleural field (tr.); tapers to bluntly rounded posterior tip; more or less effaced dorsally, ventral surface shows faint abaxial impressions of three axial rings plus a terminal piece. Articulating half ring crescent-shaped, extends full width of axis; posteriorly defined by weak furrow that shallows axially. Pleural field weakly vaulted; inner portion horizontal, distal portion sloping ventrally at approximately 30° before flattening into narrow, subhorizontal border that narrows posteriorly; border furrow not developed. First pleural furrow and weaker first interpleural furrow clear on dorsal surface of pleural field; each deepens and widens (exsag.) away from axial furrow, does not extend to margin. Distal portion of second pleural furrow very faintly expressed dorsally. Pygidial doublure broadest at anterolateral corner of pygidium, narrowing posteriorly, absent sagittally; innermost margin below and paralleling break in slope defining pygidial border.

Hypostome, rostral plate, and thorax thoroughly described by Palmer (1958).

Ontogeny.—The ontogeny of *C.*? *metalaspis* was originally described by Palmer (1958, as *C. walcotti*) based on silicified material collected from the One Wheel Canyon section (Fig. 1.2). Morphometric analysis herein of cranidia ranging from 1.71 mm to 5.43 mm in sagittal length from ICS-10124 (Log Cabin Mine section; Fig. 1.2) reveals several ontogenetic trends in cranidial morphology (above; Figs. 5, 6, 16.2), confirming and expanding upon the observations made by Palmer (1958). The glabella proportionally narrows (tr.) anteriorly and widens (tr.) posteriorly, becoming more anteriorly tapered; L1 proportionally expands (tr.) more dramatically than more anterior glabellar lobes. Sagittal glabellar length is approximately 73% to 75% of sagittal cranidial length on the smallest sampled specimens (sagittal cephalic length <2.2 mm) and decreases to approximately 68% to 74% of sagittal cranidial length over the sampled portion of ontogeny (Fig. 24.2). Glabellar furrows anterior to SO and ocular ridges are extremely weak or not defined on cranidia <3.4 mm in sagittal length (Fig. 6.1–6.16). SO is straighter (tr.) and shallows only slightly over the axis on cranidia <2.1 mm in sagittal length relative to larger specimens (Fig. 6.1). The portion of the posterior cranidial margin distal to the fulcrum becomes less strongly posterolaterally oriented. The anterior cranidial margin and the anterior branch of the facial suture migrate away from the anterior margin of the glabella as the anterior cranidial border widens (tr., sag., exsag.). The anterior end of the palpebral lobe more or less initially contacts the anterior border furrow (Fig. 6.3, 4), but becomes separated from it as a strip of exoskeleton anterior to the ocular ridge elongates (exsag.). The palpebral lobe proportionally shortens (exsag.), and its distal edge (bounded by the facial suture) becomes slightly more strongly crescent-shaped.

Silicified material is almost invariably disarticulated. In the absence of instar size clusters, assignment of isolated cranidia to particular meraspid degrees is impossible. Palmer (1958) divided post-protaspid development of *C.*? *metalaspis* into three broad stages, recognized by differences in cranidial, hypostomal, and pygidial morphology. Specimens included in the morphometric analyses herein fall within the ''late meraspid and holaspid'' developmental stage as defined by Palmer (1958). Rarely, silicified sclerites remain articulated. In most such cases the hypostome, rostral plate, and librigena are more or less in life position, and these specimens are interpreted as carcasses. Several articulated specimens of *C.*? *metalaspis* were recovered from ICS-10124 (Figs. 26, 27), offering the potential to relate cranidial morphology to that of other sclerites and to the traditional divisions of trilobite ontogeny based on thoracic segment number (reviewed by Chatterton and Speyer in Whittington et al., 1997; Hughes et al., 2006).

Palmer (1958, p. 159) stated that the mature thorax of *C.*? *metalaspis* consisted of at least 15 segments, based on an specimen bearing a thorax of 15 segments associated with a pygidium but lacking a cranidium (Palmer, 1958, pl. 25, figs. 19, 23). Palmer (1958, p. 168) suggested that the transition into the holaspid period occurred at a sagittal cranidial length of at least 2 mm. The newly collected articulated specimens illustrated herein are consistent with these earlier findings. One specimen 1.53 mm in sagittal cephalic length (Fig. 26.1–26.5) bears 11 thoracic segments and a pygidium with sagittal length approximately 0.24 mm. The associated hypostome is approximately 0.55 mm long. This is undoubtedly a meraspis. Slightly larger specimens 1.77 mm and 2.10 mm in sagittal cephalic length (Fig. 26.6–26.9 and Fig. 27.1–27.8) bear 12 and 14 thoracic segments but lack pygidia: it is therefore unknown whether these represent later meraspis or holaspis exoskeletons. The hypostome associated with the larger of these specimens is broken (Fig. 27.2) but is estimated to have

←

showing slightly displaced pygidium, FMNH PE58334, ×22; *6–9,* articulated dorsal exoskeleton with 12 thoracic segments but lacking pygidium, in dorsal, ventral, and right lateral views, FMNH PE58335, ×20; *10–12,* articulated dorsal exoskeleton with associated hypostome, in dorsal, ventral, and left lateral views, FMNH PE58336, ×15. All from ICS-10124, Combined Metals Member, Pioche Formation, Log Cabin Mine section, Highland Range.

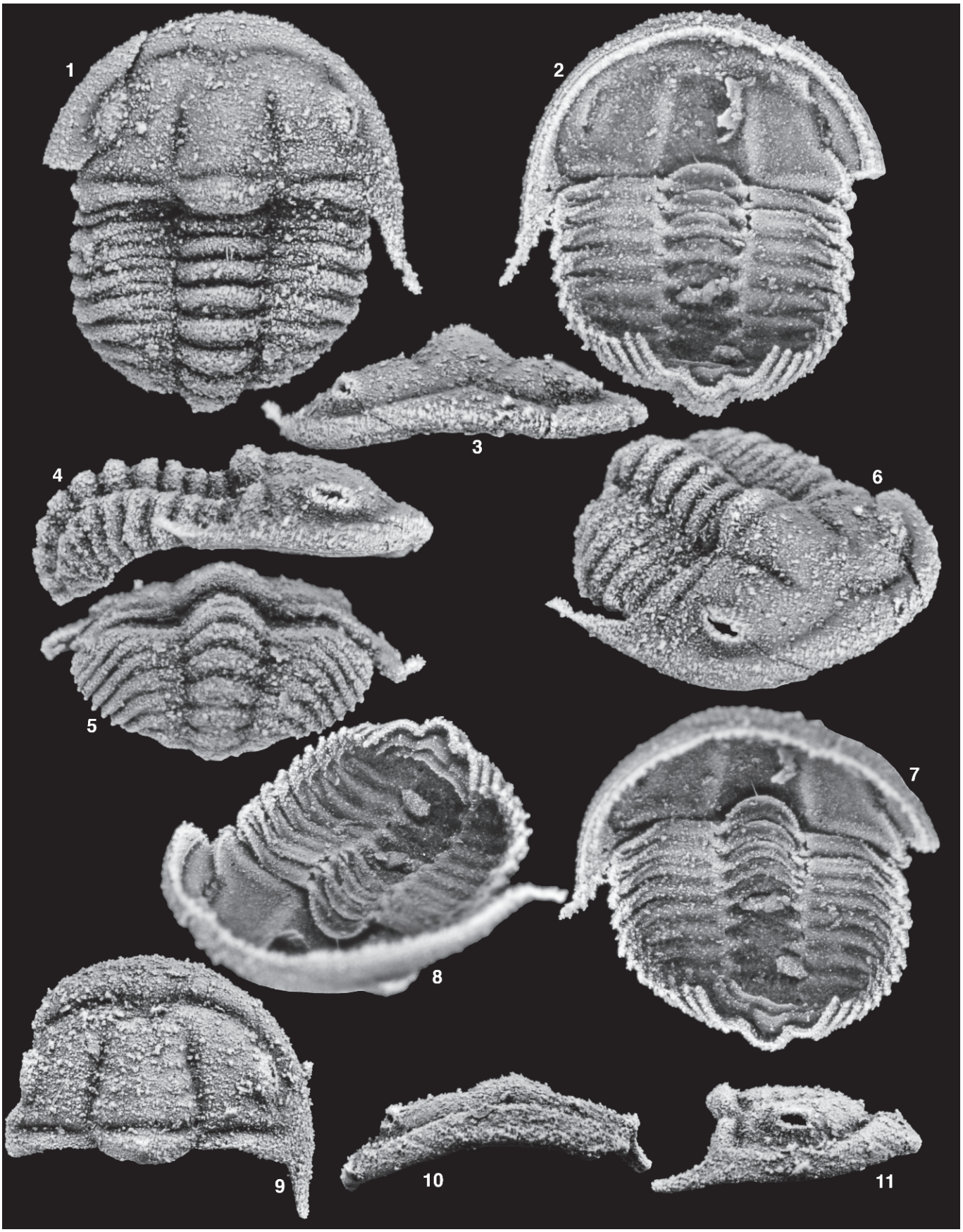

FIGURE *27*—Articulated specimens of *Crassifimbra*? *metalaspis*: *1–8,* articulated dorsal exoskeleton with 14 thoracic segments, rostral plate, and hypostome, but lacking pygidium, in dorsal, ventral, anterior, right lateral, posterior, oblique dorsoanterolateral, oblique ventral, and oblique ventroanterolateral views, FMNH PE58337, ×18; *9–11,* cranidium and associated right librigena in dorsal, anterior, and right lateral views, FMNH PE58338, ×10. Both from ICS-10124, Combined Metals Member, Pioche Formation, Log Cabin Mine section, Highland Range.

been approximately 0.73 mm long. The articulating half ring of T1 is proportionally longer (sag.) than that of more posterior segments (Fig. 27.2, 7, 8; see also Fig. 25.24). The largest articulated specimen is 2.38 mm in sagittal cephalic length (Fig. 26.10–26.12) and has a hypostome length of approximately 0.85 mm; the number of thoracic segments on this specimen is unclear. These specimens demonstrate that the sagittal length of the hypostome is approximately one-third of the sagittal cranidial length. The only complete specimen (Fig. 26.1–26.5) confirms that the pygidium was strongly micropygous (sagittal pygidial length approximately 16% of sagittal cranidial length) during meraspid degree 11.

Holotype.—USNM 133202c, figured by Palmer (1958, pl. 25, fig. 11), from USGS locality 1400-CO (Fig. 1.2).

Other material examined.—Descriptions and morphometric analyses presented herein based on examination of FMNH PE58270-PE58289, FMNH PE58326-PE58338, plus >200 other cranidia in the ICS collections, all from ICS-10124 (stratigraphic and locality details above).

Discussion.—The description of new material from the Log Cabin Mine section (above) expands Palmer's (1958) work on *C.*? *metalaspis* by incorporating quantification of the degree of intracollection variation in mature cranidial morphology, and by providing a more extensive description of librigenal and pygidial morphology. This permits more detailed comparison to other basal ptychoparioids.

As discussed above, Palmer (1958) considered the silicified material from USGS localities 1399-CO and 1400-CO to be conspecific with *C. walcotti* from USGS locality 30. Small but significant differences in cranidial dimensions between these localities were interpreted as geographic variation. Later workers (Fritz, 1968; Sundberg and McCollum, 2000) considered these differences to be of a magnitude sufficient to warrant species- and genus-level distinction between these collections, resulting in the establishment of "*Eokochaspis*" *metalaspis* Sundberg and McCollum, 2000. Sundberg and McCollum (2000, p. 619) stated that "*E.*" *metalaspis* differs from *C. walcotti* by having a more trapezoidal cranidial outline (rather than subtriangular outline); a higher convexity of the glabella and anterior border; more prominently developed axial, occipital, posterior border, and anterior border furrows; a less distally tapering anterior border; a less tapered, narrower, and longer glabella (although Fritz [1968, p. 224] stated that the glabella of *C. walcotti* was the larger); a narrower occipital ring; in the occipital furrow being continuous across axis and connected with axial furrows; wider posterior areas of fixigena; and a non-granular internal surface. Fritz (1968, p. 224) also noted that *C. walcotti* had smaller and less raised palpebral lobes; wider (sag.) anterior border; and more wedge-shaped posterior fixigenal wings.

The present study largely confirms these previous statements. Differences in mean cranidial shape at standard size are discussed in the morphometric analyses above (Fig. 20). Additional differences are also revealed based on the new material illustrated herein: in *C. walcotti* the posterior cranidial margin distal to the fulcrum slopes less steeply ventrally; the anterior border slopes ventrally away from anterior border furrow; and the anterior margin of the doublure below the posterior cranidial border distal to the fulcrum is oriented anteriorly. However, the present study demonstrates that intraspecific variation renders some supposed distinctions less diagnostic. For example, some large cranidia from ICS-10124 (e.g., Fig. 5.12–5.16) combine a cranidial outline and glabellar furrow depth similar to *C. walcotti* with a convexity and axial furrow depth similar to "typical" *C.*? *metalaspis*.

Sundberg and McCollum (2000, p. 614) assigned the new species to *Eokochaspis* based on "similar cranidial outlines, facial sutures, median inbending of the anterior border, thoracic segments, and pygidium" between it and *E. nodosa* (type species of the genus), and suggested that *E. nodosa* may have been derived from the stratigraphically older *E. metalaspis*. This proposed derivation was not supported by subsequent cladistic work (Sundberg, 2004), which demonstrated polyphyly of the genus. "*Eokochaspis*" *nodosa* was a member of a kochaspid clade, while "*E.*" *metalaspis* was member of a paraphyletic stem group basal to the kochaspids. Nine internal nodes separated the species, although branch lengths were very short (Sundberg, 2004, fig. 2). *Crassifimbra walcotti* was not included in the analysis but, as discussed above, coding for this species would be very similar to that for "*E.*" *metalaspis* and the two are strongly supported as sister species in an expanded and modified run of Sundberg's (2004) analysis (not presented herein). Librigenal, thoracic, and pygidial morphology is much more similar between these species than between either of these species and *E. nodosa*. "*Eokochaspis*" *metalaspis* is therefore here provisionally reassigned to the genus *Crassifimbra*. This assignment is provisional because of the ambiguity regarding the diagnosis of *Crassifimbra* (above), but is deemed useful in that it at least removes one factor contributing to the polyphyly of "*Eokochaspis*."

The present study also reveals some problems in Sundberg's (2004) character state coding of *C.*? *metalaspis* (as *Eokochaspis metalaspis*). The occipital node or spine (character 11) was coded as absent, but this is clearly incorrect. The sagittal length of the occipital ring relative to sagittal cranidial length (character 14) was somewhat overestimated. This may be related to Sundberg's (2004) coding of the medial orientation of SO (characters 12, 13) which differs from the description herein. Sundberg (2004, characters 23, 25) states that *C.*? *metalaspis* possesses a V-shaped median inbend of the anterior border furrow, but that a plectrum is absent. The median inbend is herein interpreted as being related to the presence of a plectrum. The dorsal transverse arching of the anterior border (character 26) was coded as being flat. The new material illustrated herein clearly demonstrates that it is vaulted to form an anterior arch. Relative to the material examined herein, the transverse width of the fixigena between the axial furrow and palpebral furrow relative to basal glabellar width (character 28), the transverse width of the posterior area of fixigena relative to basal glabellar width (character 34), and the orientation of the palpebral lobe relative to the exsagittal axis (character 37), were each somewhat underestimated in Sundberg's (2004) coding.

A low process projecting ventrally and slightly adaxially from the posterior margin of the axial furrow on the ventral surface (Figs. 25.13–26.19) was considered by Palmer (1958, p. 159) to be an apodeme. Articulated specimens (Figs. 25.24–25.26, 26, 27) reveal that this process is more prominently developed on anterior segments, and that it nestles into a subtle socket in the ventral surface of the anterior margin of the axial furrow of the segment located immediately posteriorly, weakly "hugging" the distal tips of the articulating half ring of that segment. This structure therefore also likely served in segment articulation. Analogous axial process and socket structures are known in other trilobites (e.g., Whittington in Whittington et al., 1997, figs. 40, 47).

Genus "EOKOCHASPIS" Sundberg and McCollum, 2000

Discussion.—As currently defined, this genus is polyphyletic (Sundberg, 2004). Reassignment of "*E.*" *metalaspis* to *Crassifimbra* (above) removes one element of this polyphyly, but a complete revision of this genus is still needed. While assigned to *Eokochaspis*, *C.*? *metalaspis* represented the oldest member of the genus and of the kochaspid clade. However, a new species of kochaspid (to be described elsewhere) occurs at very low abundance with *C.*? *metalaspis* in ICS-10124, and the lowest occurrence of the clade remains in the uppermost Dyeran.

EOKOCHASPIS NODOSA Sundberg and McCollum, 2000
Figures 7, 8, 28, 29

Eoptychoparia piochensis PALMER, 1998a (part), p. 650, 651, fig. 4 [silicified occurrences only]; ?SMITH, 1998, p. 104 [morphometric data only].

Eokochaspis nodosa SUNDBERG AND MCCOLLUM, 2000, p. 611–614, figs. 7.1–7.20; SUNDBERG AND MCCOLLUM, 2003, p. 967, pl. 2, figs. 1, 2, 4; Jell in JELL AND ADRAIN, 2003, p. 373 [mentioned in list]; SUNDBERG, 2004, p. 923, 924 [in cladogram], 925 [in cladogram], 926, 927, 928, 934 [character codings], 939 [apomorphy list].

Description.—Cranidia >4 mm in sagittal glabellar length (Fig. 7) wide (tr.), subtrapezoidal in outline; sagittal length 62–77% of transverse distance between posterolateral corners of posterior limbs; distance (tr.) between anterior branches of facial suture at γ 68–78% of distance between posterolateral corners of posterior limbs. Facial suture opisthoparian; anterior branches anteriorly convergent or divergent (each side oriented from 11° outwards to 19° inwards relative to exsagittal axis when followed anteriorly; compare Fig. 7.11 to Fig. 7.12) and dipping ventrally at 40–50° between contact with palpebral lobes and anterior border furrow, subparallel and dipping ventrally at approximately 5–20° across posterior portion of anterior border, strongly anteriorly convergent across anterior portion of anterior border, merging smoothly with anterior cranidial margin in dorsal view; posterior branches sigmoidal or convex abaxially, dipping at approximately 30–40° posteroventrally away from palpebral lobe, gently dorsally arched across posterior cranidial margin. Glabella trapezoidal, length 71–76% of cranidial length (sag.); glabellar width at SO (tr.) 65–78% of glabellar length (sag.), tapering anteriorly, width (tr.) at contact with ocular ridge 46–55% of glabellar length (sag.); highest and prominently dorsally arched (tr.) posteriorly, less vaulted anteriorly; relatively strongly arched (sag., exsag.). Occipital ring semilunate in plan view; sagittal length 19–23% of glabellar length (sag.); exsagittal length from anterolateral corner (contact between axial furrow and SO) to contact with posterior cranidial margin approximately 12–15% of glabellar length (sag.); width (tr.) between contacts with posterior cranidial margins 88–98% of width (tr.) between anterolateral corners; posterior margin convex posteriorly. SO transglabellar; very broad (sag., exsag.), shallow, and transverse over sagittal axis; narrows, deepens, and becomes convex posteriorly each side of axis. L1 subtriangular, narrowing anteriorly, lateral margins bow slightly outwards. S1, S2, and S3 clear but slightly shallower than abaxial portions of SO, absent over axis. S1 convex anteriorly, oriented strongly posterolaterally when traced adaxially from axial furrow. S1 transverse or oriented very weakly posterolaterally when traced adaxially from axial furrow. Lateral margins of L2 bow slightly outwards. Contact between S2 and axial furrow located opposite point approximately three-fifths of distance along sagittal axis from SO to anterior glabellar margin. S3 weakly convex anteriorly either side of axis and oriented strongly anterolaterally when traced adaxially from axial furrow. S4 defined only distally by very shallow furrow; oriented strongly anterolaterally when traced adaxially from axial furrow. Frontal lobe bluntly rounded anteriorly. Axial furrows converge between contact with SO and contact with S2, less convergent anterior to this; clear all around glabella, deepest and broadest between lateral margins of S1 and S2. Anterior cranidial border crescent-shaped with distal portions weakly flexed posteriorly relative to sagittal portion in plan view and dorsally flexed into broad anterior arch (tr.); broad (sag., exsag.), accounting for approximately one-half of frontal area close to sagittal axis (excluding plectrum), tapering distally to anterior facial suture; convex dorsally (sag., exsag.), subhorizontal or slopes slightly ventrally out of anterior border furrow, slope steeper in anterior two-thirds. Medial portion of anterior border furrow widens (exsag.), shallows, and deflects slightly posteriorly at broad (tr.), low, poorly defined plectrum extending from anterior border across anterior half of preglabellar field. Palpebral lobe crescent-shaped in plan view, width (tr.) just posterior to midlength 20–30% of length (exsag.), length (exsag.) 28–32% of cranidial length (sag.), defined adaxially by break in slope that strengthens posterolaterally, suture-bound margin convex abaxially; axis between anterior and posterior tips oriented outwards by 6–17° relative to sagittal axis); anterior tip located opposite point 75–88% of distance from posterior to anterior end of glabella along sagittal axis, posterior tip located opposite point 37–48% of distance from posterior to anterior end of glabella along sagittal axis; gently convex dorsally (tr.); palpebral suture horizontal along summit of palpebral lobe, dipping ventrally at approximately 60–70° anteriorly and posteriorly to merge with anterior and posterior branches of facial suture. Clearly defined ocular ridge contacts axial furrow just anterior to S4, gently arcs posterolaterally across interocular area; also prominently defined on ventral surface. Fixigenal field anterior to ocular ridge arcs steeply ventrally into anterior border furrow. Interocular area semicircular; width (tr.) opposite posterior tip of palpebral lobe 40–47% of sagittal glabellar length; slightly to strongly arched dorsally (tr. and exsag.), distal portion lower than proximal portion, dorsal summit of palpebral lobe at lower dorsal elevation than axial furrow. Posterior limb of fixigena projects laterally well beyond posterior tip of palpebral lobe; width (tr.) from axial furrow to posterolateral tip 90–110% of distance between intersections of posterior cranidial margins with occipital ring. Proximal portion of posterior margin of fixigena transversely oriented and horizontal; distal portion flexing posteriorly by 17–35° relative to transverse line and dipping ventrally at 30–45° relative to horizontal plane at fulcrum. Posterior border well defined by more or less transversely or weakly posterolaterally oriented broad border furrow that slightly shallows adjacent to axial furrow and at distal end of posterior limb of fixigena; slightly narrower (exsag.) than distance (exsag.) from anterolateral corner of occipital ring to intersection of posterior cranidial margin with posterior margin of occipital ring; proportionally widening (exsag.) distally. Prominent occipital node on posterior portion of occipital ring. Anterior margin of doublure below occipital ring runs almost transversely or slightly convex anteriorly between posterolateral corners of occipital ring. Triangular doublure below posterior cranidial border extends from fulcrum to terminate slightly adaxial to facial suture, broadening (exsag.) abaxially;

anterior margin approximately transverse but for distinct subtriangular extension projecting anteriorly at abaxial end. Low boss-like process projects slightly posteriorly and ventrally at posterior margin of axial furrow on ventral surface. Rostral suture runs slightly inside margin on ventral cranidial surface. External surface of cranidium with fine granular ornament over glabella (except in furrows), fixigenal area, and possibly anterior border; interspersed with moderately coarse granules on interocular area and more subdued coarse granules on posterior fixigenal wing anterior to posterior border furrow and on anterior fixigenal wing anterior to ocular ridge.

Rostral plate (Fig. 28.1, 2) subrectangular in plan view, width (tr.) between anterolateral corners almost seven times distance between anterior and posterior tips of connective sutures; transversely bowed dorsally into broad arch. Anterior and posterior margins very weakly convex anteriorly; anterior margin steeply upturned dorsally; posterior margin bears broad, subcentral posterior extension mirroring sagittal posterior deflection of anterior cranidial border. Connective sutures concave adaxially; narrowest (tr.) point of rostral plate approximately one-third of distance from anterior to posterior end of connective sutures. Terrace ridges run transversely along anterior margin.

Mature hypostome (Fig. 28.22–28.29) subtrapezoidal in outline, tapering slightly posteriorly, maximum length approximately 150–160% of width across anterior margin (excluding anterior wings). Anterior margin convex anteriorly; posterior margin strongly rounded posteriorly (tr.). Anterior and lateral border narrow, separated from middle body by distinct furrow. Anterior wing slender, elongate, blunt-tipped, oriented strongly dorsolaterally, distance (tr.) between tips of anterior wings approximately equal to maximum hypostome length (sag.); base located approximately one-fifth distance down hypostomal length on large specimens, more anteriorly located on smaller specimens (Fig. 28.14–28.21). Posterior wing short, slender, oriented dorsally; base located approximately 70% of distance down hypostomal length from anterior end. Middle body weakly inflated (tr., sag., exsag.); central portion of anterior lobe not preserved and perhaps not strongly mineralized in life on large specimens; posterior lobe crescentic, maximum width 70–80% of maximum hypostomal width, length (sag.) approximately one-quarter that of middle body. Narrow doublure developed interior to lateral and posterior border.

Librigena (Fig. 28.3–28.13) moderately broad (tr.). Librigenal field slightly wider (tr.) than lateral border opposite midlength of eye socle, sloping from eye socle into broad, shallow lateral border furrow. Posterior border furrow and posterior portion of lateral border furrow shallow; extremely shallow, broad extensions run onto base of genal spine. Posterior librigenal margin very short, curving to merge smoothly with adaxial margin of genal spine. Lateral border weakly convex dorsally in cross-section, broadening slightly posteriorly to base of genal spine. Base of genal spines developed opposite lateral margin of occipital lobe. Genal spine very broad-based, evenly tapering to pointed tip; length approximately 35–45% of distance between anteriormost and posteriormost points of facial suture (proportionally shorter on smaller librigenae; Fig. 28.3–28.7); curvature of distal margin more or less continuous with that of lateral librigenal margin; genal spine slopes ventrally at 10–20° relative to plane defined by summit of eye socle, slope at tip decreases to become approximately coplanar with summit of eye socle on some specimens (Fig. 28.10). Doublure broadly convex ventrally, terminates below lateral border furrow; broadest at base of genal spine; projects adaxially beyond facial suture below anterior and posterior cranidial borders. Connective suture weakly concave adaxially. Doublure of lateral border and ventral surface of genal spine ornamented with terrace ridges; external surface otherwise smooth. Visual surface unknown.

Total number of thoracic segments at maturity unknown. Isolated segment (Fig. 29.1–29.6) with horizontal inner pleural region, dipping ventrally at approximately 45° relative to horizontal plane at fulcrum located approximately midway (tr.) across pleura. Axial ring subrectangular in plan view, width (tr.) approximately 200% width (tr.) of distance from axial furrow to fulcrum; strongly arched dorsally (tr.). Articulating half ring semilunate; maximum length (sag.) approximately 85% length (sag.) of axial ring; well defined by broad articulating furrow that broadens (exsag.) and slightly shallows adaxially, anterior limit of furrow almost transerve, posterior limit of furrow convex posteriorly. Axial furrow convex abaxially. Anterior and posterior margins of pleura straight (tr.) but for small swelling along anterior margin approximately two-thirds of distance from fulcrum to pleural tip; posterior margin immediately below axial furrow bears low process projecting ventrally and slightly adaxially on the ventral surface. Pleural furrow runs more or less transversely across pleura from axial furrow, terminating short of pleural tip; deepest distal to fulcrum. Pleural tip bears small, sentate pleural spine. Semilunate doublure beneath posterior margin of axial ring. Narrow triangular doublure extends along posterior margin from fulcrum to pleural tip, broadening (exsag.) distally to cover much of posterior portion of pleural tip; doublure extends as narrow strip along anterior margin from pleural tip to fulcrum.

Mature pygidium (Fig. 29.15–29.31) micropygous, wingnut-shaped in dorsal outline; sagittal length (sag., excluding articulating half ring) approximately one-quarter of maximal width (tr.); anterior margin horizontal when traced away from axial furrow, more or less transversely oriented to fulcrum located approximately 45% of distance along margin from axial furrow to anterolateral corner of pygidium; anterior margin distal to fulcrum oriented slightly posteriorly, dips ventrally at approximately 45° relative to horizontal plane to anterolateral corner of pygidium; maximum pygidial width (tr.) slightly posterior to anterolateral corner. Posterior pygidial margin with prominent sagittal notch in plan view; vaulted dorsally into strong posterior arch (less prominent on smaller pygidia [Fig. 29.7–29.14]). Pygidial axis defined by weak axial furrow; dorsally vaulted above summit of pleural field (tr.); length (sag., excluding articulating half ring) approximately 90% of pygidial length (sag.), anterior width approximately equal to that of pleural field (tr.); tapers to bluntly rounded posterior tip; two axial rings plus terminal piece faintly defined by shallow ring furrows that shallow over axis, posterior ring furrow extremely shallow. Articulating half ring crescent-shaped, extends full width of axis; posteriorly defined by broad furrow that shallows axially. Pleural field moderately strongly vaulted; inner portion horizontal, distal portion sloping ventrally at approximately 45° before flattening into narrow, subhorizontal border that narrows posteriorly; border furrow not developed. Two pleural furrows and weaker first interpleural furrow clear on dorsal surface of pleural field; all deepen (exsag.) away from axial furrow, do not extend to margin. Pygidial doublure broadest at widest (tr.) point of pygidium, narrows to anterolateral corner of

FIGURE *28*—Rostral plate, librigenae, and hypostomes of *Eokochaspis nodosa*: *1, 2,* rostral plate, ventral and posterior views, FMNH PE58339, ×15; *3, 4,* left librigena, dorsal and ventral views, FMNH PE58340, ×20; *5–7,* right librigena, ventral, dorsal, and right lateral views, FMNH PE58341, ×15;

pygidium and posteriorly, absent sagittally; innermost margin below and paralleling break in slope defining pygidial border.

Ontogeny.—Morphometric analysis herein of cranidia ranging from 1.62 mm to 4.90 mm in sagittal length reveals several ontogenetic trends in cranidial morphology (Figs. 7, 8, 16.3). The glabella proportionally narrows (tr.) anteriorly and widens (tr.) posteriorly, becoming more anteriorly tapered; L1 proportionally expands (tr.) more dramatically than more anterior glabellar lobes. Sagittal glabellar length is approximately 76% to 79% of sagittal cranidial length on the smallest sampled specimens (sagittal cephalic length <1.8 mm) and decreases to approximately 71% to 76% of sagittal cranidial length over the sampled portion of ontogeny (Fig. 24.3). SO is straighter (tr.) and shallows only slightly over the axis on cranidia <2.0 mm in sagittal length (Fig. 8) relative to larger specimens. The posterior cranidial margin distal to the fulcrum becomes less strongly posterolaterally oriented. The anterior cranidial margin and the anterior branch of the facial suture migrate away from the anterior margin of the glabella as the anterior cranidial border widens (tr., sag., exsag.). The strip of exoskeleton anterior to the ocular ridge elongates (exsag.), and the anterior end of the palpebral lobe becomes more widely separated from the anterior border. The palpebral lobe proportionally shortens (exsag.), and its distal edge (bounded by the facial suture) becomes slightly more strongly arcuate.

Holotype.—USNM 497818, figured by Sundberg and McCollum (2000, fig. 7.1–7.3), from USNM locality 41447 (Grassy Spring section, Delamar Mountains: see Webster, 2009, figs. 2, 12).

Other material examined.—Descriptions and morphometric analyses presented herein based on examination of FMNH PE58290-PE58313, FMNH PE58339-PE58354, plus >80 other cranidia in the ICS collections, all from ICS-1192 (stratigraphic and locality details above). For comparative purposes, the holotype and seven additional topotype specimens from the Grassy Spring section were also examined.

Discussion.—Based on examination of cranidia ranging in length from 2.7 mm to 5.5 mm, Sundberg and McCollum (2000, p. 614) stated that *Eokochaspis nodosa* differs from *C.*? *metalaspis* (as *E. metalaspis*) in the following respects: *E. nodosa* has a relatively narrower cranidium (sag. length relative to maximum tr. width); a longer (sag., relative to sag. cranidial length), wider (tr. across base, relative to sag. cranidial length), and more tapered glabella; a shorter occipital ring (sag., relative to sag. cranidial length); a shorter frontal area (sag., relative to sag. cranidial length) with a proportionally shorter anterior border (sag., relative to sag. cranidial length and to sag. frontal area length) and longer preglabellar field (sag., relative to sag. frontal area length); shorter palpebral lobes (exsag., relative to sag. glabellar length); a more prominent occipital node, glabellar furrows, ocular ridges, and frontal lobe; less curvature of the anterior border; a less prominent median inbend of the anterior border furrow; a sharper termination to the posterior fixigena; and a greater length of the anterior branch of the facial suture between the palpebral lobe and anterior border. *Eokochaspis nodosa* bears a granular ornament, which is absent in *C.*? *metalaspis*.

The present study confirms these differences (morphometric analyses above; Fig. 20), and also demonstrates that *E. nodosa* markedly differs from both *C. walcotti* and *C.*? *metalaspis* in non-cranidial morphology. The free cheek of *E. nodosa* is proportionally wider (tr.) than that of *C.*? *metalaspis* and *C. walcotti*, with a broader (tr.) librigenal field and genal spine base. Thoracic segments of *E. nodosa* (Fig. 29.1–29.6) are more elongate (tr.) with deeper furrows, a broader (sag., exsag.) articulating furrow, and apparently lack a panderian notch and panderian protuberance. They also possess a swelling on the anterior margin of the thoracic pleura near the pleural tip that presumably functioned in segment articulation. The wingnut-shaped pygidium of *E. nodosa* is also markedly different from the suboval pygidium of *C. walcotti* and *C.*? *metalaspis*. The similarity between *E. nodosa* and *C.*? *metalaspis* in thoracic segment and pygidial morphology noted by Sundberg and McCollum (2000, p. 614) is limited compared to the similarity in these sclerites (and librigena) between *C.*? *metalaspis* and *C. walcotti* documented herein.

The present study also reveals some problems in Sundberg's (2004) character state coding of *E. nodosa*. The occipital node or spine (character 11) was incorrectly coded as absent. Sundberg (2004, characters 23, 25) states that *E. nodosa* possesses a weak V-shaped median inbend of the anterior border furrow and that a plectrum is absent. The median inbend is herein interpreted as being related to the presence of a plectrum. The anterior branches of the facial suture (character 35) were coded as being weakly convergent anteriorly between the palpebral lobe and anterior border furrow, but large cranidia from ICS-1192 exhibit anterior branches of the facial suture that are anteriorly convergent (Fig. 7.11) to divergent (Fig. 7.12) in this location. Relative to the material studied herein, the transverse width of the posterior area of fixigena relative to basal glabellar width (character 34), the orientation of the palpebral lobe relative to the exsagittal axis (character 37), and the length of the palpebral lobe relative to the sagittal glabellar length (character 41), are each underestimated in Sundberg's (2004) coding. Coarse granules (character 47) were coded as absent, but such granules are developed on the interocular area. The effects of these revised findings on kochaspid phylogeny will be presented elsewhere.

Smith's (1998) study of intraspecific variation in Lower Paleozoic trilobites included a silicified sample identified as "*Eoptychoparia piochensis*" from the basal Delamaran Comet Shale Member of the Pioche Formation. The collection information provided by Smith (1995, 1998) is insufficient to relocate the specimens that he examined. However, *Eoptychoparia piochensis* has since been restricted to non-silicified specimens in shale of the Comet Shale Member (Sundberg and McCollum, 2000): silicified specimens formerly assigned to this species were reassigned to *Eokochaspis nodosa* by Sundberg and McCollum (2000). It is therefore possible that Smith's (1998) analysis included both *C.*? *metalaspis* (as *C.*

←

8–10, right librigena, ventral, dorsal, and right lateral views, FMNH PE58342, ×12; *11–13,* left librigena, dorsal, ventral, and left lateral views, FMNH PE58343, ×9; *14–17,* hypostome, ventral, dorsal, lateral, and posterior views, FMNH PE58344, ×40; *18–21,* hypostome, ventral, lateral, posterior, and anterior views, FMNH PE58345, ×20; *22–25,* hypostome, ventral, dorsal, lateral, and posterior views, FMNH PE58346, ×17; *26–29,* hypostome, ventral, dorsal, lateral, and posterior views, FMNH PE58347, ×15. All from ICS-1192, Comet Shale Member, Pioche Formation, Ruin Wash section, Chief Range.

FIGURE *29*—Thoracic segments and pygidia of *Eokochaspis nodosa*: *1–6,* isolated thoracic segment (right pleura missing), dorsal, ventral, anterior, posterior, left lateral, and oblique interior views, FMNH PE58348, ×15; *7–10,* pygidium, dorsal, ventral, anterior, and posterior views, FMNH

walcotti) and *Eokochaspis nodosa* (as *Eoptychoparia piochensis*). However, the silicified samples examined by Smith (1998) must have come from horizons and/or localities different from those examined herein.

ACKNOWLEDGMENTS

J. Thompson and D. Levin are thanked for the loan of material from the USNM. H. D. Sheets fixed a bug in the SemiLand software at short notice and provided helpful technical comments regarding size-standardization. Material from ICS-1029 and ICS-1192 was initially collected by A. R. Palmer in 1992 and 1996, respectively. The latter horizon was recollected by MW in 1997 and 1999. ICS-10124 was collected by MW in 2001. Assistance to MW in the field on these occasions was generously provided by N. C. Hughes, R. R. Gaines, L. McCollum, and M. McCollum. Comments by T. Karim and an anonymous reviewer helped improve the manuscript.

REFERENCES

ADRAIN, J. M. AND S. R. WESTROP. 2005. Late Cambrian ptychaspidid trilobites from western Utah: implications for trilobite systematics and biostratigraphy. Geological Magazine, 142:377–398.

ADRAIN, J. M. AND S. R. WESTROP. 2006. New earliest Ordovician trilobite genus *Millardicurus*: the oldest known hystricurid. Journal of Paleontology, 80:650–671.

ANDRESEN, P. R., F. L. BOOKSTEIN, K. CONRADSEN, B. ERSBØLL, J. MARSH, AND S. KREIBORG. 2000. Surface-bounded growth modeling applied to human mandibles. IEEE Transactions in Medical Imaging, 19:1053–1063.

AVISE, J. C. 2000. Phylogeography. Harvard University Press, Cambridge, Massachusetts, 447 p.

BARRANDE, J. 1846. Notice préliminaire sur le systême Silurien et les Trilobites de Bohême. Hirschfeld, Leipzig, 97 p.

BLAKER, M. R. AND J. S. PEEL. 1997. Lower Cambrian trilobites from North Greenland. Meddelelser om Grønland, Geoscience, 35:1–145.

BOOKSTEIN, F. L. 1991. Morphometric Tools for Landmark Data: Geometry and Biology. Cambridge Univeristy Press, 435 p.

BOOKSTEIN, F. L. 1997. Landmark methods for forms without landmarks: morphometrics of group differences in outline shape. Medical Image Analysis, 1:97–118.

BOOKSTEIN, F. L., A. P. STREISSGUTH, P. D. SAMPSON, P. D. CONNOR, AND H. M. BARR. 2002. Corpus callosum shape and neuropsychological deficits in adult males with heavy fetal alcohol exposure. Neuroimage, 15:233–251.

BRIGHT, R. C. 1959. A paleoecologic and biometric study of the Middle Cambrian trilobite *Elrathia kingii* (Meek). Journal of Paleontology, 33:83–98.

COTTON, T. J. 2001. The phylogeny and systematics of blind Cambrian ptychoparioid trilobites. Palaeontology, 44:167–204.

DRYDEN, I. L. AND K. V. MARDIA. 1998. Statistical Shape Analysis. John Wiley and Sons, Chichester, England, 347 p.

FORTEY, R. A. 2001. Trilobite systematics: The last 75 years. Journal of Paleontology, 75:1141–1151.

FRANCE, S. C. 1993. Geographic variation among three isolated populations of the hadal amphipod *Hirondellea gigas* (Crustacea: Amphipoda: Lysianassoidea). Marine Ecology Progress Series, 92:277–287.

FRITZ, W. H. 1968. Lower and early Middle Cambrian trilobites from the Pioche Shale, east-central Nevada, U.S.A. Palaeontology, 11:183–235.

GEYER, G. AND J. M. MALINKY. 1997. Middle Cambrian fossils from Tizi N'Tichka, the High Atlas, Morocco. Part 1. Introduction and trilobites. Journal of Paleontology, 71:620–637.

GOODALL, C. 1991. Procrustes methods in the statistical analysis of shape. Journal of the Royal Statistical Society, Series B (Methodological), 53:285–339.

GREEN, W. D. K. 1996. The thin-plate spline and images with curving features, p. 79–87. *In* K. V. Mardia, C. A. Gill and I. L. Dryden (eds.), Image Fusion and Shape Variability. University of Leeds Press, Leeds.

GUNZ, P., P. MITTEROECKER, AND F. L. BOOKSTEIN. 2005. Semilandmarks in three dimensions, p. 73–98. *In* D. E. Slice (ed.), Modern Morphometrics in Physical Anthropology. Kluwer Academic Publishers/Plenum, New York.

HALL, J. AND R. P. WHITFIELD. 1877. Palaeontology. United States Geological Exploration of the Fortieth Parallel, 4:198–302.

HALLGRÍMSSON, B. AND B. K. HALL. 2005. Variation: A Central Concept in Biology. Elsevier Academic Press, Burlington, MA, 568 p.

HOPKINS, M. J. AND C. L. THURMAN. 2010. The geographic structure of morphological variation in eight species of fiddler crabs (Ocypodidae: genus *Uca*) from the eastern United States and Mexico. Biological Journal of the Linnean Society, 100:248–270.

HOPKINS, M. J. AND M. WEBSTER. 2009. Ontogeny and geographic variation of a new species of the corynexochine trilobite *Zacanthopsis* (Dyeran, Cambrian). Journal of Paleontology, 83:524–547.

HUGHES, N. C. 1994. Ontogeny, intraspecific variation, and systematics of the Late Cambrian trilobite *Dikelocephalus*. Smithsonian Contributions to Paleobiology, 79:1–89.

HUGHES, N. C., A. MINELLI, AND G. FUSCO. 2006. The ontogeny of trilobite segmentation: a comparative approach. Paleobiology, 32:602–627.

HUNT, G. 2004a. Phenotypic variation in fossil samples: modeling the consequences of time-averaging. Paleobiology, 30:426–443.

HUNT, G. 2004b. Phenotypic variance inflation in fossil samples: an empirical assessment. Paleobiology, 30:487–506.

HUNT, G. 2007. Evolutionary divergence in directions of high phenotypic variance in the ostracode genus *Poseidonamicus*. Evolution, 61:1560–1576.

HUPE, P. 1953. Classe de trilobites, p. 22–246. *In* J. Piveteau (ed.), Traité de Paléontologie, vol. 3. Les formes ultimes d'Invertébrés: morphologie et évoltion: Onychophores-Arthropodes-Échinodermes-Stomocordés. Masson et Cie, Paris.

JELL, P. A. AND J. M. ADRAIN. 2003. Available generic names for trilobites. Memoirs of the Queensland Museum, 48:331–553.

LEROSEY-AUBRIL, R. AND K. J. MCNAMARA. 2008. The cephalic median organ of trilobites, p. 229–235. *In* I. Rábano, R. Gozalo, and D. García-Bellido (eds.), Advances In Trilobite Research. Cuadernos del Museo Geominero 9. Instituto Geológico y Minero de España, Madrid.

LOCHMAN, C. 1947. Analysis and revision of eleven Lower Cambrian trilobite genera. Journal of Paleontology, 21:59–71.

MATTHEW, G. F. 1887. Illustrations of the fauna of the St. John Group continued. III–Descriptions of new genera and species, (including a description of a new species of Solenopleura by J. F. Whiteaves). Transactions of the Royal Society of Canada, 3:29–84.

MEEK, F. B. 1870. Descriptions of fossils collected by the U.S. Geological Survey, under charge of Clarence King. Proceedings of the Academy of Natural Sciences of Philadelphia, Second Series, 14:56–64.

NIXON, K. C. AND Q. D. WHEELER. 1990. An amplification of the phylogenetic species concept. Cladistics, 6:211–223.

PALMER, A. R. 1958. Morphology and ontogeny of a Lower Cambrian ptychoparioid trilobite from Nevada. Journal of Paleontology, 32:154–170.

PALMER, A. R. 1968. Cambrian trilobites of East-Central Alaska. United States Geological Survey Professional Paper, 559-B:1–115.

PALMER, A. R. 1998a. Terminal Early Cambrian extinction of the Olenellina: Documentation from the Pioche Formation, Nevada. Journal of Paleontology, 72:650–672.

PALMER, A. R. 1998b. A proposed nomenclature for stages and series for the Cambrian of Laurentia. Canadian Journal of Earth Sciences, 35:323–328.

PALMER, A. R. AND R. B. HALLEY. 1979. Physical stratigraphy and trilobite biostratigraphy of the Carrara Formation (Lower and Middle Cambrian) in the southern Great Basin. United States Geological Survey Professional Paper, 1047:1–131.

PEREZ, S. I., V. BERNAL, AND P. N. GONZALEZ. 2006. Differences between sliding semi-landmark methods in geometric morphometrics, with an

←

PE58349, ×25; *11–14,* pygidium, dorsal, ventral, anterior, and posterior views, FMNH PE58350, ×20; *15–19,* pygidium, dorsal, ventral, anterior, posterior, and right lateral views, FMNH PE58351, ×18; *20–22,* pygidium, dorsal, ventral, and anterior views, FMNH PE58352, ×12; *23–26,* pygidium with incipiently released anterior segment, dorsal, ventral, anterior, and posterior views, FMNH PE58353, ×10; *27–31,* pygidium, dorsal, ventral, anterior, posterior, and left lateral views, FMNH PE58354, ×10. All from ICS-1192, Comet Shale Member, Pioche Formation, Ruin Wash section, Chief Range.

application to human craniofacial and dental variation. Journal of Anatomy, 208:769–784.
RASETTI, F. 1951. Middle Cambrian stratigraphy and faunas of the Canadian Rocky Mountains. Smithsonian Miscellaneous Collections, 116:1–277.
RASETTI, F. 1955. Lower Cambrian ptychopariid trilobites from the conglomerates of Quebec. Smithsonian Miscellaneous Collections, 128:1–35.
RENAUD, S., J.-C. AUFFREY, AND J. MICHAUX. 2006. Conserved phenotypic variation patterns, evolution along lines of least resistance, and departure due to selection in fossil rodents. Evolution, 60:1701–1717.
RESSER, C. E. 1936. Second contribution to nomenclature of Cambrian trilobites. Smithsonian Miscellaneous Collections, 95:1–29.
RESSER, C. E. 1937. Third contribution to nomenclature of Cambrian trilobites. Smithsonian Miscellaneous Collections, 95:1–29.
RESSER, C. E. 1938. Cambrian System (restricted) of the southern Appalachians. Geological Society of America Special Papers, 15:1–140.
RISKA, B. 1981. Morphological variation in the horseshoe crab *Limulus polyphemus*. Evolution, 35:647–658.
ROHLF, F. J. 2003. tpsSmall. Version 1.20. Department of Ecology and Evolution, State University of New York. Available at <http://life.bio.sunysb.edu.morph/>.
ROHLF, F. J. 2009. tpsDig. Version 2.14. Department of Ecology and Evolution, State University of New York. Available at <http://life.bio.sunysb.edu.morph/>.
ROHLF, F. J. AND D. SLICE. 1990. Extensions of the Procrustes method for the optimal superimposition of landmarks. Systematic Zoology, 39:40–59.
SAMPSON, P. D., F. L. BOOKSTEIN, H. SHEEHAN, AND E. L. BOLSON. 1996. Eigenshape analysis of left ventricular outlines from contrast ventriculograms, p. 131–152. *In* L. F. Marcus, M. Corti, A. Loy, G. J. P. Naylor and D. E. Slice (eds.), Advances in Morphometrics. Nato ASI Series, Series A: Life Science, New York.
SCHLUTER, D. 1996. Adaptive radiation along genetic lines of least resistance. Evolution, 50:1766–1774.
SCHWIMMER, D. R. 1975. Quantitative taxonomy and biostratigraphy of Middle Cambrian trilobites from Montana and Wyoming. Mathematical Geology, 7:149–166.
SHAW, A. B. 1957. Quantitative trilobite studies II. Measurement of the dorsal shell of non-agnostidean trilobites. Journal of Paleontology, 31:193–207.
SHAW, A. B. 1962. Paleontology of northwestern Vermont IX. Fauna of the Monkton Quartzite. Journal of Paleontology, 36:322–345.
SHEETS, H. D. 2001. Standard6beta. Department of Physics, Canisius College, Buffalo, New York. Available at <http://www.canisius.edu/~sheets/morphsoft.html>.
SHEETS, H. D. 2003. VecCompare6c. Department of Physics, Canisius College, Buffalo, New York. Available at <http://www.canisius.edu/~sheets/morphsoft.html>.
SHEETS, H. D. 2005. TwoGroup6h. Department of Physics, Canisius College, Buffalo, New York. Available at <http://www.canisius.edu/~sheets/morphsoft.html>.
SHEETS, H. D. 2007a. PCAGen6p. Department of Physics, Canisius College, Buffalo, New York. Available at <http://www.canisius.edu/~sheets/morphsoft.html>.
SHEETS, H. D. 2007b. DisparityBox6i. Department of Physics, Canisius College, Buffalo, New York. Available at <http://www.canisius.edu/~sheets/morphsoft.html>.
SHEETS, H. D. 2008. Regress6N. Department of Physics, Canisius College, Buffalo, New York. Available at <http://www.canisius.edu/~sheets/morphsoft.html>.
SHEETS, H. D. 2009. SemiLand6. 7th Beta Version. Department of Physics, Canisius College, Buffalo, New York. Available at <http://www.canisius.edu/~sheets/morphsoft.html>.
SHEETS, H. D., K. KIM, AND C. E. MITCHELL. 2004. A combined landmark and outline-based approach to ontogenetic shape change in the Ordovician trilobite *Triarthrus becki*, p. 67–82. *In* A. M. T. Elewa (ed.), Morphometrics: Applications in Biology and Paleontology. Springer-Verlag, Berlin.
SIMPSON, G. G. 1944. Tempo and Mode in Evolution. Columbia University Press, New York, 237 p.
SLICE, D. E. 2007. Geometric morphometrics. Annual Review of Anthropology, 36:261–281.
SMITH, L. H. 1995. The role of species level phenotypic and developmental variability in the early evolution of animals. Unpublished Ph.D. Thesis, Harvard University, 201 p.
SMITH, L. H. 1998. Species level phenotypic variation in lower Paleozoic trilobites. Paleobiology, 24:17–36.
SNIEGOWSKI, P. D. AND H. A. MURPHY. 2006. Evolvability. Current Biology, 16:R831–R834.
SUNDBERG, F. A. 1999. Redescription of *Alokistocare subcoronatum* (Hall and Whitfield, 1877), the type species of *Alokistocare*, and the status of Alokistocaridae Resser, 1939b (Ptychopariida: Trilobita, Middle Cambrian). Journal of Paleontology, 73:1126–1143.
SUNDBERG, F. A. 2004. Cladistic analysis of Early–Middle Cambrian kochaspid trilobites (Ptychopariida). Journal of Paleontology, 78:920–940.
SUNDBERG, F. A. 2005. The Topazan Stage, a new Laurentian stage (Lincolnian Series–"Middle" Cambrian). Journal of Paleontology, 79:63–71.
SUNDBERG, F. A. AND L. B. MCCOLLUM. 2000. Ptychopariid trilobites of the Lower-Middle Cambrian boundary interval, Pioche Shale, southeastern Nevada. Journal of Paleontology, 74:604–630.
SUNDBERG, F. A. AND L. B. MCCOLLUM. 2003. Early and Mid Cambrian trilobites from the outer-shelf deposits of Nevada and California, USA. Palaeontology, 46:945–986.
WAGNER, G. P. AND L. ALTENBERG. 1996. Complex adaptations and the evolution of evolvability. Evolution, 50:967–976.
WALCOTT, C. D. 1886. Second contribution to the studies on the Cambrian faunas of North America. United States Geological Survey Bulletin, 30, 369 p.
WALCOTT, C. D. 1890. The fauna of the Lower Cambrian or *Olenellus* Zone, p. 509–774. In Tenth Annual Report of the Director, 1888–1889, United States Geological Survey.
WALCOTT, C. D. 1916. Cambrian Geology and Paleontology. III. No. 3. Cambrian Trilobites. Smithsonian Miscellaneous Collections, 64:157–258.
WEBSTER, M. 2007a. A Cambrian peak in morphological variation within trilobite species. Science, 317:499–502.
WEBSTER, M. 2007b. Ontogeny and evolution of the Early Cambrian trilobite genus *Nephrolenellus* (Olenelloidea). Journal of Paleontology, 81:1168–1193.
WEBSTER, M. 2009. Systematic revision of the Cambrian trilobite *Bathynotus* Hall, 1860, with documentation of new occurrences in western Laurentia and implications for intercontinental biostratigraphic correlation. Memoirs of the Association of Australasian Palaeontologists, 37:369–406.
WEBSTER, M. AND N. C. HUGHES. 1999. Compaction-related deformation in Cambrian olenelloid trilobites and its implications for fossil morphometry. Journal of Paleontology, 73:355–371.
WEBSTER, M. AND H. D. SHEETS. 2010. A practical introduction to landmark-based geometric morphometrics, p. 163–188. *In* J. Alroy and G. Hunt (eds.), Quantitative Methods in Paleobiology. Paleontological Society Papers, Vol. 16.
WEBSTER, M. AND M. L. ZELDITCH. 2005. Evolutionary modifications of ontogeny: heterochrony and beyond. Paleobiology, 31:354–372.
WEBSTER, M. AND M. L. ZELDTICH. 2008. Integration and regulation of developmental systems in trilobites, p. 427–433. *In* I. Rábano, R. Gozalo, and D. García-Bellido (eds.), Advances In Trilobite Research. Cuadernos del Museo Geominero 9. Instituto Geológico y Minero de España, Madrid.
WEBSTER, M. AND M. L. ZELDITCH. 2009. Testing hypotheses of developmental constraints on macroevolutionary diversification: Studying modularity of ancient developmental systems. Cincinnati Museum Center Scientific Contributions Number, 3:115.
WEBSTER, M., H. D. SHEETS, and N. C. HUGHES. 2001. Allometric patterning in trilobite ontogeny: testing for heterochrony in *Nephrolenellus*, p. 105–144. *In* M. L. Zelditch (ed.), Beyond Heterochrony: The Evolution of Development. Wiley and Sons, New York.
WEBSTER, M., R. R. GAINES, and N. C. HUGHES. 2008. Microstratigraphy, trilobite biostratinomy, and depositional environment of the "Lower Cambrian" Ruin Wash Lagerstätte, Pioche Formation, Nevada. Palaeogeography, Palaeoclimatology, Palaeoecology, 264: 100–122.
WESTROP, S. R. AND J. M. ADRAIN. 2007. *Bartonaspis* new genus, a trilobite species complex from the base of the Upper Cambrian Sunwaptan Stage in North America. Canadian Journal of Earth Sciences, 44:987–1003.
WHEELER, Q. D. AND R. MEIER. 2000. Species Concepts and Phylogenetic Theory: A Debate. Columbia University Press, New York, 230 p.
WHITTINGTON, H. B. 1965. Trilobites of the Ordovician Table Head Formation, western Newfoundland. Bulletin of the Museum of Comparative Zoology, 132:277–442.
WHITTINGTON, H. B., B. D. E. CHATTERTON, S. E. SPEYER, R. A. FORTEY, R. M. OWENS, W. T. CHANG, W. T. DEAN, P. A. JELL, J. R. LAURIE, A. R. PALMER, L. N. REPINA, A. W. A. RUSHTON, J. H.

SHERGOLD, E. N. K. CLARKSON, N. V. WILMOT, AND S. R. A. KELLY. 1997. Treatise on Invertebrate Paleontology. Part O. Arthropoda 1. Trilobita, Revised. Volume 1: Introduction, Order Agnostida, Order Redlichiida. Geological Society of America and Univeristy of Kansas, Boulder, Colorado and Lawrence, Kansas, 530 p.

ZELDITCH, M. L., D. L. SWIDERSKI, H. D. SHEETS, AND W. L. FINK. 2004. Geometric Morphometrics of Biologists: A Primer. Elsevier Academic Press, San Diego, 443 p.

ACCEPTED 8 NOVEMBER 2010